

Chapter 1

Energy Band Structures of Semiconductors

Abstract The physical properties of semiconductors can be understood with the help of the energy band structures. This chapter is devoted to energy band calculations and interpretation of the band structures. Bloch theorem is the starting point for the energy band calculations. Bloch functions in periodic potentials is derived here and a periodic function is shown to be expressed in terms of Fourier expansion by means of reciprocal wave vectors. Brillouin zones are then introduced to understand energy band structures of semiconductors. The basic results obtained here are used throughout the text. Nearly free electron approximation is shown as the simplest example to understand the energy band gap (forbidden gap) of semiconductors and the overall features of the energy band structure. The energy band calculation is carried out first by obtaining free-electron bands (empty lattice bands) which are based on the assumption of vanishing magnitude of crystal potentials and of keeping the crystal periodicity. Next we show that the energy band structures are calculated with a good approximation by the local pseudopotential method with several Fourier components of crystal potential. The nonlocal pseudopotential method, where the nonlocal properties of core electrons are taken into account, is discussed with the spin-orbit interaction. Also $\mathbf{k} \cdot \mathbf{p}$ perturbation method for energy band calculation is described in detail. The method is extended to obtain the full band structures of the elementary and compound semiconductors. Another method “tight binding approximation” will be discussed in connection with the energy band calculation of superlattices in Chap. 8.

1.1 Free-Electron Model

It is well known that the physical properties of semiconductors are understood with the help of energy band structures. The energy states or energy band structures of electrons in crystals reflect the periodic potential of the crystals and they can be calculated when we know the exact shape and the magnitude of the crystal potentials. The shape and the magnitude of the potential are not determined directly from any experimental methods, and thus we have to calculate or estimate the energy bands by using the assumed potentials. Many different approaches to calculations of energy

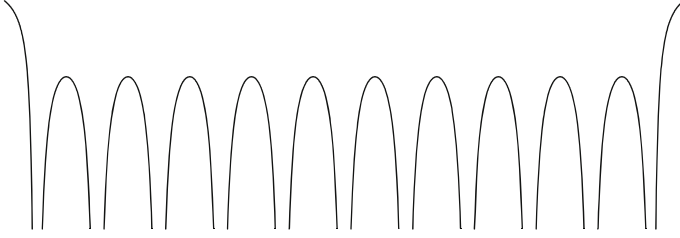


Fig. 1.1 One-dimensional crystal with periodic potential

bands have been reported, but in this textbook we will deal with several methods, which are not so difficult to understand. We begin with the most simplified method to calculate electronic states in a model crystal.

For simplicity we consider a one-dimensional crystal with a periodic potential as shown in Fig. 1.1, and assume that each atom provides one free electron and that the atom has a charge of $+e$, forming an ion.

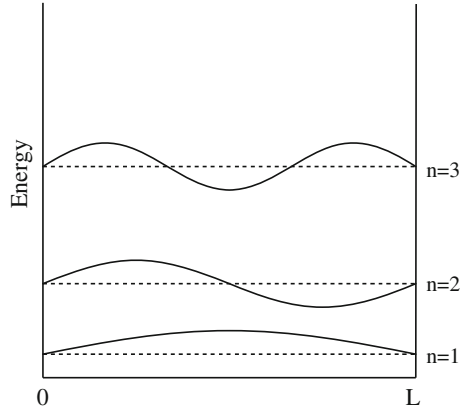
The ion provides potential energy $V(r) = -e^2/4\pi\epsilon_0 r$, where r is the distance from the central position of the ion. Therefore, the one-dimensional crystal has a potential energy consisting of the superposition of that of each atom, as shown in Fig. 1.1. From the figure we find the potential energy of the walls is higher than the inside potential and thus the electrons are confined between the walls. However, we have to note that the above results are derived from a very simplified assumption and the potential distribution is obtained without electrons. In a crystal there are many electrons and thus electron–electron interactions play a very important role in the potential energy distribution. Electron–electron interaction will be discussed in the case of plasmon scattering in Chap. 2 and in calculating the electronic states in quantum dots in Sect. 8. In the discussion of the energy band structure we will not deal with the electron–electron interactions and consider a simplified case where we calculate the electronic states for a single electron and then put many electrons in the energy states by taking the Pauli exclusion principle into account.

The large conductivity in metals is understood to arise from the fact that many free electrons exist in the conduction band. Therefore such electrons have an energy higher than the potential maxima and lower than the confining wall potentials. In the extreme case we can make an approximation that the electrons are confined in a square potential well, as shown in Fig. 1.2, where we assume the potential is infinite at $x = 0$ and $x = L$. In such a case the electron energy may be obtained by solving the one-dimensional Schrödinger equation

$$\left[-\frac{\hbar^2}{2m} \frac{d^2}{dx^2} + V(x) \right] \Psi(x) = \mathcal{E} \Psi(x), \quad (1.1)$$

and the solutions are given by the following relations:

Fig. 1.2 Simplified quantum well model and electronic states



$$\begin{aligned}
 \Psi(x) &= A \sin(k_n) = A \sin\left(\frac{\pi}{L} \cdot n\right), \\
 \mathcal{E} &= \frac{\hbar^2}{2m} k_n^2 = \frac{\hbar^2}{2m} \cdot \left(\frac{\pi n}{L}\right)^2, \\
 k_n &= \frac{\pi}{L} \cdot n \quad (n = 1, 2, 3, \dots)
 \end{aligned} \tag{1.2}$$

Eigenfunctions and their energy level for $n = 1, 2, 3, \dots$ are shown in Fig. 1.2. It is very easy to extend this one-dimensional model to the three-dimensional model, which will not be given here. We have to note that energy band structures are well understood by introducing periodic boundary conditions and the Bloch theorem.

1.2 Bloch Theorem

When we introduce a translational vector \mathbf{T} , the crystal potential has the periodicity $V(\mathbf{r}) = V(\mathbf{r} + \mathbf{T})$, and thus the squared wave function of the electron $|\Psi(\mathbf{r})|^2$ has the same periodicity. The amplitude of the wave function $\Psi(\mathbf{r})$ has an ambiguity of a phase factor $\exp(i\mathbf{k} \cdot \mathbf{r})$. The cyclic boundary condition in the case of a one-dimensional crystal requires the condition that the wave function including the phase factor is the same at x and at $x + L$, and thus $\Psi(x) = \Psi(x + L)$, where L is the length of the crystal. The results are summarized as follows [1]:

$$\Psi(\mathbf{r}) = \exp(i\mathbf{k} \cdot \mathbf{r}) u_k(\mathbf{r}), \tag{1.3}$$

$$u_k(\mathbf{r} + \mathbf{T}) = u_k(\mathbf{r}), \tag{1.4}$$

$$\mathbf{k} = \frac{2\pi}{N}(n_x \mathbf{a}^* + n_y \mathbf{b}^* + n_z \mathbf{c}^*), \quad (1.5)$$

where \mathbf{k} is called the electron wave vector and $\mathbf{T} = n_1 \mathbf{a} + n_2 \mathbf{b} + n_3 \mathbf{c}$ is the translational vector defined by using the fundamental vectors $\mathbf{a}, \mathbf{b}, \mathbf{c}$ with $n_1, n_2, n_3 = 0, \pm 1, \pm 2, \dots$. The function $\Psi(\mathbf{r})$ is called the Bloch function and the function $u(\mathbf{r})$ is the periodic function of the translational vector,

$$u(\mathbf{r} + \mathbf{T}) = u(\mathbf{r}). \quad (1.6)$$

The wave vector \mathbf{k} is expressed in terms of the reciprocal lattice [1],

$$\mathbf{a}^* = \frac{\mathbf{b} \times \mathbf{c}}{\mathbf{a} \cdot (\mathbf{b} \times \mathbf{c})}, \quad (1.7)$$

$$\mathbf{b}^* = \frac{\mathbf{c} \times \mathbf{a}}{\mathbf{a} \cdot (\mathbf{b} \times \mathbf{c})}, \quad (1.8)$$

$$\mathbf{c}^* = \frac{\mathbf{a} \times \mathbf{b}}{\mathbf{a} \cdot (\mathbf{b} \times \mathbf{c})}, \quad (1.9)$$

which satisfy the following relations [1]:

$$\mathbf{a}^* \cdot \mathbf{a} = \mathbf{b}^* \cdot \mathbf{b} = \mathbf{c}^* \cdot \mathbf{c} = 1, \quad (1.10)$$

$$\mathbf{a}^* \cdot \mathbf{b} = \mathbf{a}^* \cdot \mathbf{c} = \dots = \mathbf{c}^* \cdot \mathbf{a} = \mathbf{c}^* \cdot \mathbf{b} = 0. \quad (1.11)$$

The reciprocal lattice vector is defined by

$$\mathbf{G}_n = 2\pi(n_1 \mathbf{a}^* + n_2 \mathbf{b}^* + n_3 \mathbf{c}^*), \quad \text{where } n_1, n_2, n_3 \text{ are integers.} \quad (1.12)$$

Periodic functions with the lattice vectors $\mathbf{a}, \mathbf{b}, \mathbf{c}$ are Fourier expanded with the reciprocal lattice vectors,

$$u_k(\mathbf{r}) = \sum_m A(\mathbf{G}_m) \exp(-i\mathbf{G}_m \cdot \mathbf{r}), \quad (1.13)$$

$$V(\mathbf{r}) = \sum_n V(\mathbf{G}_n) \exp(-i\mathbf{G}_n \cdot \mathbf{r}), \quad (1.14)$$

where $A(\mathbf{G}_m)$ and $V(\mathbf{G}_n)$ are Fourier coefficients. The coefficients are obtained by the inverse Fourier transformation,

$$A(\mathbf{G}_i) = \frac{1}{\Omega} \int_{\Omega} \exp(+i\mathbf{G}_i \cdot \mathbf{r}) u_k(\mathbf{r}) d^3\mathbf{r}, \quad (1.15)$$

$$V(\mathbf{G}_j) = \frac{1}{\Omega} \int_{\Omega} \exp(+i\mathbf{G}_j \cdot \mathbf{r}) V(\mathbf{r}) d^3\mathbf{r}, \quad (1.16)$$

where Ω is the volume of the unit cell of the crystal. From the definition of the reciprocal lattice vector (1.12), we can easily prove the following important relation (see Appendix A.2),

$$\frac{1}{\Omega} \int_{\Omega} \exp [i (\mathbf{G}_m - \mathbf{G}_n) \cdot \mathbf{r}] d^3\mathbf{r} = \delta_{mn} . \quad (1.17)$$

Here we have used the Kronecker delta function defined by

$$\delta_{mn} = \begin{cases} 1 & \text{for } m = n \\ 0 & \text{for } m \neq n \end{cases} . \quad (1.18)$$

1.3 Nearly Free Electron Approximation

For simplicity we begin with the one-dimensional case. From (1.16) we obtain

$$V(G_n) = \frac{1}{a} \int_0^a V(x) \exp(iG_n x) dx , \quad (1.19)$$

which gives the following zeroth-order Fourier coefficient, $V(0)$, when we put $G_n = 0$ in the above equation

$$V(0) = \frac{1}{a} \int_0^a V(x) dx . \quad (1.20)$$

The coefficient $V(0)$ gives the average of the potential energy. In the case of three-dimensional crystals, the coefficient

$$V(0) = \frac{1}{\Omega} \int_{\Omega} V(\mathbf{r}) d^3\mathbf{r} \quad (1.21)$$

also gives the average value of the potential energy $V(\mathbf{r})$ in the unit cell Ω . In the following we measure the energy from $V(0)$ and thus we put $V(0) = 0$. The electronic states of an electron in the periodic potential $V(\mathbf{r})$ are given by solving the Schrödinger equation,

$$\left[-\frac{\hbar^2}{2m} \nabla^2 + V(\mathbf{r}) \right] \Psi(\mathbf{r}) = \mathcal{E}(\mathbf{k}) \Psi(\mathbf{r}) . \quad (1.22)$$

Putting (1.13) into (1.3), we obtain

$$\begin{aligned}
\Psi(\mathbf{r}) &= \frac{1}{\sqrt{\Omega}} \exp(i\mathbf{k} \cdot \mathbf{r}) \sum_n A(\mathbf{G}_n) \exp(-i\mathbf{G}_n \cdot \mathbf{r}), \\
&= \frac{1}{\sqrt{\Omega}} \sum_n A(\mathbf{G}_n) \exp[i(\mathbf{k} - \mathbf{G}_n) \cdot \mathbf{r}],
\end{aligned} \tag{1.23}$$

where the factor $1/\sqrt{\Omega}$ is introduced to normalize the wave function $\Psi(\mathbf{r})$ in the unit cell. Putting (1.14) and (1.23) into (1.22), the following result is obtained:

$$\begin{aligned}
\frac{1}{\sqrt{\Omega}} \sum_n \left[\frac{\hbar^2}{2m} (\mathbf{k} - \mathbf{G}_n)^2 - \mathcal{E}(\mathbf{k}) + \sum_m V(\mathbf{G}_m) \exp(-i\mathbf{G}_m \cdot \mathbf{r}) \right] \\
\times A(\mathbf{G}_n) \exp[i(\mathbf{k} - \mathbf{G}_n) \cdot \mathbf{r}] = 0.
\end{aligned} \tag{1.24}$$

Multiplying $(1/\sqrt{\Omega}) \exp[-i(\mathbf{k} - \mathbf{G}_l) \cdot \mathbf{r}]$ to the both sides of the above equation and integrating in the unit cell with the help of (1.17), we find that the first and the second terms are not 0 for $n = l$, and that the third term is not 0 for $-(\mathbf{G}_m + \mathbf{G}_n) = -\mathbf{G}_l$ (or $\mathbf{G}_l - \mathbf{G}_n = \mathbf{G}_m$). Therefore, the integral is not 0 only in the case of $m = l - n$, and we obtain the following result:

$$\left[\frac{\hbar^2}{2m} (\mathbf{k} - \mathbf{G}_l)^2 - \mathcal{E}(\mathbf{k}) \right] A(\mathbf{G}_l) + \sum_n V(\mathbf{G}_l - \mathbf{G}_n) A(\mathbf{G}_n) = 0. \tag{1.25}$$

In the free-electron approximation of Sect. 1.1, we assumed the potential is given by the square well shown in Fig. 1.2, and thus the Fourier coefficients are $V(\mathbf{G}_m) = 0$ ($m \neq 0$). As stated above, we take the energy basis at $V(0)$ and put $V(\mathbf{r}) = 0$. Then (1.22) gives the following solution:

$$\mathcal{E}(\mathbf{k}) = \frac{\hbar^2 k^2}{2m}, \tag{1.26}$$

$$\Psi(\mathbf{r}) = \frac{1}{\sqrt{\Omega}} A(0) \exp(i\mathbf{k} \cdot \mathbf{r}). \tag{1.27}$$

In the nearly free electron approximation, the potential energy is assumed to be very close to the square well shown in Fig. 1.2 and the Fourier coefficients $V(\mathbf{G}_l)$ are assumed to be negligible except for $V(0)$. Therefore, we replace the energy $\mathcal{E}(\mathbf{k})$ by (1.26) in (1.25) and only the term including $A(0)$ is kept in the second term. This assumption results in

$$\left[\frac{\hbar^2}{2m} (\mathbf{k} - \mathbf{G}_l)^2 - \frac{\hbar^2 k^2}{2m} \right] A(\mathbf{G}_l) + V(\mathbf{G}_l) A(0) = 0. \tag{1.28}$$

From this equation we obtain

$$A(\mathbf{G}_l) = \frac{V(\mathbf{G}_l)A(0)}{(\hbar^2/2m)[k^2 - (\mathbf{k} - \mathbf{G}_l)^2]}. \quad (1.29)$$

In the nearly free electron approximation, the electron wave function may be approximated by (1.27). In other words, the terms $A(\mathbf{G}_l)$ are very small except $\mathbf{G}_l = 0$. From the result given by (1.29), however, we find that the term $A(\mathbf{G}_l)$ is very large when $(\mathbf{k} - \mathbf{G}_l)^2 \approx k^2$. The condition is shown by the following equation:

$$(\mathbf{k} - \mathbf{G}_l)^2 = k^2, \quad (1.30)$$

which gives rise to Bragg's law (law of Bragg reflection) and determines the Brillouin zones of crystals. When the electron wave vector ranges close to the value given by (1.30), we keep the term $A(\mathbf{G}_l)$ in addition to the term $A(0)$, and neglect the other terms. Then we obtain the following relations from (1.25):

$$\left[\frac{\hbar^2}{2m}k^2 - \mathcal{E}(\mathbf{k}) \right] A(0) + V(-\mathbf{G}_l)A(\mathbf{G}_l) = 0, \quad (1.31a)$$

$$\left[\frac{\hbar^2}{2m}(\mathbf{k} - \mathbf{G}_l)^2 - \mathcal{E}(\mathbf{k}) \right] A(\mathbf{G}_l) + V(\mathbf{G}_l)A(0) = 0. \quad (1.31b)$$

The solutions of the above equations are obtained under the condition that the coefficients $A(0)$ and $A(\mathbf{G}_l)$ are both not equal to 0 at the same time. The condition is satisfied when the determinant of (1.31a) and (1.31b) is 0, which is given by

$$\begin{bmatrix} (\hbar^2/2m)k^2 - \mathcal{E}(\mathbf{k}) & V(-\mathbf{G}_l) \\ V(\mathbf{G}_l) & (\hbar^2/2m)(\mathbf{k} - \mathbf{G}_l)^2 - \mathcal{E}(\mathbf{k}) \end{bmatrix} = 0. \quad (1.32)$$

From this we obtain

$$\begin{aligned} \mathcal{E}(\mathbf{k}) &= \frac{1}{2} \left[\frac{\hbar^2}{2m} \{k^2 + (\mathbf{k} - \mathbf{G}_l)^2\} \right. \\ &\quad \left. \pm \sqrt{\left(\frac{\hbar^2}{2m} \right)^2 \{k^2 - (\mathbf{k} - \mathbf{G}_l)^2\}^2 + 4|V(\mathbf{G}_l)|^2} \right], \end{aligned} \quad (1.33)$$

where the relation $V(-\mathbf{G}_l) = V^*(\mathbf{G}_l)$ is used. When $k^2 = (\mathbf{k} - \mathbf{G}_l)^2$ and thus $2\mathbf{k} \cdot \mathbf{G}_l = G_l^2$, we find

$$\mathcal{E}(\mathbf{k}) = \frac{\hbar^2 k^2}{2m} \pm |V(\mathbf{G}_l)|, \quad (1.34)$$

which means that there exists an energy gap of $2|V(\mathbf{G}_l)|$.

Here we will apply the results to a one-dimensional crystal. Replacing \mathbf{G}_l by \mathbf{G}_n in (1.33) and using the relation $\mathbf{G}_n = 2\pi n/a$ ($n = 0, \pm 1, \pm 2, \pm 3, \dots$), we have the following equation:

$$\mathcal{E}(k) = \frac{1}{2} \left[\frac{\hbar^2}{2m} \left\{ k^2 + \left(k - \frac{2\pi n}{a} \right)^2 \right\} \pm \sqrt{\left(\frac{\hbar^2}{2m} \right)^2 \left\{ k^2 - \left(k - \frac{2\pi n}{a} \right)^2 \right\}^2 + 4|V(G_n)|^2} \right]. \quad (1.35)$$

Therefore, $\mathcal{E}(k) \cong \hbar^2 k^2 / 2m$ is satisfied, except in the region close to the condition $k^2 = G_n^2 = (k - 2\pi n/a)^2$ or $k = n\pi/a$. This result gives the choice of \pm in (1.35). Taking account of the sign of the square root, in the region $k < (k - G_n)^2$ we should choose the minus sign and in the region $k > (k - G_n)^2$ we have to choose the plus sign in (1.35). Therefore, in the region $k \approx n\pi/a > 0$, we find we obtain the following relations:

$$k \leq \frac{n\pi}{a} : \quad \mathcal{E}(k) = \frac{\hbar^2 k^2}{2m} - |V(G_n)|, \quad (1.36)$$

$$k \geq \frac{n\pi}{a} : \quad \mathcal{E}(k) = \frac{\hbar^2 k^2}{2m} + |V(G_n)|. \quad (1.37)$$

Using the above relations and plotting $\mathcal{E}(\mathbf{k})$ as a function of k , we obtain the results shown in Fig. 1.3a. Such a plot of energy in the whole region of the k vector shown in Fig. 1.3a is called the “extended zone representation”. In such a one-dimensional crystal model with N atoms, however, the electron system has N degrees of freedom and thus the wave vector of the electron may take N values in the range $-\pi/a < k \leq \pi/a$, corresponding to the first Brillouin zone. When we take this fact into account, the energy can be shown in the first Brillouin zone $-\pi/a < k \leq \pi/a$. This may be understood from the fact that the wave vectors \mathbf{k} and $\mathbf{k} + \mathbf{G}_m$ are equivalent because of the equivalence of the wave functions with these two wave vectors from

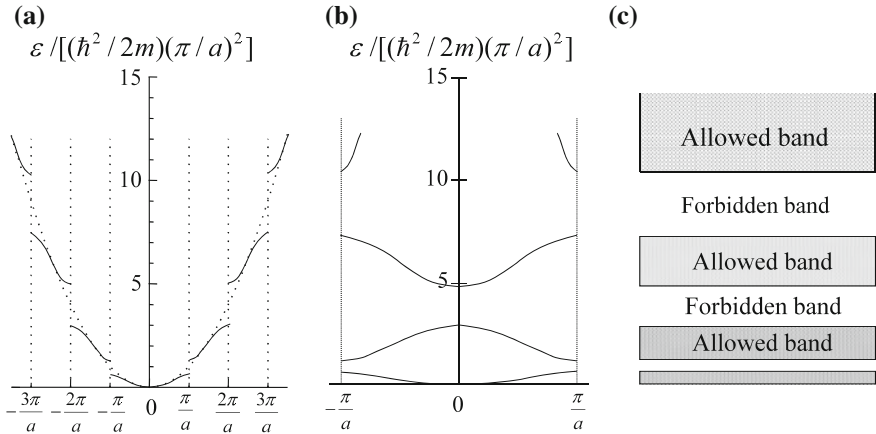


Fig. 1.3 Energy band structure of one-dimensional crystal obtained from the nearly free electron approximation. **a** extended zone representation, **b** reduced zone representation, and **c** energy bands in real space. Energy in units of $(\hbar^2/2m)(\pi/a)^2$

the result shown by (1.23) (see Sect. 1.4). Using this result we easily find that the region $-2\pi/a < k \leq -\pi/a$ in Fig. 1.3a is moved in the region $0 \leq k \leq \pi/a$ of the first Brillouin zone by adding $G = 2\pi/a$ and that $\pi/a \leq k \leq 2\pi/a$ is moved into $-\pi/a \leq k \leq 0$ by adding $G = -2\pi/a$. The region $-2\pi/a < k \leq -\pi/a$ and $\pi/a \leq k \leq 2\pi/a$ is called the second Brillouin zone. The 3rd Brillouin zone, 4th Brillouin zone, ... are defined in the same manner and they can be reduced to the first Brillouin zone. The energy plotted in the first Brillouin zone is shown in Fig. 1.3b and this is called the “reduced zone representation”. Usually the energy band structure is shown in the reduced zone scheme. Figure 1.3c shows the allowed energy region with the shaded portion and the region is called the “allowed band”, while electrons cannot occupy the region in between the allowed bands, which is called the “forbidden band” or “energy band gap”, where the horizontal axis corresponds to the coordinate of real space.

1.4 Reduced Zone Scheme

The Bloch function in a crystal is given by

$$\psi(\mathbf{r}) = \frac{1}{\sqrt{\Omega}} \sum_l A(\mathbf{G}_l) e^{i(\mathbf{k} - \mathbf{G}_l) \cdot \mathbf{r}}. \quad (1.38)$$

Let us examine the phase between two Bloch functions with \mathbf{k} -vectors $\mathbf{k} - \mathbf{G}_l$ and \mathbf{k} . The phase difference at \mathbf{r} between $\exp[i\mathbf{k} \cdot \mathbf{r}]$ and $\exp[i(\mathbf{k} - \mathbf{G}_l) \cdot \mathbf{r}]$ is $\mathbf{G}_l \cdot \mathbf{r}$. The phase difference of the Bloch functions at a point displaced by the translational vector \mathbf{T} , $\mathbf{r} + \mathbf{T}$, is easily obtained in the following way. Since we have the relations

$$\mathbf{T} = n_1 \mathbf{a} + n_2 \mathbf{b} + n_3 \mathbf{c}, \quad (1.39)$$

$$\mathbf{G}_l = 2\pi(m_1 \mathbf{a}^* + m_2 \mathbf{b}^* + m_3 \mathbf{c}^*), \quad (1.40)$$

$$\mathbf{G}_l \cdot \mathbf{T} = 2\pi(m_1 n_1 + m_2 n_2 + m_3 n_3) = 2\pi n, \quad (1.41)$$

and we obtain

$$\begin{aligned} \mathbf{k} \cdot (\mathbf{r} + \mathbf{T}) - (\mathbf{k} - \mathbf{G}_l) \cdot (\mathbf{r} + \mathbf{T}) &= \mathbf{G}_l \cdot \mathbf{r} + \mathbf{G}_l \cdot \mathbf{T} \\ &= \mathbf{G}_l \cdot \mathbf{r} + 2\pi n, \end{aligned} \quad (1.42)$$

where n is an integer and the relation $\mathbf{a}^* \cdot \mathbf{a} = 1$ is used.

From the above considerations we find the following results. The phase differences between the two functions $\exp[i\mathbf{k} \cdot \mathbf{r}]$ and $\exp[i(\mathbf{k} - \mathbf{G}_l) \cdot \mathbf{r}]$ at two different positions \mathbf{r} and $\mathbf{r} + \mathbf{T}$ differs by the amount $2\pi n$ and thus the Bloch function $\psi(\mathbf{r})$ behaves in the same way at the position displaced by the translational vector \mathbf{T} . In other words, we can conclude that electrons with \mathbf{k} and $\mathbf{k} - \mathbf{G}_l$ are equivalent. Therefore, we can reduce the electronic state of an electron with wave vector \mathbf{k} into the state $\mathbf{k} - \mathbf{G}_l$, and represent the electronic states in the first Brillouin zone. This procedure is called the **reduced zone scheme** and the energy band representation in the reduced zone scheme. On the other hand, the energy band representation over the whole \mathbf{k} region is called the **extended zone scheme**.

1.5 Free-Electron Bands (Empty-Lattice Bands)

1.5.1 First Brillouin Zone

In order to calculate energy band structures of a semiconductor the following procedures are required to carry out the calculations. These are

1. Calculate the first Brillouin zone.
2. Calculate the energy band structures in the limit of zero potential energy. This procedure is to obtain the free-electron bands or empty-lattice bands and plot the energy as a function of wave vector \mathbf{k} in the reduced zone scheme.
3. Then calculate the energy bands using an appropriate method.

In the energy band calculation the most important procedure is to obtain the empty-lattice bands, which are calculated by assuming zero lattice potential $V(\mathbf{r}) = 0$ and keeping the lattice periodicity. In other words we assume the wave functions are given by the free-electron model with the wave vectors of the electrons in the periodic potential. Such an energy band structure is called empty-lattice bands or free-electron bands and thus the band structure exhibits the characteristics of the lattice periodicity.

Here we will show an example of empty-lattice bands in the case of the face-centered cubic (fcc) lattice. First, we calculate the Brillouin zone of the fcc lattice. Figure 1.4a shows the fcc structure. The diamond structure is obtained by displacing the lattice atoms by the amount $(a/4, a/4, a/4)$, which is shown in Fig. 1.4b. Therefore, the diamond structure belongs to the fcc structure. Diamond (C), Si and Ge have this diamond structure. On the other hand, the displaced lattice atoms are different from the original atoms, and the structure is called the zinc-blende structure, which is shown in Fig. 1.4c. Crystals such as GaAs, GaP, AlAs, InAs, InSb belong to the zinc-blende structure. The fundamental vectors and volume v of a fcc lattice are defined by

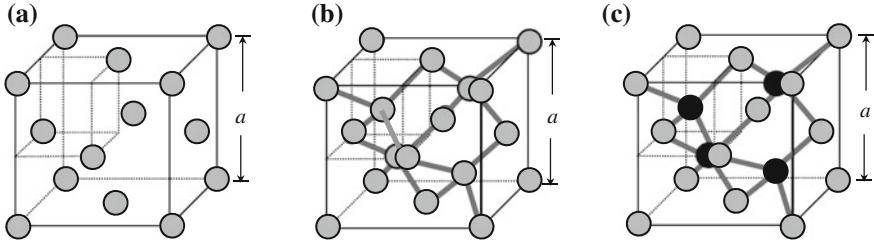


Fig. 1.4 **a** face-centered cubic lattice, **b** the diamond crystal lattice is obtained by displacing the lattice atoms of **a** by $(a/4, a/4, a/4)$, **c** when the displaced lattice atoms are different from the original lattice atoms, the crystal structure is called the zinc-blende crystal structure

$$\begin{aligned}
 \mathbf{a} &= \frac{a}{2}(\mathbf{e}_x + \mathbf{e}_y), \quad \mathbf{b} = \frac{a}{2}(\mathbf{e}_y + \mathbf{e}_z), \quad \mathbf{c} = \frac{a}{2}(\mathbf{e}_z + \mathbf{e}_x), \\
 v &= \mathbf{a} \cdot (\mathbf{b} \times \mathbf{c}) \\
 &= \left(\frac{a}{2}\right)^3 (\mathbf{e}_x + \mathbf{e}_y) \cdot [(\mathbf{e}_y + \mathbf{e}_z) \times (\mathbf{e}_z + \mathbf{e}_x)] = 2 \left(\frac{a}{2}\right)^3 = \frac{1}{4}a^3,
 \end{aligned} \tag{1.43}$$

where \mathbf{e} is the unit vector. The reciprocal vectors of the fcc structure are obtained as follows:

$$\begin{aligned}
 \mathbf{a}^* &= \frac{\mathbf{b} \times \mathbf{c}}{v} = \left(\frac{a}{2}\right)^2 \frac{(\mathbf{e}_y + \mathbf{e}_z) \times (\mathbf{e}_z + \mathbf{e}_x)}{v} = \left(\frac{a}{2}\right)^2 \frac{(\mathbf{e}_x - \mathbf{e}_z + \mathbf{e}_y)}{a^3/4} \\
 &= \frac{1}{a}(\mathbf{e}_x + \mathbf{e}_y - \mathbf{e}_z),
 \end{aligned} \tag{1.44}$$

$$\mathbf{b}^* = \frac{1}{a}(-\mathbf{e}_x + \mathbf{e}_y + \mathbf{e}_z), \tag{1.45}$$

$$\mathbf{c}^* = \frac{1}{a}(\mathbf{e}_x - \mathbf{e}_y + \mathbf{e}_z). \tag{1.46}$$

From these results we find that the reciprocal lattices of the fcc lattice form body-centered cubic lattices. Therefore, the reciprocal lattice vectors \mathbf{G} of the fcc lattice are given by

$$\mathbf{G} = 2\pi(n_1\mathbf{a}^* + n_2\mathbf{b}^* + n_3\mathbf{c}^*). \tag{1.47}$$

The Brillouin zone of the fcc lattice is defined by

$$k^2 = (\mathbf{k} - \mathbf{G}_l)^2 \tag{1.48}$$

or

$$2\mathbf{k} \cdot \mathbf{G}_l = G_l^2. \tag{1.49}$$

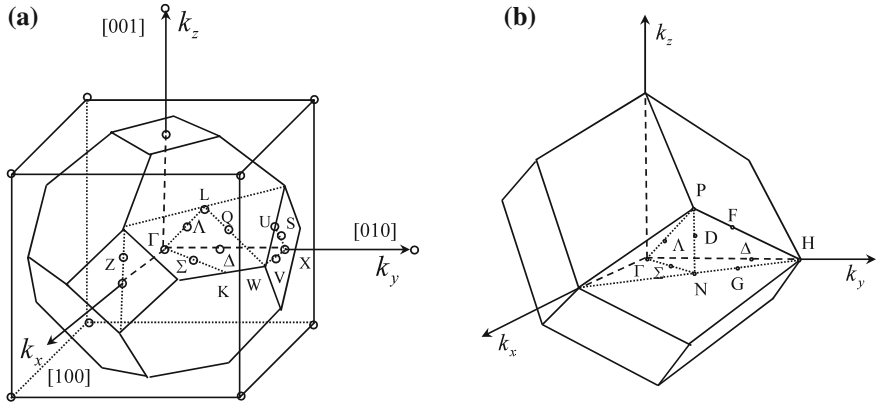


Fig. 1.5 The first Brillouin zone of **a** face-centered cubic lattice and **b** body-centered cubic lattice

Using the above equation the first Brillouin zone is easily calculated, as shown in Fig. 1.5a. For comparison the first Brillouin zone of body-centered cubic lattices, which form face-centered cubic lattices, is shown in Fig. 1.5b.

Since the lattice potential is 0 in the empty-lattice model, the energy of an electron is given by the free-electron model:

$$\mathcal{E}(\mathbf{k}) = \frac{\hbar^2}{2m} k^2. \quad (1.50)$$

We plot the energy $\mathcal{E}(\mathbf{k})$ versus wave vector \mathbf{k} curves in the reduced zone scheme, using the relation

$$\mathbf{k}' = \mathbf{k} - \mathbf{G}, \quad (1.51)$$

and choose \mathbf{k}' in the first Brillouin zone. Then the empty lattice bands are given by

$$\mathcal{E}(\mathbf{k}') = \frac{\hbar^2}{2m} (\mathbf{k}' + \mathbf{G})^2. \quad (1.52)$$

1.5.2 Reciprocal Lattice Vectors of fcc Crystal

In the next Sect. 1.6, we discuss detailed treatment of pseudopotential method for energy band calculations and show how to program the energy band calculation. For this purpose we evaluate the matrix elements of the pseudopotential Hamiltonian of a face centered cubic (fcc) crystal. First, we calculate the reciprocal lattice vectors. Inserting (1.44) ~ (1.46) into (1.47), we obtain the following relations for the reciprocal vectors

$$\mathbf{G} = \frac{2\pi}{a} \left[(n_1 - n_2 + n_3)\mathbf{e}_x + (n_1 + n_2 - n_3)\mathbf{e}_y + (-n_1 + n_2 + n_3)\mathbf{e}_z \right] \quad (1.53)$$

and thus the x , y , z components of \mathbf{G} , and G^2 are

$$G_x = \frac{2\pi}{a} (n_1 - n_2 + n_3) , \quad (1.54)$$

$$G_y = \frac{2\pi}{a} (n_1 + n_2 - n_3) , \quad (1.55)$$

$$G_z = \frac{2\pi}{a} (-n_1 + n_2 + n_3) , \quad (1.56)$$

$$G^2 = [G_x^2 + G_y^2 + G_z^2] \quad (1.57)$$

$$\equiv \left(\frac{2\pi}{a} \right)^2 \left[(n_1 - n_2 + n_3)^2 + (n_1 + n_2 - n_3)^2 + (-n_1 + n_2 + n_3)^2 \right] . \quad (1.58)$$

Using these relations the reciprocal wave vectors of a face-centered cubic lattice are easily evaluated, by putting $n_1, n_2, n_3 = \pm 0, \pm 1, \pm 2, \pm 4, \pm 5, \dots$. It is very convenient to introduce dimensionless lattice vectors \mathbf{K} defined by,

$$\mathbf{K} = \left(\frac{a}{2\pi} \right) \mathbf{G} . \quad (1.59)$$

The calculated reciprocal lattice vectors \mathbf{K} are listed in Table 1.1, where G_x, G_y, G_z are obtained by multiplying \mathbf{K} by $(2\pi/a)$ and they are tabulated for $K^2 = K_x^2 + K_y^2 + K_z^2 = 0 \sim 27$.

1.5.3 Free Electron Bands

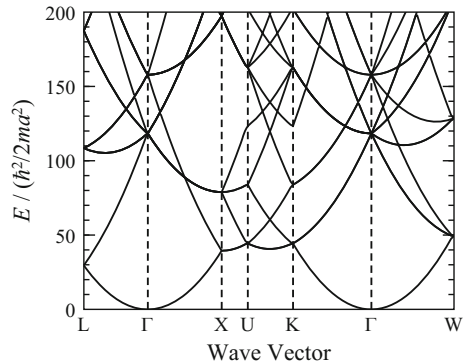
Free electron bands (empty lattice bands) are easily calculated using the results of Table 1.1, which are shown in Fig. 1.6 in the range of electron energy less than 200 in units of $[\hbar^2/2ma^2]$.

For better understanding we list several reciprocal lattice vectors from the lowest orders, which are given by (see (1.53) and Table 1.1)

Table 1.1 Reciprocal lattice vectors of a face-centered cubic lattice calculated from (1.53), where $K_x = (a/2\pi)G_x$, $K_y = (a/2\pi)G_y$, $K_z = (a/2\pi)G_z$. Here the vectors are obtained for $K^2 = K_x^2 + K_y^2 + K_z^2$ from 0 to 27

[K]	Permutations								K^2
[000]	[000]								0
[111]	[$\bar{1}\bar{1}\bar{1}$]	[$\bar{1}\bar{1}1$]	[$\bar{1}1\bar{1}$]	[$\bar{1}11$]	[$1\bar{1}\bar{1}$]	[$1\bar{1}1$]	[$11\bar{1}$]	[111]	3
[200]	[0 $\bar{2}$ 0]	[$\bar{2}$ 00]	[00 $\bar{2}$]	[002]	[200]	[020]			4
[220]	[$\bar{2}\bar{2}$ 0]	[0 $\bar{2}\bar{2}$]	[$\bar{2}$ 0 $\bar{2}$]	[0 $\bar{2}$ 2]	[$\bar{2}$ 02]	[2 $\bar{2}$ 0]	[$\bar{2}$ 20]	[20 $\bar{2}$]	8
	[0 $\bar{2}\bar{2}$]	[202]	[022]	[220]					
[311]	[$\bar{1}\bar{3}\bar{1}$]	[$\bar{3}\bar{1}\bar{1}$]	[$\bar{1}\bar{3}1$]	[$\bar{3}\bar{1}1$]	[$\bar{1}\bar{1}\bar{3}$]	[$\bar{1}\bar{3}\bar{1}$]	[$\bar{1}\bar{3}1$]	[$\bar{3}\bar{1}\bar{1}$]	11
	[$\bar{3}\bar{1}1$]	[$\bar{1}\bar{1}\bar{3}$]	[$\bar{1}\bar{1}\bar{3}$]	[$\bar{1}\bar{1}3$]	[$\bar{1}1\bar{3}$]	[$\bar{1}\bar{1}3$]	[$\bar{1}13$]	[$\bar{3}\bar{1}\bar{1}$]	
	[$\bar{3}\bar{1}\bar{1}$]	[$\bar{1}\bar{1}\bar{3}$]	[$\bar{1}\bar{1}3$]	[$\bar{1}1\bar{3}$]	[$\bar{3}\bar{1}\bar{1}$]	[$\bar{1}\bar{3}\bar{1}$]	[$\bar{3}\bar{1}1$]	[$\bar{1}\bar{3}\bar{1}$]	
[222]	[$\bar{2}\bar{2}\bar{2}$]	[$\bar{2}\bar{2}2$]	[$\bar{2}2\bar{2}$]	[$\bar{2}22$]	[$2\bar{2}\bar{2}$]	[$2\bar{2}2$]	[$22\bar{2}$]	[222]	12
[400]	[040]	[$\bar{4}$ 00]	[004]	[004]	[400]	[040]			16
[331]	[$\bar{3}\bar{3}\bar{1}$]	[$\bar{3}\bar{3}1$]	[$\bar{1}\bar{3}\bar{3}$]	[$\bar{3}\bar{1}\bar{3}$]	[$\bar{1}\bar{3}\bar{3}$]	[$\bar{3}\bar{1}\bar{3}$]	[$\bar{1}\bar{3}\bar{3}$]	[$\bar{3}\bar{1}\bar{3}$]	19
	[$\bar{1}\bar{3}\bar{3}$]	[$\bar{3}\bar{1}\bar{3}$]	[$\bar{3}\bar{3}\bar{1}$]	[$\bar{3}\bar{3}1$]	[$\bar{3}\bar{3}\bar{1}$]	[$\bar{3}\bar{3}1$]	[$\bar{3}\bar{1}\bar{3}$]	[$\bar{1}\bar{3}\bar{3}$]	
	[$\bar{3}\bar{1}\bar{3}$]	[$\bar{1}\bar{3}\bar{3}$]	[$\bar{3}\bar{1}\bar{3}$]	[$\bar{1}\bar{3}\bar{3}$]	[$\bar{1}\bar{3}\bar{3}$]	[$\bar{3}\bar{3}\bar{1}$]	[$\bar{3}\bar{3}1$]	[$\bar{3}\bar{1}\bar{3}$]	
[420]	[$\bar{2}\bar{4}$ 0]	[$\bar{4}\bar{2}$ 0]	[04 $\bar{2}$]	[$\bar{4}$ 0 $\bar{2}$]	[042]	[402]	[0 $\bar{2}$ 4]	[$\bar{2}$ 04]	20
	[$\bar{2}\bar{4}$ 0]	[$\bar{4}\bar{2}$ 0]	[0 $\bar{2}$ 4]	[$\bar{2}$ 04]	[204]	[02 $\bar{4}$]	[4 $\bar{2}$ 0]	[$\bar{2}$ 40]	
	[$\bar{2}$ 04]	[024]	[40 $\bar{2}$]	[$\bar{4}$ 0 $\bar{2}$]	[402]	[042]	[420]	[240]	
[422]	[$\bar{2}\bar{4}\bar{2}$]	[$\bar{4}\bar{2}\bar{2}$]	[$\bar{2}\bar{4}\bar{2}$]	[$\bar{4}\bar{2}\bar{2}$]	[$\bar{2}\bar{2}\bar{4}$]	[$\bar{2}\bar{2}\bar{4}$]	[$\bar{2}\bar{4}\bar{2}$]	[$\bar{4}\bar{2}\bar{2}$]	24
	[$\bar{4}\bar{2}\bar{2}$]	[$\bar{4}\bar{2}\bar{2}$]	[$\bar{2}\bar{2}\bar{4}$]	[$\bar{2}\bar{2}\bar{4}$]	[$\bar{2}\bar{2}\bar{4}$]	[$\bar{2}\bar{2}\bar{4}$]	[$\bar{4}\bar{2}\bar{2}$]	[$\bar{4}\bar{2}\bar{2}$]	
	[$\bar{2}\bar{4}\bar{2}$]	[$\bar{2}\bar{4}\bar{2}$]	[$\bar{2}\bar{2}\bar{4}$]	[$\bar{2}\bar{2}\bar{4}$]	[$\bar{4}\bar{2}\bar{2}$]	[$\bar{2}\bar{4}\bar{2}$]	[$\bar{4}\bar{2}\bar{2}$]	[$\bar{2}\bar{4}\bar{2}$]	
[511]	[$\bar{5}\bar{1}\bar{1}$]	[$\bar{1}\bar{5}\bar{1}$]	[$\bar{1}\bar{5}\bar{1}$]	[$\bar{5}\bar{1}\bar{1}$]	[$\bar{5}\bar{1}\bar{1}$]	[115]	[$\bar{1}\bar{5}\bar{1}$]	[$\bar{1}\bar{5}\bar{1}$]	27
	[$\bar{5}\bar{1}\bar{1}$]	[$\bar{5}\bar{1}\bar{1}$]	[$\bar{1}\bar{1}\bar{5}$]	[$\bar{1}\bar{1}\bar{5}$]	[$\bar{1}\bar{1}\bar{5}$]	[$\bar{5}\bar{1}\bar{1}$]	[$\bar{1}\bar{1}\bar{5}$]	[$\bar{5}\bar{1}\bar{1}$]	
	[$\bar{1}\bar{1}\bar{5}$]	[$\bar{1}\bar{1}\bar{5}$]	[$\bar{1}\bar{1}\bar{5}$]	[$\bar{1}\bar{5}\bar{1}$]	[$\bar{1}\bar{5}\bar{1}$]	[511]	[$\bar{1}\bar{5}\bar{1}$]	[$\bar{1}\bar{5}\bar{1}$]	
[333]	[333]	[$\bar{3}\bar{3}\bar{3}$]	[$\bar{3}\bar{3}\bar{3}$]	[$\bar{3}\bar{3}\bar{3}$]	[$\bar{3}\bar{3}\bar{3}$]	[$\bar{3}\bar{3}\bar{3}$]	[$\bar{3}\bar{3}\bar{3}$]	[$\bar{3}\bar{3}\bar{3}$]	27

Fig. 1.6 Free electron bands (empty lattice bands) of a face-centered lattice are plotted as a function of electron wave vector along the direction shown in Fig. 1.22, where the energy range is 0 ~ 200 in units of $[\hbar^2/2ma^2]$



$$\mathbf{G}_0 = \frac{2\pi}{a}[0, 0, 0], \quad (1.60a)$$

$$\mathbf{G}_3 = \frac{2\pi}{a}[\pm 1, \pm 1, \pm 1], \quad (1.60b)$$

$$\mathbf{G}_4 = \frac{2\pi}{a}[\pm 2, 0, 0], \quad (1.60c)$$

$$\mathbf{G}_8 = \frac{2\pi}{a}[\pm 2, \pm 2, 0], \quad (1.60d)$$

$$\mathbf{G}_{11} = \frac{2\pi}{a}(\pm 3, \pm 1, \pm 1). \quad (1.60e)$$

Putting these values in (1.52), the empty-lattice bands (free-electron bands) are easily calculated. In the following we use \mathbf{k} instead of \mathbf{k}' and take account of \mathbf{k} in the first Brillouin zone. As an example we calculate the energy bands along the direction $\langle 100 \rangle$ in the \mathbf{k} -space shown in Fig. 1.5. In other words, we calculate the energy band structures \mathcal{E} versus \mathbf{k} from the Γ point to the X point. Since $k_y = k_z = 0$ in this direction, putting the reciprocal lattice vectors into (1.50), the energy is given by the following equations:

$$\mathbf{G}_0 : \mathcal{E} = k_x^2, \quad (1.61a)$$

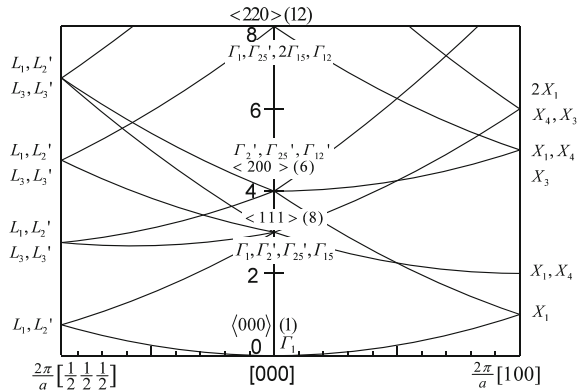
$$\begin{aligned} \mathbf{G}_3 : \mathcal{E} &= (k_x \pm 1)^2 + (\pm 1)^2 + (\pm 1)^2, \\ &= \begin{cases} (k_x - 1)^2 + 2 & (4\text{-fold degeneracy}) \\ (k_x + 1)^2 + 2 & (4\text{-fold degeneracy}) \end{cases}, \end{aligned} \quad (1.61b)$$

$$\mathbf{G}_4 : \mathcal{E} = \begin{cases} k_x^2 + 4 & (4\text{-fold degeneracy}) \\ (k_x - 2)^2 & (\text{single state}) \\ (k_x + 2)^2 & (\text{single state}) \end{cases}, \quad (1.61c)$$

where the energy is measured in the units $\hbar^2(2\pi/a)^2/2m$ and the wave vector \mathbf{k} in the units $2\pi/a$. When we plot these relations, we obtain the curves shown in Fig. 1.7.

Next we calculate the \mathcal{E} versus \mathbf{k} curves in the $\langle 111 \rangle$ direction of \mathbf{k} -space, or along the direction from the Γ point to the L point. The results are

Fig. 1.7 Empty-lattice bands (free-electron bands) of a face-centered cubic lattice. $\langle 000 \rangle$, $\langle 111 \rangle$, $\langle 200 \rangle$, and $\langle 220 \rangle$ represent the reciprocal lattice vectors \mathbf{G}_0 , \mathbf{G}_3 , \mathbf{G}_4 , and \mathbf{G}_8 , respectively, and the numbers in () show the degeneracy of the wave functions



$$G_0 : \mathcal{E} = k_x^2 + k_y^2 + k_z^2 \equiv k_{111}^2, \quad (1.62a)$$

$$G_3 : \mathcal{E} = (k_x \pm 1)^2 + (k_y \pm 1)^2 + (k_z \pm 1)^2, \quad (1.62b)$$

$$G_4 : \mathcal{E} = \begin{cases} (k_x \pm 2)^2 + k_y^2 + k_z^2 & (2\text{-fold degeneracy}) \\ k_x^2 + (k_y \pm 2)^2 + k_z^2 & (2\text{-fold degeneracy}) \\ k_x^2 + k_y^2 + (k_z \pm 2)^2 & (2\text{-fold degeneracy}) \end{cases}, \quad (1.62c)$$

where $k_x^2 + k_y^2 + k_z^2 = k_{111}^2$ and $k_x = k_y = k_z = k_{111}/\sqrt{3}$. Using these results we obtain the energy bands, $\mathcal{E} - \mathbf{k}$ curves in the direction $\langle 111 \rangle$, which are shown in the left half of Fig. 1.7. In Fig. 1.7, the notation of the point group for O_h is used to represent the symmetry properties of the Brillouin zone edge. Note here that the energy \mathcal{E} is expressed in units of $\hbar^2(2\pi/a)^2/2m$.

1.6 Pseudopotential Method

In this section we will concern with the energy band calculations based on the pseudopotential method. First we introduce local pseudopotential theory in which the nonlocality of the core states are ignored, and we will show how to calculate the energy band structures of the diamond and zinc blende semiconductors by using small number of the pseudopotentials. In the later section we will discuss the nonlocal pseudopotential theory in which the core potential of the occupied states is taken into account.

1.6.1 Local Pseudopotential Theory

The electronic states in a crystal are obtained by solving the following non-relativistic Schrödinger equation in the one-electron approximation:

$$\left[-\frac{\hbar^2}{2m} \nabla^2 + V(\mathbf{r}) \right] \psi_n(\mathbf{r}) = \mathcal{E}_n(\mathbf{k}) \psi_n(\mathbf{r}). \quad (1.63)$$

However, it is possible only when we know the crystal potential $V(\mathbf{r})$. In the following we will express the wavefunction $\psi_n(\mathbf{r})$ by the ket vector as $|\psi_n(\mathbf{r})\rangle$ and show how the Schrödinger equation is solved to a good approximation by using empirical parameters, known as pseudopotentials, and the orthogonality of the wave functions [2–7]. The idea of the pseudopotential method is based on the assumption that the real crystal potential $V(\mathbf{r})$ is given by the sum of the attractive core potential and the weak repulsive potential (to keep the valence electrons out of the core). The addition of the repulsive potential to the core potential cancels the real potential, resulting in a weak net potential (pseudopotential). The introduction of the pseudopotential enables us to treat valence electrons as nearly free electron approximation or to solve Schrödinger equation with a small number of Fourier components of the pseudopotential.

First, we assume the electron wave functions of the core states and their energies are given by $|\phi_j\rangle$ and \mathcal{E}_j , respectively. We then have

$$H|\phi_j\rangle = [H_0 + V_c(\mathbf{r})]|\phi_j\rangle = \mathcal{E}_j|\phi_j\rangle, \quad (1.64)$$

where $V_c(\mathbf{r})$ is the attractive core potential, and

$$H_0 = -\frac{\hbar^2}{2m}\nabla^2. \quad (1.65)$$

The true wave function $|\Psi\rangle$ of an electron is then expressed as the sum of a smooth wave function $|\chi_n(\mathbf{r})\rangle$ of a valence electron (subscript n is the band index) and a sum over occupied core states $|\phi_j\rangle$;

$$|\Psi\rangle = |\chi_n\rangle + \sum_j b_j |\phi_j\rangle. \quad (1.66)$$

Since the true wave function is orthogonal to the core states, the expansion coefficient $b_{j'}$ is determined by the orthogonality $\langle\phi_{j'}|\Psi\rangle = 0$ as follows.

$$\begin{aligned} \langle\phi_{j'}|\Psi\rangle &= \langle\phi_{j'}|\chi_n\rangle + \sum_j \langle\phi_{j'}|b_j\phi_j\rangle \\ &= \langle\phi_{j'}|\chi_n\rangle + b_{j'} = 0, \end{aligned} \quad (1.67)$$

which gives $b_{j'} = -\langle\phi_{j'}|\chi_n\rangle$ and thus we obtain

$$|\Psi(\mathbf{k}, \mathbf{r})\rangle = |\chi_n(\mathbf{k}, \mathbf{r})\rangle - \sum_j \langle\phi_j|\chi_n\rangle |\phi_j\rangle. \quad (1.68)$$

We have to note here that $|\chi_n\rangle$ is defined as a smooth wave function for a valence electron and called as the pseudo-wave-function. As in the case of nearly free electron approximation, we calculate energy band structures by using plane waves for $|\chi_n(\mathbf{k}, \mathbf{r})\rangle$ and in this scheme (1.68) is called the OPW (orthogonalized plane wave). Substituting (1.68) into (1.63) we find

$$H|\chi_n\rangle - \sum_j \langle\phi_j|\chi_n\rangle H|\phi_j\rangle = \mathcal{E}_n(\mathbf{k}) \left\{ |\chi_n\rangle - \sum_j \langle\phi_j|\chi_n\rangle |\phi_j\rangle \right\}, \quad (1.69)$$

and then we obtain the following relation:

$$H|\chi_n\rangle + \sum_j [\mathcal{E}_n(\mathbf{k}) - \mathcal{E}_j] \langle\phi_j|\chi_n\rangle |\phi_j\rangle = \mathcal{E}_n(\mathbf{k}) |\chi_n\rangle. \quad (1.70)$$

We introduce a new parameter according to the definition of Cohen and Chelikowsky [2]

$$V_r(\mathbf{r}) = \sum_j [\mathcal{E}_n(\mathbf{k}) - \mathcal{E}_j] |\phi_j\rangle \langle \phi_j|, \quad (1.71)$$

or

$$V_r(\mathbf{r})|\chi_n\rangle = \sum_j [\mathcal{E}_n(\mathbf{k}) - \mathcal{E}_j] |\phi_j\rangle \langle \phi_j|\chi_n\rangle. \quad (1.72)$$

This term acts like a short-ranged non-Hermitian repulsive potential. Using this definition we obtain the following equation.

$$[H + V_r(\mathbf{r})]|\chi_n\rangle = \mathcal{E}_n(\mathbf{k})|\chi_n\rangle. \quad (1.73)$$

If H is separated into a kinetic energy $H_0 = -(\hbar^2/2m)\nabla^2$ and attractive core potential $V_c(\mathbf{r})$, then (1.73) becomes

$$\left[-\frac{\hbar^2}{2m}\nabla^2 + V_c(\mathbf{r}) + V_r(\mathbf{r}) \right] |\chi_n\rangle = \mathcal{E}_n(\mathbf{k})|\chi_n\rangle, \quad (1.74)$$

where $\mathcal{E}_n(\mathbf{k})$ is the energy of the band we are interested in. There exists the following inequality between the energies of the core states, \mathcal{E}_j , and the energies of the valence and conduction bands, $\mathcal{E}_n(\mathbf{k})$:

$$\mathcal{E}_n(\mathbf{k}) > \mathcal{E}_j, \quad (1.75)$$

and thus we find from (1.72) that

$$V_r(\mathbf{r}) > 0. \quad (1.76)$$

We may rewrite (1.74) as

$$[H_0 + V_{ps}(\mathbf{r})]|\chi_n\rangle = \mathcal{E}_n(\mathbf{k})|\chi_n\rangle, \quad (1.77)$$

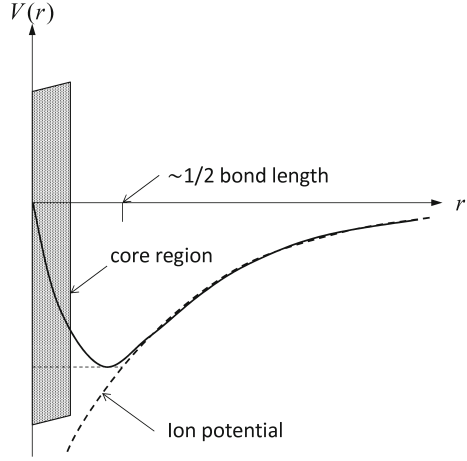
$$V_{ps}(\mathbf{r}) = V_c(\mathbf{r}) + V_r(\mathbf{r}), \quad (1.78)$$

and it may be possible to make V_{ps} small enough, since the attractive core potential $V_c(\mathbf{r}) < 0$ and the repulsive potential $V_r(\mathbf{r}) > 0$ cancel each other. The new potential $V_{ps}(\mathbf{r})$ is called the **pseudopotential**. Since the pseudopotential V_{ps} is the sum of the attractive long-range potential V_c and a short-range repulsive potential V_r , V_{ps} becomes weak long-range attractive regions away from the core and weakly repulsive or attractive regions near the core (see Fig. 1.8 [2]).

The pseudopotential $V_{ps}(\mathbf{r})$ is also periodic, and we can expand it as the Fourier series

$$V_{ps}(\mathbf{r}) = \sum_j V_{ps}(\mathbf{G}_j) e^{-i\mathbf{G}_j \cdot \mathbf{r}}, \quad (1.79)$$

Fig. 1.8 Schematic plot of pseudopotential in real space (after Cohen and Chelikowsky [2])



where the Fourier coefficients $V_{\text{ps}}(\mathbf{G}_j)$ are given by

$$V_{\text{ps}}(\mathbf{G}_j) = \frac{1}{\sqrt{\Omega}} \int_{\Omega} V_{\text{ps}}(\mathbf{r}) e^{i\mathbf{G}_j \cdot \mathbf{r}} d^3\mathbf{r}. \quad (1.80)$$

For the reason stated above the potential $V_{\text{ps}}(\mathbf{r})$ may be chosen as small as possible, and thus we choose $V_{\text{ps}}(\mathbf{G}_j)$ so that the potential $V_{\text{ps}}(\mathbf{G}_j)$ is expressed with a small number of the Fourier coefficients $V_{\text{ps}}(\mathbf{G}_j)$; in other words, we may keep several values of $V_{\text{ps}}(\mathbf{G}_j)$ and neglect the other values because of their smallness. We should note that $|V_{\text{ps}}(\mathbf{r})|$ is smaller than $|V(\mathbf{r})|$, but it does not mean that $V(\mathbf{r})$ converges with only a small number of its Fourier coefficients. The **empirical pseudopotential method** is based on the approximation that the Fourier coefficients of $V_{\text{ps}}(\mathbf{r})$ are empirically chosen so that the shape of the critical points and their energies show good agreement with experimental observation.

Energy band calculations based on the empirical pseudopotential method take into account as few the pseudopotentials $V_{\text{ps}}(\mathbf{G}_j)$ as possible and use the Bloch functions of the free-electron bands for the wave functions $|\chi_n\rangle$. The energy bands are obtained by solving

$$\left[-\frac{\hbar^2}{2m} \nabla^2 + V_{\text{ps}}(\mathbf{r}) \right] |\chi_n(\mathbf{r})\rangle = \mathcal{E}_n |\chi_n(\mathbf{r})\rangle, \quad (1.81)$$

$$|\chi_n(\mathbf{r})\rangle = \frac{1}{\sqrt{\Omega}} \sum_j e^{i(\mathbf{k} + \mathbf{G}_j) \cdot \mathbf{r}}, \quad (1.82)$$

$$V_{\text{ps}}(\mathbf{r}) = \sum_{j'} V_{\text{ps}}(\mathbf{G}_{j'}) e^{i\mathbf{G}_{j'} \cdot \mathbf{r}}. \quad (1.83)$$

Then the energy band structures are calculated by solving the following equation, where the j -th component is given by dropping the factor $(1/\sqrt{\Omega}) \sum_j$:

$$\left[-\frac{\hbar^2}{2m} \nabla^2 + \sum_{j'} V_{\text{ps}}(\mathbf{G}_{j'}) e^{i\mathbf{G}_{j'} \cdot \mathbf{r}} \right] e^{i(\mathbf{k} + \mathbf{G}_j) \cdot \mathbf{r}} = \mathcal{E}_n(\mathbf{k}) e^{i(\mathbf{k} + \mathbf{G}_j) \cdot \mathbf{r}}. \quad (1.84)$$

The eigenvalues and eigen functions of the above equation are easily obtained by solving the following matrix equation. First, we introduce pseudopotential Hamiltonian by

$$H_{\text{ps}} = -\frac{\hbar^2}{2m} \nabla^2 + V_{\text{ps}}(\mathbf{r}), \quad (1.85)$$

and rewrite (1.84) as

$$H_{\text{ps}}|\mathbf{k} + \mathbf{G}_j\rangle = \mathcal{E}_n(\mathbf{k})|\mathbf{k} + \mathbf{G}_j\rangle, \quad (1.86)$$

$$|\mathbf{k} + \mathbf{G}_j\rangle = \frac{1}{\sqrt{\Omega}} e^{i(\mathbf{k} + \mathbf{G}_j) \cdot \mathbf{r}}. \quad (1.87)$$

Then the solutions are equivalently obtained by solving the determinant

$$||\langle \mathbf{k} + \mathbf{G}_i | H_{\text{ps}} | \mathbf{k} + \mathbf{G}_j \rangle - \mathcal{E}(\mathbf{k}) \delta_{i,j} || = 0, \quad (1.88)$$

where the matrix elements of the Hamiltonian H_{ps} are written as

$$\langle \mathbf{k} + \mathbf{G}_i | H_{\text{ps}} | \mathbf{k} + \mathbf{G}_j \rangle = \frac{\hbar^2}{2m} (\mathbf{k} + \mathbf{G}_i)^2 \delta_{\mathbf{G}_i, \mathbf{G}_j} + V_{\text{ps}}(\mathbf{G}_j - \mathbf{G}_i). \quad (1.89)$$

When we know the pseudopotential form factors $V_{\text{ps}}(\mathbf{G}_j - \mathbf{G}_i)$, the energy band calculations are straightforward by solving the eigen equation (1.88). In the next subsection we will deal with the evaluation of non-vanishing pseudopotential form factors.

1.6.2 Pseudopotential Form Factors

Once we know the Fourier coefficients $V_{\text{ps}}(\mathbf{G}_j)$, the solutions of (1.88) are easily calculated with a personal computer. It is very interesting to point out that the calculated energy bands using the reciprocal wave vectors given by (1.60a)–(1.60e)

Table 1.2 Pseudopotentials for several semiconductors in units of Rydberg [Ry] and lattice constants a in [Å] (from [5])

	$a[\text{Å}]$	V_3^S	V_8^S	V_{11}^S	V_3^A	V_4^A	V_{11}^A
Si	5.43	-0.21	+0.04	+0.08	0	0	0
Ge	5.66	-0.23	+0.01	+0.06	0	0	0
Sn	6.49	-0.20	0.00	+0.04	0	0	0
GaP	5.44	-0.22	+0.03	+0.07	+0.12	+0.07	+0.02
GaAs	5.64	-0.23	+0.01	+0.06	+0.07	+0.05	+0.01
AlAs	5.66	-0.221	0.025	0.07	0.08	0.05	-0.004
AlSb	6.13	-0.21	+0.02	+0.06	+0.06	+0.04	+0.02
InP	5.86	-0.23	+0.01	+0.06	+0.07	+0.05	+0.01
GaSb	6.12	-0.22	0.00	+0.05	+0.06	+0.05	+0.01
InAs	6.04	-0.22	0.00	+0.05	+0.08	+0.05	+0.03
InSb	6.48	-0.20	0.00	+0.04	+0.06	+0.05	+0.01
ZnS	5.41	-0.22	+0.03	+0.07	+0.24	+0.14	+0.04
ZnSe	5.65	-0.23	+0.03	+0.06	+0.18	+0.12	+0.03
ZnTe	6.07	-0.22	0.00	+0.05	+0.13	+0.10	+0.01
CdTe	6.41	-0.20	0.00	+0.04	+0.15	+0.09	+0.04

and the free-electron Bloch functions show very reasonable results, where only several pseudopotential parameters derived by Cohen and Bergstresser [5] shown in Table 1.2 are taken into account.

First we explain the pseudopotential parameters. In general a unit cell of a crystal contains a single atom or multi-atoms and thus the pseudopotential is expressed as [6]

$$V_{\text{ps}}(\mathbf{r}) = \sum_j V(\mathbf{G}_j) e^{-i\mathbf{G}_j \cdot \mathbf{r}}, \quad (1.90a)$$

$$V(\mathbf{G}_j) = \sum_{\alpha} S_{\alpha}(\mathbf{G}_j) V_{\alpha}(\mathbf{G}_j), \quad (1.90b)$$

$$S_{\alpha}(\mathbf{G}_j) = \frac{1}{N_{\alpha}} \sum_{\text{cell } m} e^{-i\mathbf{G}_j \cdot \mathbf{R}_m^{\alpha}}, \quad (1.90c)$$

$$V_{\alpha}(\mathbf{G}_j) = \frac{1}{\Omega_{\alpha}} \int e^{i\mathbf{G}_j \cdot \mathbf{r}} V_{\text{ps}}^{\alpha}(\mathbf{r}) d^3\mathbf{r}. \quad (1.90d)$$

Derivation of the above relations is understood by taking account of multi-atoms in the unit cell

$$\sum_j V(\mathbf{G}_j) e^{-i\mathbf{G}_j \cdot \mathbf{r}} \rightarrow \sum_j \sum_{\alpha} \sum_{\text{cell } m} V_{\alpha}(\mathbf{G}_j) e^{-i\mathbf{G}_j \cdot (\mathbf{r} + \mathbf{R}_m^{\alpha})},$$

where $S_\alpha(\mathbf{G})$ is called a **structure factor**, N_α is the number of atomic species α present, \mathbf{R}_m^α is the position of the m -th atom of the α -th species, and Ω_α is the atomic volume. Here the crystalline potential is assumed to be a sum of local atomic pseudopotential $V_{\text{ps}}^\alpha(\mathbf{r})$.

The diamond-type crystal structure such as Ge and Si contains two atoms A and B ($A = B$) in the unit cell ($N_\alpha = 2$), and the zinc-blende-type crystal structure has two different atoms A and B ($A \neq B$) ($N_\alpha = 2$). When a new vector $\boldsymbol{\tau} = (a/8)(111)$ is defined, the atomic positions of A and B are given by $\mathbf{R}^A = -\boldsymbol{\tau}$ and $\mathbf{R}^B = +\boldsymbol{\tau}$, respectively. Taking the origin of coordinates to be the center of those two atoms, the structure factors are written as

$$S_A(\mathbf{G}_j) = \frac{1}{2}e^{i\mathbf{G}_j \cdot \boldsymbol{\tau}}, \quad S_B(\mathbf{G}_j) = \frac{1}{2}e^{-i\mathbf{G}_j \cdot \boldsymbol{\tau}} \quad (1.91)$$

and thus the pseudopotential form factor $V(\mathbf{G})$ is given by

$$\begin{aligned} V(\mathbf{G}_j) &= \frac{1}{2} [V_A(\mathbf{G}_j)e^{i\mathbf{G}_j \cdot \boldsymbol{\tau}} + V_B(\mathbf{G}_j)e^{-i\mathbf{G}_j \cdot \boldsymbol{\tau}}] \\ &= V^S(\mathbf{G}_j) \cos(\mathbf{G}_j \cdot \boldsymbol{\tau}) + iV^A(\mathbf{G}_j) \sin(\mathbf{G}_j \cdot \boldsymbol{\tau}). \end{aligned} \quad (1.92)$$

Here we introduce following new parameters

$$V^S(\mathbf{G}_j) = [V_A(\mathbf{G}_j) + V_B(\mathbf{G}_j)]/2, \quad (1.93a)$$

$$V^A(\mathbf{G}_j) = [V_A(\mathbf{G}_j) - V_B(\mathbf{G}_j)]/2, \quad (1.93b)$$

where V^S and V^A are called the symmetric and antisymmetric form factors, respectively. The structure factor plays an important role in electronic properties such as energy band structure, diffraction effect and so on. $S^S(\mathbf{G}_j) = \cos(\mathbf{G}_j \cdot \boldsymbol{\tau})$ and $S^A(\mathbf{G}_j) = \sin(\mathbf{G}_j \cdot \boldsymbol{\tau})$ are the real part and imaginary part of the structure factor. From the definition of diamond-type crystal we have $V^A(\mathbf{G}_j) = 0$ and the structure factor reduces to $\cos(\mathbf{G}_j \cdot \boldsymbol{\tau})$. In Table 1.2 the pseudopotentials are defined by using the relations $V^S(\mathbf{G}_j) = V_j^S$ and $V^A(\mathbf{G}_j) = V_j^A$, where \mathbf{G}_j is defined by (1.60a)–(1.60e). As shown in Table 1.2 some of the pseudopotentials $V^S(\mathbf{G}_j)$ and $V^A(\mathbf{G}_j)$ vanish. This may be understood from the following considerations. The symmetric component of the pseudopotential is written as

$$V^S(\mathbf{G}_j) \cos(\mathbf{G}_j \cdot \boldsymbol{\tau}) = V^S(\mathbf{G}_j) \cos\left(\frac{a}{8} [G_{jx} + G_{jy} + G_{jz}]\right). \quad (1.94)$$

Let's examine the pseudopotentials for the reciprocal vectors (1.60a)–(1.60e). The pseudopotentials for smaller values of \mathbf{G}_j are evaluated as

$$\begin{aligned}
V^S(\mathbf{G}_0) \cos(\mathbf{G}_0 \cdot \boldsymbol{\tau}) &= V^S(\mathbf{G}_0), \\
V^S(\mathbf{G}_3) \cos(\mathbf{G}_3 \cdot \boldsymbol{\tau}) &= V^S(\mathbf{G}_3) \cos\left(\frac{\pi}{4} [\pm 1 \pm 1 \pm 1]\right) \neq 0, \\
V^S(\mathbf{G}_4) \cos(\mathbf{G}_4 \cdot \boldsymbol{\tau}) &= V^S(\mathbf{G}_4) \cos\left(\frac{\pi}{4} [\pm 2]\right) = 0, \\
V^S(\mathbf{G}_8) \cos(\mathbf{G}_8 \cdot \boldsymbol{\tau}) &= V^S(\mathbf{G}_8) \cos\left(\frac{\pi}{4} [\pm 2 \pm 2]\right) \neq 0, \\
V^S(\mathbf{G}_{11}) \cos(\mathbf{G}_{11} \cdot \boldsymbol{\tau}) &= V^S(\mathbf{G}_{11}) \cos\left(\frac{\pi}{4} [\pm 3 \pm 1 \pm 1]\right) \neq 0.
\end{aligned}$$

Therefore the symmetric components of the pseudopotentials $V^S(\mathbf{G}_0) = V_0^S$, $V^S(\mathbf{G}_3) = V_3^S$, $V^S(\mathbf{G}_8) = V_8^S$, $V^S(\mathbf{G}_{11}) = V_{11}^S$ remain and $V^S(\mathbf{G}_4) = V_4^S$ will not contribute. In a similar fashion, there is no contribution from the antisymmetric components of the pseudopotential $V^A(\mathbf{G}_0) = V_0^A$ and $V^A(\mathbf{G}_8) = V_8^A$. These results give the pseudopotentials for smaller values of $|\mathbf{G}_j|$ in Table 1.2, where we find that pseudopotentials of large $|\mathbf{G}_j|$ are diminished. Since the energy bands calculated with these pseudopotentials given in Table 1.2 show good agreement with experimental observation, higher order components of the pseudopotentials are usually neglected. The term $V^S(\mathbf{G}_0) = V_0^S$ results in a shift of the energy reference and thus we put $V_0^S = 0$.

1.6.3 Nonlocal Pseudopotential Theory

Here we will be concerned with the energy band calculations by the pseudopotential method where the nonlocality of the core potential is considered. The method described above is called local pseudopotential method, where the core potential is assumed to be uniform neglecting the angular orbitals of the core electrons.

The nonlocal pseudopotential method takes account of nonlocal properties of the core electrons. The core potential $V_c(\mathbf{r})$ consists of a sum over the occupied core states ϕ_j , and it consists of the various states with the respective angular momentum symmetry as discussed by Cohen and Chelikowsky [2, 6, 7] (see also the references listed there). Therefore the core potential is given by the sum of s -, p -, and d -components of the respective angular momentum quantum number $l = 0, 1, 2, \dots$

$$V_c(\mathbf{r}) = V_s + V_p + V_d + \dots \quad (1.95)$$

As an example we consider carbon atom C. Its core states are $(1s)^2$ and thus carbon has no p -repulsive potential. The $(2p)$ electrons of the valence states $(2s)^2(2p)^2$ are affected by the core potential. This repulsive core potential is expected to be stronger because of its closer distance to the core than in Si and Ge. In general, the core potential is energy dependent and the nonlocal (NL) correction term to the local atomic potential term is expressed as the following [2, 4, 7]

$$V_{\text{NL}}^{\alpha}(\mathbf{r}, \mathcal{E}) = \sum_{l=0}^{\infty} A_l^{\alpha}(\mathcal{E}) f_l(r) \mathcal{P}_l, \quad (1.96)$$

and

$$f_l^{\alpha}(r) = \begin{cases} 1, & r \leq R_m \\ 0, & r \geq R_m \end{cases}, \quad (1.97)$$

where $A_l^{\alpha}(\mathcal{E})$ is an energy-dependent well depth of the α species, R_m is the model radius, which is taken to be the same for all l , and \mathcal{P}_l is projects out the l -th angular momentum component of the wave function.

When we assume a square well for the model potential defined by (1.97), the matrix element of the nonlocal potential is given by

$$V_{\text{NL}}(\mathbf{K}, \mathbf{K}') = \frac{4\pi}{\Omega_{\alpha}} \sum_{l,\alpha} A_l^{\alpha}(\mathcal{E})(2l+1) \\ \times P_l(\cos(\theta_{\mathbf{K},\mathbf{K}'})) S^{\alpha}(\mathbf{K} - \mathbf{K}') F_l^{\alpha}(K, K'), \quad (1.98)$$

where $S^{\alpha}(\mathbf{K})$ is the structure factor defined by (1.90c) with $\mathbf{K} = \mathbf{k} + \mathbf{G}$ and $\mathbf{K}' = \mathbf{k} + \mathbf{G}'$, $\theta_{\mathbf{K},\mathbf{K}'}$ is the angle between \mathbf{K} and \mathbf{K}' , and the sum of α is carried out over the atomic species present.

$$F_l(K, K') = \begin{cases} \frac{R_m^3}{2} \{ [j_l(K R_m)]^2 - j_{l-1}(K R_m) j_{l+1}(K R_m) \}, & K = K', \\ \frac{R_m^2}{K^2 - K'^2} [K j_{l+1}(K R_m) j_l(K' R_m) - K' j_{l+1}(K' R_m) j_l(K R_m)], & K \neq K'. \end{cases}$$

$P_l(x)$ is a Legendre polynomial and $j_l(x)$ is a spherical Bessel function, which are given for smaller values of the subscript l :

$$P_0(x) = 1, \quad P_1(x) = x, \quad P_2(x) = (1/2)(3x^2 - 1), \\ j_0(x) = x^{-1} \sin x, \quad j_1(x) = x^{-2} \sin x - x^{-1} \cos x, \\ j_2(x) = (3x^{-3} - x^{-1}) \sin x - 3x^{-2} \cos x, \quad j_3(x) = 5x^{-1} j_2(x) - j_1(x).$$

Energy band calculations require the estimation of energy dependent term $A_l^{\alpha}(\mathcal{E})$ and radii $R_m = R_0$, which are reported by Cohen and Chelikowsky [7]. They make the approximation for $A_0(\mathcal{E})$ for the s state as

$$A_0(\mathcal{E}) = \alpha_0 + \beta_0 \{ [\mathcal{E}^0(K) E^0(K')]^{1/2} - E^0(K_F) \}, \quad (1.99)$$

where $E^0(K) = \hbar^2 K^2 / 2m$, $K_F = (6\pi^2 Z / \Omega)^{1/3}$ and Z is the valence of the atomic species of interest [6, 7].

Now the energy band calculations with local and nonlocal pseudopotentials are straight forward. The eigenvalues and eigenvectors are obtained by solving the secular equation

$$\det |H_{\mathbf{G},\mathbf{G}'}(\mathbf{k}) - \mathcal{E}(\mathbf{k})\delta_{\mathbf{G},\mathbf{G}'}| = 0. \quad (1.100)$$

For the local pseudopotential approximation, we have

$$H_{\mathbf{G},\mathbf{G}'}^L = \frac{\hbar^2}{2m}(\mathbf{k} + \mathbf{G})^2 + V_{\text{ps}}(|\mathbf{G} - \mathbf{G}'|). \quad (1.101)$$

When we include the nonlocal pseudopotential term we obtain

$$\begin{aligned} H_{\mathbf{G},\mathbf{G}'} &= H_{\mathbf{G},\mathbf{G}'}^L + V_{\text{NL}}(\mathbf{K}, \mathbf{K}') \\ &= H_{\mathbf{G},\mathbf{G}'}^L + \frac{4\pi}{\Omega_\alpha} \sum_{l,\alpha} A_l^\alpha(\mathcal{E})(2l+1)P_l(\cos(\theta_{\mathbf{K},\mathbf{K}'})) \\ &\quad \times S^\alpha(\mathbf{G} - \mathbf{G}')F_l^\alpha(K, K'), \end{aligned} \quad (1.102)$$

where the sum is carried out over the atomic species α .

Nonlocal pseudopotential parameters reported by Chelikowsky and Cohen [7] are listed in Table 1.3. In their calculations, the model radius of the R_l for the pseudopotential is taken to be the same for all l and $\alpha_0 = 0$ for the cations. Energy band calculations based on the nonlocal pseudopotentials require many parameters, but the calculated results differ only a little compared to the simple local pseudopotential method. We will present only the energy band structure of GaAs calculated by the nonlocal pseudopotential method in Sect. 1.6.6. Before dealing with the energy band calculations by nonlocal pseudopotential, we present energy band structures calculated by the local pseudopotential method for diamond and zinc blende semiconductors without spin-orbit interaction in Sect. 1.6.4. Later in Sect. 1.6.6 we

Table 1.3 Nonlocal pseudopotential parameters for the diamond and zinc blende semiconductors (after Chelikowsky and Cohen [7])

Materials	Pseudopotential form factors [Ry]						Lattice constant [Å]
	V_3^S	V_8^S	V_{11}^S	V_3^A	V_4^A	V_{11}^A	
Si	-0.257	-0.040	0.033				5.43
Ge	-0.221	0.019	0.056				5.65
GaP	-0.230	0.020	0.057	0.100	0.070	0.025	5.45
GaAs	-0.254*	0.014	0.067	0.055	0.038	0.010*	5.65
GaSb	-0.220	0.005	0.045	0.040	0.030	0.000	6.10
InP	-0.235	0.000	0.053	0.080	0.060	0.030	5.86
InAs	-0.230	0.000	0.045	0.055	0.045	0.010	6.05
InSb	-0.200	-0.010	0.044	0.044	0.030	0.015	6.47

The pseudopotential values of GaAs with asterisk differ from the values $V_3^S = -0.214$ and $V_{11}^A = 0.001$ of Chelikowsky and Cohen [7]

Nonlocal parameters for Si and Ge					
Material	α_0 [Ry]	β_0	A_2 [Ry]	R_0 [Å]	R_2 [Å]
Si	0.55	0.32	0	1.06	0
Ge	0	0	0.275	0	1.22

Nonlocal parameters for zinc blende semiconductors
($R_0 = 1.27$ for the cation and 1.06 Å for the anion)

Material	Cation			Anion		
	α_0 [Ry]	β_0	A_2 [Ry]	α_0 [Ry]	β_0	A_2 [Ry]
GaP	0	0.30	0.40	0.32	0.05	0.45
GaAs	0	0	0.125	0	0	0.625
GaSb	0	0.20	0.20	0	0.30	0.60
InP	0	0.25	0.55	0.30	0.05	0.35
InAs	0	0.35	0.50	0	0.25	1.00
InSb	0	0.45	0.55	0	0.48	0.70

will show calculated results for Ge and GaAs with the spin–orbit interaction for comparison, and finally we present the energy band calculation of GaAs by the nonlocal pseudopotential method.

1.6.4 Energy Band Calculation by Local Pseudopotential Method

In this section we show the calculated results of the energy band structures with the local pseudopotential method by neglecting the spin–orbit interaction. After the discussion of the spin–orbit interaction in Sect. 1.6.5 we will present energy band calculations with the spin–orbit interaction in Sect. 1.6.6. As discussed by Chelikowsky and Cohen [6, 7], the overall feature of the calculated results by the local pseudopotential method shows a good agreement with the results by the nonlocal pseudopotential method, except a small change in the region near some critical points. Instead, the spin–orbit interaction plays a more important role in the energy regions near the critical points. In order to understand the energy band calculation by the pseudopotential, first we will concern with the energy band calculation by the local pseudopotential method.

Since we have only few numbers of the pseudopotential form factors, the energy band calculations are straight forward. However, the accuracy of the calculated energy band structures depends on the number of plane waves used for the pseudopotential Hamiltonian matrix. When the number of plane waves are increased, a large computation time is required to diagonalize the matrix. Therefore we have to limit the

number of the plane waves. One of the most popular method is to limit the number of plane waves to form the matrix elements in a reasonable size and the higher energy states are taken into account by using the perturbation method proposed by Löwdin [8] as reported by Brust [9] and Cohen and Bergstresser [5]. Now high performance PC's such as Windows 7 with Intel core i-7 are available and 200×200 matrix is solved to give the eigen energies and eigenstates in a reasonable time. In the next section we will deal with $\mathbf{k} \cdot \mathbf{p}$ perturbation method to calculate energy bands, where 15 eigenstates are used. In this textbook the energy band structures are calculated by the empirical pseudopotential method with 113 plane waves and thus 226 plane waves with spin-up and -down states, and higher energy states up to 169 are treated by Löwdin's perturbation which are believed to be enough number to get accurate energy band structures. The energy bands without the spin-orbit interaction with 59 plane waves and Löwdin's perturbation for the higher states exhibit no noticeable difference with the present results and thus we recommend the readers to use 59 plane waves for the purpose of time saving.

It is very interesting to compare two different results with 15 plane waves and 169 plane waves because these results provide an information of the convergence of the energy band calculation by the pseudopotential method. A beginner for the energy band calculations is recommended to calculate the energy bands of Si for example using 15 plane waves [000], [111] and [200] ($K^2 \leq 4$ in Table 1.1) and disregarding the spin-orbit interaction. The overall features of the calculated energy band structure of Si are quite similar to the result obtained by 169 plane waves as shown in Fig. 1.9,

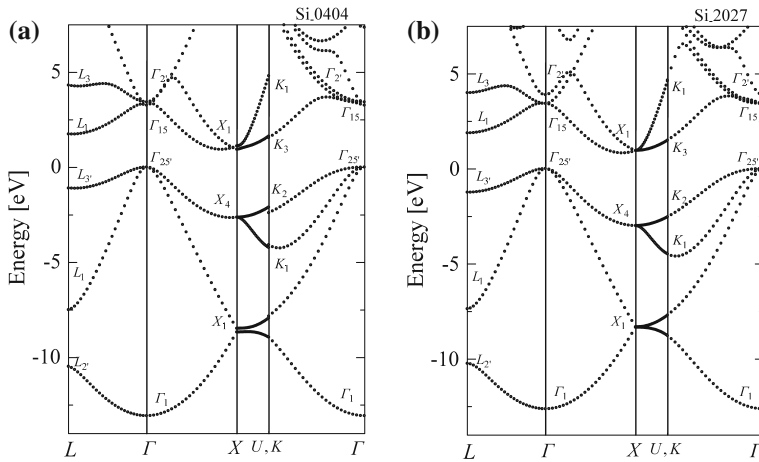
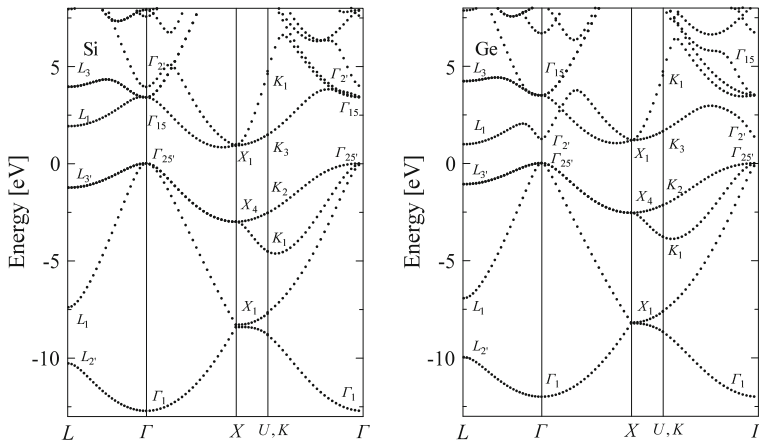


Fig. 1.9 Energy bands of Si calculated by the local empirical pseudopotential method with 15 plane waves (a) and 169 plane waves (b). The curves of (b) are obtained by diagonalizing 113 plane waves $0 \leq \mathcal{E}(\mathbf{K}) \leq \mathcal{E}(\mathbf{K}) = 20$ (where $\mathcal{E}(\mathbf{K}) = (\hbar^2/2m)(2\pi/a)^2 K^2$) exactly and 56 higher energy states of $20 < \mathcal{E}(\mathbf{K}) \leq \mathcal{E}(\mathbf{K}) = 27$ by Löwdin's perturbation method. Note the curves of (a) exhibit discontinuity at U, K points and a curve of higher conduction band in the region K_1 to Γ is missing

where energy band structures calculated by 15 plane waves are shown by the curves in (a) and the curves in (b) are calculated by 169 plane waves. We find here that overall features are in good agreement but some disagreement exists as follows. The curves obtained by 169 plane waves show smooth continuity at the points U and K (at K_2). The points U and K in the Brillouin zone are equivalent because of the symmetry of the representation as seen in Figs. 1.5 and 1.22 and thus obtained bands are expected to be continuous through the points U and K . In addition to the discontinuity, a higher conduction band obtained by 169 plane waves is missing in the bands of 15 plane waves calculation in the region K_1 to Γ and the conduction bands of Γ_{15} and Γ_2 are almost degenerate in Fig. 1.9a. This will be discussed in Sect. 1.7, where energy band calculations by $\mathbf{k} \cdot \mathbf{p}$ perturbation method of 15 states will be discussed.

The energy band calculations carried out by Cohen and Bergstresser [5] reveal that the choice of appropriate values for the pseudopotentials V_3^S , V_8^S , V_{11}^S , V_3^A , V_8^A , V_{11}^A and the neglect of higher-order values give the band structures in good agreement with experimental results. The pseudopotential values determined by Cohen and Bergstresser [5] for typical semiconductors are given in Table 1.2. As discussed by Brust [9], and Cohen and Bergstresser [5], the energy bands are obtained by limited number of plane waves to form pseudopotential Hamiltonian matrix and plane waves with higher free electron energies are taken into account by the perturbation method proposed by Löwdin [8]. Energy band structures calculated by (1.84) with 169 plane waves are shown for Ge and Si in Fig. 1.10, for GaAs, GaP, AlAs and AlSb in Fig. 1.11, for InP, InAs, GaSb and InSb in Fig. 1.12, and for ZnS, ZnSe, ZnTe and CdTe in Fig. 1.13. In the calculations, the pseudopotential matrix of the 113 free-electron states of $0 \leq \mathcal{E}(\mathbf{K}) \leq \mathcal{E}(\mathbf{K}) = 20$ (where $\mathcal{E}(\mathbf{K}) = (\hbar^2/2m)(2\pi/a)^2 K^2$) are exactly diagonalized. For example, the calculated band gap of GaAs is 1.42 [eV]



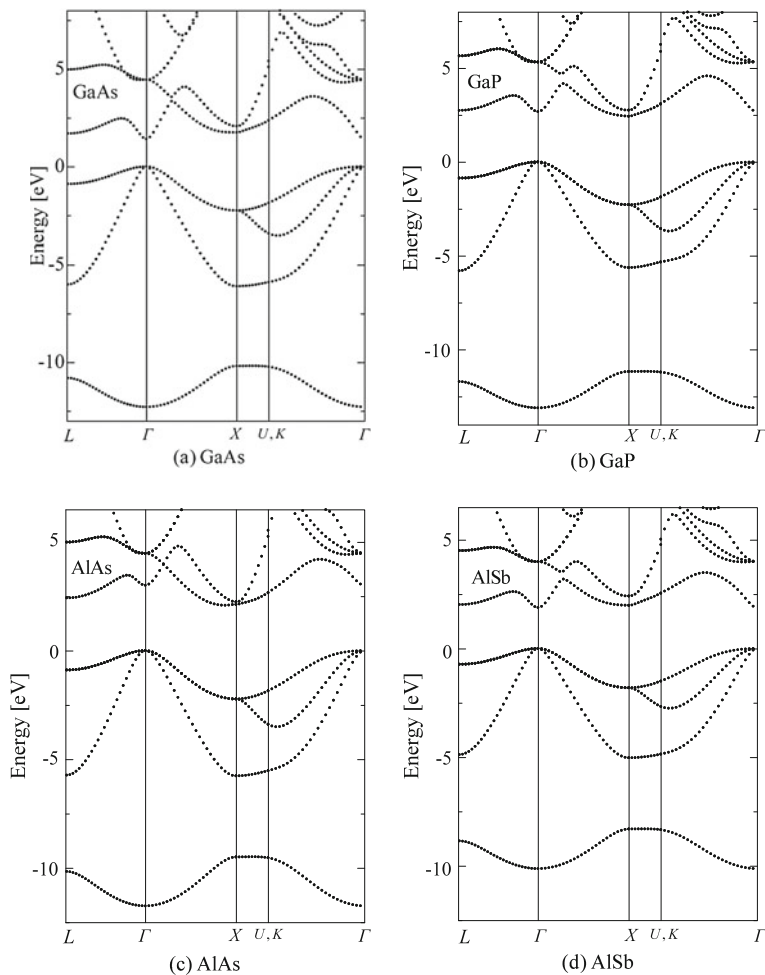


Fig. 1.11 Energy band structures calculated by the empirical pseudopotential method for **a** GaAs, **b** GaP, **c** AlAs, and **d** AlSb. The spin–orbit interaction is not included

which is obtained without spin–orbit interaction (compare the results with spin–orbit interaction shown in Fig. 1.21, where we obtain 1.52 eV for the direct band gap). We have to note here that energy band calculations with 59 plane waves of $0 \leq \mathcal{E}(\mathbf{K}) \leq \mathcal{E}(\mathbf{K}) = 12$ give quite reasonable results. This is understood from the fact that the next higher levels of the free electron states are $\mathcal{E}(\mathbf{K}) = 16$ and well high compared with $\mathcal{E}(\mathbf{K}) = 12$. The energy band calculations mentioned above is sometimes called the “local pseudopotential method”, and later Chelikowsky and Cohen reported the “nonlocal pseudopotential method” as described in Sect. 1.6.3 in which the spin–orbit interaction is taken into account [6, 7].

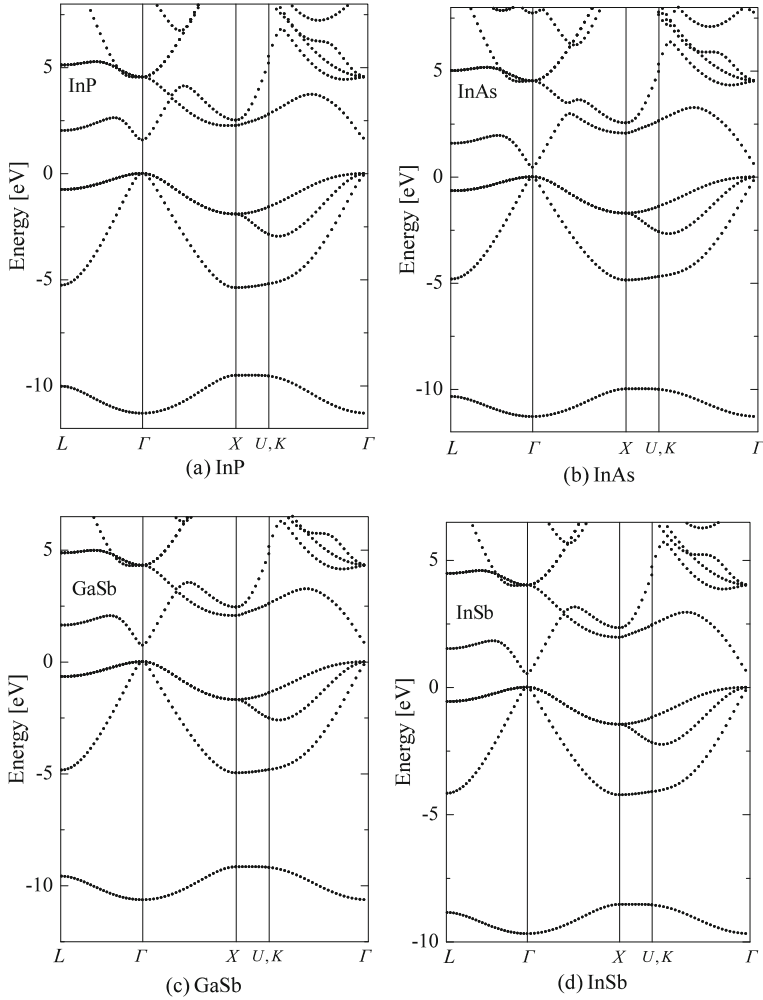


Fig. 1.12 Energy band structures calculated by the empirical pseudopotential method for **a** InP, **b** InAs, **c** GaSb, and **d** InSb. The spin-orbit interaction is not included

1.6.5 Spin-Orbit Interaction

Once the reciprocal vectors are calculated, the free-electron wave functions (1.87) (called as plane waves in this textbook) are easily formulated. Then putting the wave functions into (1.84) we obtain (1.88) which is called eigen-value equation and easily diagonalized to give eigenvalues and eigen functions. The matrix element in (1.84) is written as

$$\langle (\mathbf{k} + \mathbf{G}_i) | H_{\text{ps}} | (\mathbf{k} + \mathbf{G}_j) \rangle = T(\mathbf{k})_{G_i, G_j} + V_{G_i, G_j} + \Delta(\mathbf{k})_{G_i, G_j}, \quad (1.103)$$

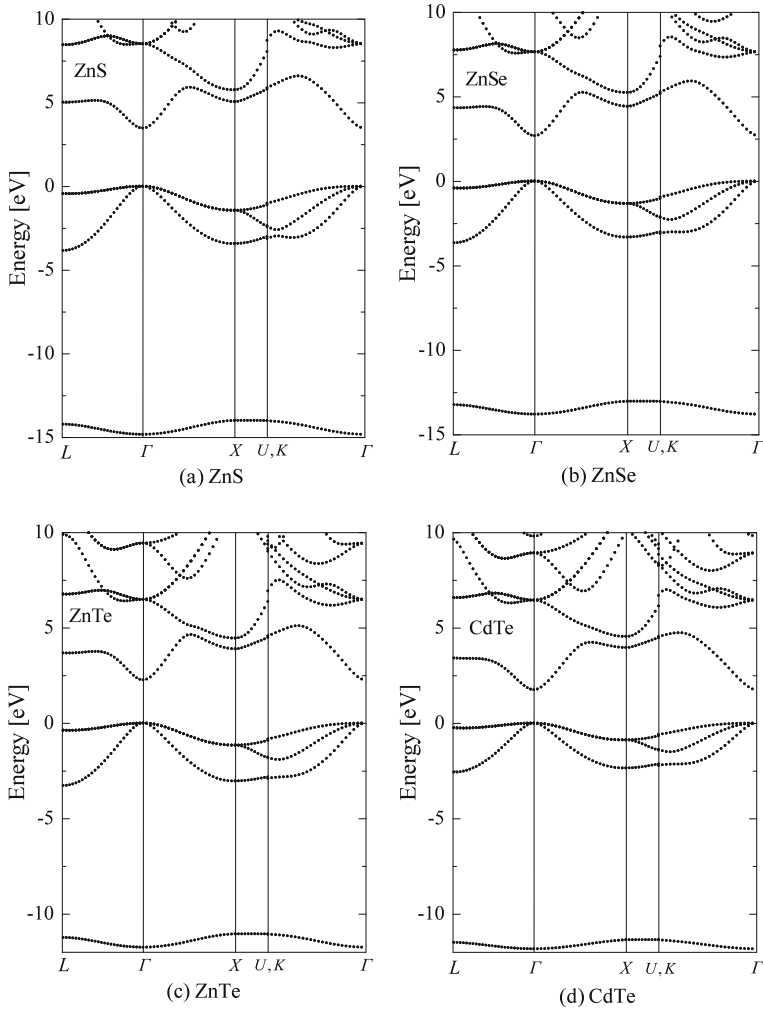


Fig. 1.13 Energy band structures calculated by the empirical pseudopotential method for **a** ZnS, **b** ZnSe, **c** ZnTe, and **d** CdTe. The spin-orbit interaction is not included

where we included spin-orbit interaction by introducing the term $\Delta(\mathbf{k})_{G_i, G_j}$. The derivation of spin-orbit interaction term is shown in Appendix H. The three terms of (1.103) are given by

$$T(\mathbf{k})_{G_i, G_j} = \frac{\hbar^2}{2m} (\mathbf{k} + \mathbf{G}_i)^2 \delta_{G_i, G_j}, \quad (1.104)$$

$$V_{G_i, G_j} = [V^S(\mathbf{Q}) \cos(\mathbf{Q} \cdot \boldsymbol{\tau}) + iV^A(\mathbf{Q}) \sin(\mathbf{Q} \cdot \boldsymbol{\tau})]_{\mathbf{Q}=\mathbf{G}_i-\mathbf{G}_j}, \quad (1.105)$$

$$\Delta(\mathbf{k})_{G_i, G_j} = i\boldsymbol{\sigma} \cdot [\mathbf{G}_i \times \mathbf{G}_j - \mathbf{k} \times (\mathbf{G}_i - \mathbf{G}_j)] \times [\lambda^S \cos(\mathbf{Q} \cdot \boldsymbol{\tau}) + i\lambda^A \sin(\mathbf{Q} \cdot \boldsymbol{\tau})], \quad (1.106)$$

where

$$\mathbf{Q} = \mathbf{G}_i - \mathbf{G}_j \equiv \frac{2\pi}{a} \mathbf{K}. \quad (1.107)$$

The term $T(\mathbf{k})_{G_i, G_j}$ has diagonal elements only and is easily formulated by using the reciprocal wave vectors listed in Table 1.1. The pseudopotential term V_{G_i, G_j} is separated in symmetric parts and antisymmetric parts (for zinc blende crystal) and their matrix elements are evaluated as follows. Using $\mathbf{K} = (a/2\pi) \mathbf{Q} = (a/2\pi)(\mathbf{G}_j - \mathbf{G}_i)$, and $\boldsymbol{\tau} = (a/8)[111]$, the symmetric parts of the pseudopotentials are

$$V^S(\mathbf{Q}) \cos(\mathbf{Q} \cdot \boldsymbol{\tau}) = V_3^S \cos\left[\frac{\pi}{4}(K_x + K_y + K_z)\right] \text{ if } |\mathbf{K}|^2 = 3 \quad (1.108a)$$

$$= V_8^S \cos\left[\frac{\pi}{4}(K_x + K_y + K_z)\right] \text{ if } |\mathbf{K}|^2 = 8 \quad (1.108b)$$

$$= V_{11}^S \cos\left[\frac{\pi}{4}(K_x + K_y + K_z)\right] \text{ if } |\mathbf{K}|^2 = 11 \quad (1.108c)$$

$$= 0 \text{ if } |\mathbf{K}|^2 > 11, \quad (1.108d)$$

and in a similar fashion we obtain the antisymmetric parts of the pseudopotentials for a zinc blende crystal

$$V^A(\mathbf{Q}) \sin(\mathbf{Q} \cdot \boldsymbol{\tau}) = V_3^A \sin\left[\frac{\pi}{4}(K_x + K_y + K_z)\right] \text{ if } |\mathbf{K}|^2 = 3 \quad (1.109a)$$

$$= V_4^A \sin\left[\frac{\pi}{4}(K_x + K_y + K_z)\right] \text{ if } |\mathbf{K}|^2 = 4 \quad (1.109b)$$

$$= V_{11}^A \sin\left[\frac{\pi}{4}(K_x + K_y + K_z)\right] \text{ if } |\mathbf{K}|^2 = 11 \quad (1.109c)$$

$$= 0 \text{ if } |\mathbf{K}|^2 > 11. \quad (1.109d)$$

The matrix elements of the spin-orbit Hamiltonian are easily evaluated by using the results shown in Appendix H (see also Sect. 1.7.5 for the evaluation of the matrix elements of the spin-orbit Hamiltonian), and the manipulation similar to the pseudopotential term leads to the following relations

$$\lambda^S \cos(\mathbf{Q} \cdot \boldsymbol{\tau}) = \lambda^S \cos\left[\frac{\pi}{4}(K_x + K_y + K_z)\right], \quad (1.110)$$

$$\lambda^A \sin(\mathbf{Q} \cdot \boldsymbol{\tau}) = \lambda^A \sin\left[\frac{\pi}{4}(K_x + K_y + K_z)\right]. \quad (1.111)$$

The expression of spin-orbit interaction shown here is based on the derivation by Melz [10] and known to be mathematically equivalent to the long-wavelength limit of the OPW formulation due to Weisz [11], but the formalism is based on the empirical

pseudopotential (local pseudopotential) method. See the paper by Chelikowsky and Cohen [7] for more detailed treatment. Since we are interested in the valence bands and lower lying conduction bands, we may restrict the number of plane waves to calculate the spin–orbit interaction term.

It is well known that the atomic spin–orbit splittings are larger for the heavier elements. Therefore we expect that the spin–orbit splitting at the valence band maximum increases with the heavier elements. For example the spin–orbit splitting of Ge is larger than Si, and it increases in order of the mass for GaP, GaAs, GaSb, InP, InAs, and InSb.

1.6.6 Energy Band Calculations by Nonlocal Pseudopotential Method with Spin–Orbit Interaction

First, we show the calculated results by the local pseudopotential method with spin–orbit interaction for Ge in Fig. 1.14(a) and GaAs in Fig. 1.14(b) with 118 plane waves of spin–up and spin–down with the spin–orbit interaction. The pseudopotential values used in the calculations are local pseudopotentials reported by Cohen and Bergstresser [5] (see Table 1.2), and the spin–orbit interaction parameters are $(2\pi/a)^2\lambda^S = 0.0008$, $(2\pi/a)^2\lambda^A = 0.0002$, where λ^S and λ^A are given by the units $(2\pi/a)^2\lambda^S$ and $(2\pi/a)^2\lambda^A$ and used as fitting parameters for simplicity throughout the textbook. These parameters are not best fitted but give the spin–orbit splitting energy about 0.340 [eV] for GaAs. There exists only a slight difference in the energies at X , L and other critical points between the present calculations and the results calculated by the nonlocal pseudopotential methods of Chelikowsky and Cohen [7] (the results of the nonlocal pseudopotential method obtained by the present authors' are shown in Fig. 1.15).

Finally we will show the energy band structure of GaAs calculated by using the nonlocal pseudopotential method with the spin–orbit interaction. In the calculation the plane waves for $0 \leq K^2 \leq \mathcal{E}_1 = 20$ (113 plane waves and thus 226 plane waves with spin–up and –down states) are exactly diagonalized, and 56 (= 169 – 113) spin–degenerate states for $\mathcal{E}_1 < K^2 \leq 27$ are treated by Löwdin's perturbation method [8]. The results are shown in Fig. 1.15, where we used the pseudopotentials $V_3^S = -0.254$ (–0.214) and $V_{11}^A = 0.010$ (0.001) instead of the parameters shown in the parentheses reported by Chelikowsky and Cohen [7], and the spin–orbit parameters is $\lambda^S = 0.00081$ and $\lambda^A = 0.000245$. The results are shown in Fig. 1.15 which give the energy gap $\mathcal{E}_G = 1.5055$ [eV] and the spin–orbit splitting at the Γ point 0.34018 [eV]. We have to note here that the calculated results depend on the energy cut values \mathcal{E}_1 and \mathcal{E}_2 . When we choose a smaller value for \mathcal{E}_1 , the convergence is very fast, but the results strongly depend on the value of \mathcal{E}_2 and the obtained result is not enough to explain the existing experimental data. On the other hand the results for $\mathcal{E}_1 = 20$ exhibit no recognizable difference between the results with and without the perturbation terms of the plane waves for $\mathcal{E}_1 < K^2 \leq 27$.

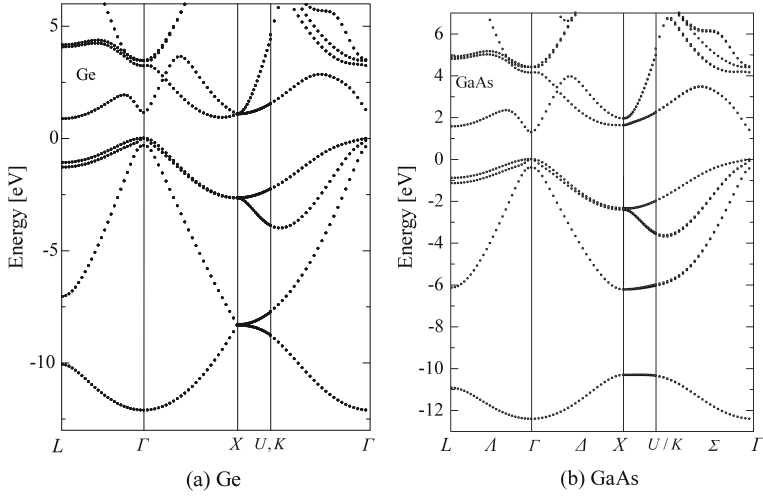


Fig. 1.14 Energy band structures of **a** Ge and **b** GaAs calculated by the local pseudopotential method with the spin-orbit interaction, where 118 plane waves with spin-up and spin-down and the spin-orbit interaction parameters are $(2\pi/a)^2\lambda^S = 0.0008$, $(2\pi/a)^2\lambda^A = 0.0002$. The pseudopotential parameters given in Table 1.2 are used ($(2\pi/a)^2\lambda^S = 0.00097$ for Ge)

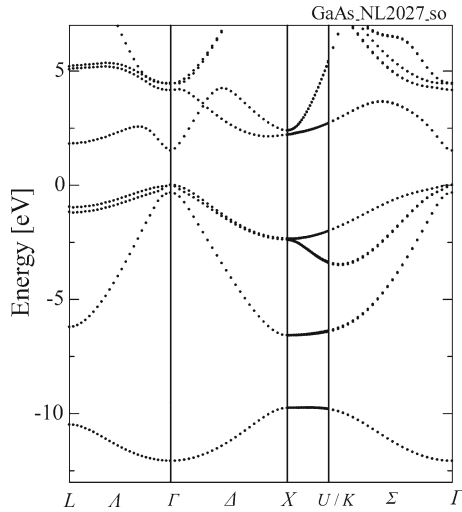


Fig. 1.15 Energy bands of GaAs calculated by the nonlocal pseudopotential method, where the spin-orbit interaction is taken into account. The states for $0 \leq K^2 \leq \mathcal{E}_1 = 20$ (113 plane waves and thus 226 plane waves with spin-up and -down states) are exactly diagonalized and the states for $\mathcal{E}_1 < K^2 \leq 27$ (degenerate 56 waves) are treated by the perturbation method

As reported by Chelikowsky and Cohen [7] the over all features of the energy bands are almost the same as the results calculated by the local pseudopotential method except some critical points. Therefore the results shown in the text are calculated by the local pseudopotential method, unless otherwise mentioned, because we have to adjust more parameters for the nonlocal pseudopotential methods. The local pseudopotential method requires fewer number of the pseudopotential parameters to get results in agreement with the experimental observation, and provides the energy bands and optical properties of various semiconductors which help us to understand the optical characteristics and transport properties based on the full band Monte Carlo simulation.

1.7 $\mathbf{k} \cdot \mathbf{p}$ Perturbation

1.7.1 $\mathbf{k} \cdot \mathbf{p}$ Hamiltonian

The $\mathbf{k} \cdot \mathbf{p}$ perturbation was introduced by Kane [12] in 1956 to analyze the energy band structures of III–V compound semiconductors and led to a successful result. The method was originally used in 1936 to discuss the character table of the symmetry points in the Brillouin zone by Bouckaert, Smoluchowski and Wigner [13]. Later Dresselhaus, Kip and Kittel [14] used the $\mathbf{k} \cdot \mathbf{p}$ perturbation method to analyze the detailed structure of the valence bands of Ge. This method is described in detail in Sect. 2.1, where the $\mathbf{k} \cdot \mathbf{p}$ perturbation method is applied to analyze the experimental results of cyclotron resonance in Ge. In this section we will consider the method used by Cardona and Pollak [15] to calculate energy band structures.

We consider the non-relativistic Schrödinger equation for a one-electron system:

$$\left[-\frac{\hbar^2}{2m} \nabla^2 + V(\mathbf{r}) \right] \Psi(\mathbf{r}) = \mathcal{E} \Psi(\mathbf{r}), \quad (1.112)$$

where $V(\mathbf{r})$ is the crystal potential energy with the lattice periodicity. The solution of (1.112) is given by the Bloch function

$$\Psi(\mathbf{r}) = e^{i\mathbf{k} \cdot \mathbf{r}} u_{n,\mathbf{k}}(\mathbf{r}), \quad (1.113)$$

where $u_{n,\mathbf{k}}$ is a function of the lattice periodicity for band index n . Putting this Bloch function into (1.112) and using the following relations

$$\nabla \Psi(\mathbf{r}) = i\mathbf{k} \Psi(\mathbf{r}) + e^{i\mathbf{k} \cdot \mathbf{r}} \nabla u_{n,\mathbf{k}}(\mathbf{r}), \quad (1.114a)$$

$$\begin{aligned} \nabla^2 \Psi(\mathbf{r}) &= -k^2 \Psi(\mathbf{r}) + 2i\mathbf{k} e^{i\mathbf{k} \cdot \mathbf{r}} \nabla u_{n,\mathbf{k}}(\mathbf{r}) + e^{i\mathbf{k} \cdot \mathbf{r}} \nabla^2 u_{n,\mathbf{k}}(\mathbf{r}), \\ &= e^{i\mathbf{k} \cdot \mathbf{r}} (-k^2 + 2i\mathbf{k} \cdot \nabla + \nabla^2) u_{n,\mathbf{k}}(\mathbf{r}), \end{aligned} \quad (1.114b)$$

we obtain

$$\left[-\frac{\hbar^2}{2m} \nabla^2 + V(\mathbf{r}) + \frac{\hbar^2}{2m} k^2 - i\frac{\hbar^2}{m} (\mathbf{k} \cdot \nabla) \right] u_{n,\mathbf{k}}(\mathbf{r}) = \mathcal{E}_n(\mathbf{k}) u_{n,\mathbf{k}}(\mathbf{r}). \quad (1.115)$$

Using the relation $-i\hbar\nabla = \mathbf{p}$ for the momentum operator, the above equation may be rewritten as

$$\left[H_0 + \frac{\hbar^2 k^2}{2m} + \frac{\hbar}{m} \mathbf{k} \cdot \mathbf{p} \right] u_{n,\mathbf{k}}(\mathbf{r}) = \mathcal{E}_n(\mathbf{k}) u_{n,\mathbf{k}}(\mathbf{r}), \quad (1.116)$$

where $H_0 = -(\hbar^2/2m)\nabla^2 + V(\mathbf{r})$ is Hamiltonian. The terms $\hbar^2 k^2/2m$ in [] on the left-hand side is a constant (c -number) without any operator and thus the term gives rise to an energy shift of $\hbar^2 k^2/2m$ from $\mathcal{E}_n(\mathbf{k})$. First solving (1.116) for $\mathbf{k} = 0$ and then treating $(\hbar/m)\mathbf{k} \cdot \mathbf{p}$ as a perturbing term, we obtain eigenstates as a function of \mathbf{k} which gives the energy band structure. Therefore, this method is called **$\mathbf{k} \cdot \mathbf{p}$ perturbation**. The eigenstates for the Hamiltonian H_0 are obtained by using the pseudopotentials, but here we show a simplified method to obtain the eigenstates by solving 2×2 matrices following the method reported by Cardona [16]. Although such a calculation is very simple, obtained eigen energies and eigenvectors are very useful to understand the band structures.

The above $\mathbf{k} \cdot \mathbf{p}$ Hamiltonian is rewritten by using atomic units as follows:

$$-\frac{\hbar^2}{2m} \nabla^2 = \frac{\hbar^2}{2m} \left(\frac{1}{a_B} \right)^2 (-ia_B \nabla)^2 = \text{Ry} \cdot (-ia_B \nabla)^2 \quad (1.117a)$$

$$\frac{\hbar^2 k^2}{2m} = \frac{\hbar^2}{2m} \left(\frac{1}{a_B} \right)^2 (a_B \mathbf{k})^2 = \text{Ry} \cdot (a_B \mathbf{k})^2 \quad (1.117b)$$

$$\frac{\hbar}{m} \mathbf{k} \cdot \mathbf{p} = \frac{\hbar^2}{2m} \left(\frac{1}{a_B} \right)^2 \left(\frac{a_B^2}{\hbar} \right) (2\mathbf{k} \cdot \mathbf{p}) = \text{Ry} \cdot \left(\frac{a_B^2}{\hbar} \right) (2\mathbf{k} \cdot \mathbf{p}), \quad (1.117c)$$

where $a_B = 4\pi\epsilon_0\hbar^2/(me^2) \simeq 0.529 \text{ [\AA]}$ is Bohr radius and $\text{Ry} = me^4/(8\epsilon^2\hbar^3c) \simeq 13.6 \text{ [eV]}$ is Rydberg constant. Using the dimensionless notation or the atomic units

$$\mathbf{k} \text{ (in [a.u.])} = a_B \mathbf{k}, \quad \mathbf{p} \text{ (in [a.u.])} = \frac{a_B}{\hbar} \mathbf{p} = -ia_B \nabla, \quad (1.118)$$

and then the $(\hbar/m)\mathbf{k} \cdot \mathbf{p}$ operator of (1.117c) is rewritten as

$$\frac{\hbar}{m} \mathbf{k} \cdot \mathbf{p} = \text{Ry} \cdot (2\mathbf{k} \cdot \mathbf{p}). \quad (1.119)$$

Finally, the length is expressed in atomic units or normalized by a_B and then the $\mathbf{k} \cdot \mathbf{p}$ Hamiltonian is rewritten as

$$H_0 + \frac{\hbar}{m} \mathbf{k} \cdot \mathbf{p} + \frac{\hbar^2 k^2}{2m} = -\nabla^2 + 2\mathbf{k} \cdot \mathbf{p} + k^2. \quad (1.120)$$

When we put $\mathbf{k} = 0$ in (1.116), we obtain

$$H_0 u_{n,0}(\mathbf{r}) = \left[-\frac{\hbar^2}{2m} \nabla^2 + V(\mathbf{r}) \right] u_{n,0}(\mathbf{r}) = \mathcal{E}_n(0) u_{n,0}(\mathbf{r}), \quad (1.121)$$

which is rewritten in atomic units as

$$[-\nabla^2 + V(\mathbf{r})] u_{n,0}(\mathbf{r}) = \mathcal{E}_n(0) u_{n,0}(\mathbf{r}). \quad (1.122)$$

Since the crystal potential $V(\mathbf{r})$ and Bloch function $u_{n,0}(\mathbf{r})$ are periodic with the lattice constant, and thus these two functions are expanded by Fourier series. Therefore we may use the pseudopotential theory stated before, and the diagonalization of the Hamiltonian matrix gives the eigenstates and the corresponding eigenvalues. In the $\mathbf{k} \cdot \mathbf{p}$ perturbation theory we need eigenstates at $\mathbf{k} = 0$ (at the Γ point) only. For this purpose we rewrite (1.86) and (1.87) as

$$[-\nabla^2 + V_{ps}(|G|^2)] |\mathbf{G}_j\rangle = \mathcal{E}_n |\mathbf{G}_j\rangle, \quad (1.123)$$

$$|\mathbf{G}_j\rangle = \frac{1}{\sqrt{\Omega}} e^{i\mathbf{G}_j \mathbf{r}}, \quad (1.124)$$

where $V_{ps}(\mathbf{r})$ is expanded with Fourier coefficients $V_{ps}(|G|^2)$ (pseudopotential form factors). Simplified solutions of the above equations are very helpful to obtain the eigenstates and to explain the group theoretical representations used in Fig. 1.7. The $\mathbf{k} \cdot \mathbf{p}$ Hamiltonian for semiconductors with inversion symmetry has off-diagonal terms only. In addition, we classify the matrix elements with the help of group theory, and so the number of the matrix elements are extremely decreased. Cardona and Pollak [15] proposed to calculate the energy band structures using 15 electronic states (wave functions) at the Γ point (at $\mathbf{k} = 0$) and obtained very accurate energy band structures of germanium and silicon. Here we will show the energy band calculations of germanium and silicon based on the $\mathbf{k} \cdot \mathbf{p}$ perturbation method of Cardona and Pollak, where the spin-orbit interaction is not included. First we classify the free electron energy bands shown in Fig. 1.7 with the help of group theory.

Here we summarize important and useful results of group theory without showing the derivation. The most important factors are to use the character table of the crystal. The character table for a face centered cubic lattice which includes diamond and zinc blende crystals is shown in Table 1.4. Although detailed description of group theory is not shown here, the character table is very useful to calculate non-vanishing matrix elements and thus selection rule of optical transition. Another important information about the symmetry properties of quantum states is the basis functions for the representations, which is summarized in Table 1.5.

In a crystalline solid the notation of atomic orbitals is classified by using the spherical harmonics $Y_{lm}(\theta, \phi)$ ($m = -l, \dots, +l$) which constitute a basis for the irreducible representation and thus the electronic states are related to the states of an atom as shown below [17],

Table 1.4 Character table of small representations of O_h group

BSW	E	$3C_4^2$	$6C_4$	$6C_2$	$8C_3$	J	$3JC_4^2$	$6JC_4$	$6JC_2$	$8JC_3$
Γ_1	1	1	1	1	1	1	1	1	1	1
Γ_2	1	1	-1	-1	1	1	1	-1	-1	1
Γ_{12}	2	2	0	0	-1	2	2	0	0	-1
$\Gamma_{15'}$	3	-1	1	-1	0	3	-1	1	-1	0
$\Gamma_{25'}$	3	-1	-1	1	0	3	-1	-1	1	0
$\Gamma_{1'}$	1	1	1	1	1	-1	-1	-1	-1	-1
$\Gamma_{2'}$	1	1	-1	-1	1	-1	-1	1	1	-1
$\Gamma_{12'}$	2	2	0	0	-1	-2	-2	0	0	1
Γ_{15}	3	-1	1	-1	0	-3	1	-1	1	0
Γ_{25}	3	-1	-1	1	0	-3	1	1	-1	0

Table 1.5 Basis function of irreducible representation of O_h group at Γ point

Representation	Degeneracy	Basis functions
Γ_1	1	1
Γ_2	1	$x^4(y^2 - z^2) + y^4(z^2 - x^2) + z^4(x^2 - y^2)$
Γ_{12}	2	$z^2 - \frac{1}{2}(x^2 + y^2), (x^2 - y^2)$
$\Gamma_{15'}$	3	$xy(x^2 - y^2), yz(y^2 - z^2), zx(z^2 - x^2)$
$\Gamma_{25'}$	3	xy, yz, zx
$\Gamma_{1'}$	1	$xyz[x^4(y^2 - z^2) + y^4(z^2 - x^2) + z^4(x^2 - y^2)]$
$\Gamma_{2'}$	1	xyz
$\Gamma_{12'}$	2	$xyz[z^2 - \frac{1}{2}(x^2 + y^2)], xyz(x^2 - y^2)$
Γ_{15}	3	x, y, z
Γ_{25}	3	$z(x^2 - y^2), x(y^2 - z^2), y(z^2 - x^2)$

State s ($l = 0$) = Γ_1 ,

State p ($l = 1$) = Γ_{15} ,

State d ($l = 2$) = $\Gamma_{25'} + \Gamma_{12}$,

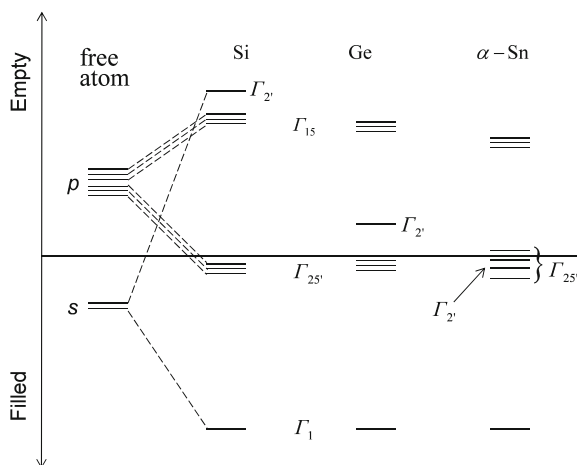
State f ($l = 3$) = $\Gamma_{15} + \Gamma_{25} + \Gamma_{2'}$,

State g ($l = 4$) = $\Gamma_{25'} + \Gamma_{15'} + \Gamma_{12} + \Gamma_1$,

State h ($l = 5$) = $\Gamma_{25} + 2\Gamma_{15} + \Gamma_{12'}$.

In a crystalline solid the wave functions of an atom and the next nearest neighbor are hybridized, resulting in bonding and anti-bonding states and thus in energy shift, as discussed below. A concept of atomic orbitals, LCAO (Linear Combination of Atomic Orbitals), is very helpful to understand the energy bands at $\mathbf{k} = 0$. Here we follow the method of Cardona [16]. First, we consider electronic states in the outer shell of an atomic Ge, where two s -states and two p -states are filled with electrons. Therefore the other two p -states and ten d -states are empty. Since two

Fig. 1.16 Splitting of the atomic states of Ge, Si and α -Sn under the presence of the crystalline field of the diamond structure at Γ point of the Brillouin zone, where a bar corresponds to a degenerate energy state with spin up and down (after Cardona [16])



atoms are included in a unit cell of diamond structure, the states are doubled when the two atoms are put together. In such a case, the electronic states are modified by linear combinations of the atomic orbitals, the bonding and anti-bonding states, and thus the states split as shown in Fig. 1.16. No mixing by the crystal field occurs between s - and p -orbitals at $\mathbf{k} = 0$. The s -orbitals contain a negligible admixture of f -orbitals while the p -orbitals may contain a significant admixture of d -orbitals of the same shell. The ordering of the states are illustrated so as to fit the observed conduction and valence bands. The ordering between the states is changed by the bonding-anti-bonding splitting. If the splitting is small, as in the case of α -Sn with large lattice constant, the Γ_1 and $\Gamma_{2'}$ are filled and $\Gamma_{25'}$ only partially filled. As the bonding-anti-bonding splitting becomes larger, the $\Gamma_{2'}$ -state becomes higher than $\Gamma_{25'}$, resulting in an energy gap. This is the case for Ge and Si as shown in Fig. 1.16.

In order to calculate the energy bands of Ge and Si by the $\mathbf{k} \cdot \mathbf{p}$ method, we have to choose the eigenstates at $\mathbf{k} = 0$ properly, not so many states but enough to lead reasonable results. First we show the free electron bands for lower energy states in Table 1.6, where the free electron energies are estimated for Ge ($a = 5.66 \text{ \AA}$), G_3 band is 1.038 a.u. (14.1 eV), and G_4 is 1.38 a.u. (18.8 eV). The fourth band G_8 is 2.77 a.u. (37.7 eV), which is well higher than the G_4 bands and we may limit the plane waves up to G_4 . This enables us to choose 15 eigenstates with the representations; Γ_1^l , $\Gamma_{25'}^l$, Γ_{15}^l , $\Gamma_{2'}^l$, Γ_1^u , $\Gamma_{25'}^u$, $\Gamma_{12'}^u$, and $\Gamma_{2'}^u$. This approximation was used by Cardona and Pollak [15].

Next, we discuss relation between the LCAO and plane waves of free electron bands expressed by a combination of the reciprocal lattice vectors [G_x , G_y , G_z] of the empty lattice bands at Γ point (at $\mathbf{k} = 0$ of the Brillouin zone). The plane waves of [000], [111] and [200] are related to the LCAO states as shown by Cardona [16].

Table 1.6 Reciprocal of smaller free electron energies, where dgn means the degeneracy of the states and the free electron energy in [a.u.] is estimated for $a = 5.66$ [Å]

G	Vector components	dgn	Representations	Energy in [a.u.]
G_0	$= (2\pi/a)[0, 0, 0]$	1	Γ_1^l	0
G_3	$= (2\pi/a)[\pm 1, \pm 1, \pm 1]$	8	$\Gamma_{25'}^l + \Gamma_{15} + \Gamma_{2'}^l + \Gamma_1^u$	1.038
G_4	$= (2\pi/a)[\pm 2, 0, 0]$	6	$\Gamma_{25'}^u + \Gamma_{12'} + \Gamma_{2'}^u$	1.38
G_8	$= (2\pi/a)[\pm 2, \pm 2, 0]$	12	$\Gamma_1 + \Gamma_{12} + 2\Gamma_{15} + \Gamma_{25'}$	2.77
G_{11}	$= (2\pi/a)[\pm 3, \pm 1, \pm 1]$	24	$\Gamma_1 + \Gamma_{12} + \Gamma_2 + \Gamma_{12'} + \Gamma_{15'} + \Gamma_{25} + 2\Gamma_{25'} + 2\Gamma_{15}$	3.81

$$\begin{aligned}
[000] & \quad \Gamma_1^l; & s\text{-bonding}; \\
[111] & \left\{ \begin{array}{ll} \Gamma_{25'}^l; & p\text{-bonding} \\ \Gamma_{15}; & p\text{-anti-bonding} \\ \Gamma_{2'}^l; & s\text{-anti-bonding} \\ \Gamma_1^u; & s\text{-bonding (next shell)}; \end{array} \right. \\
[200] & \left\{ \begin{array}{ll} \Gamma_{25'}^u; & d\text{-bonding} \\ \Gamma_{12'}; & d\text{-bonding} \\ \Gamma_{2'}^u; & s\text{-anti-bonding (next shell)}, \end{array} \right.
\end{aligned}$$

where the superscript l and u denote the lower and the upper of the two states of the same symmetry. For simplicity we use the relation (1.59) to express dimensionless reciprocal lattice vector \mathbf{K} . The group of reciprocal wave vectors $\mathbf{K}[\pm 1, \pm 1, \pm 1](8)$ have 8 components (dimension is 8), and a combinations of the 8 plane waves gives the following representations by using the character table of Table 1.4

$$\mathbf{K}[\pm 1, \pm 1, \pm 1](8) = \Gamma_1^u(1) + \Gamma_{2'}^u(1) + \Gamma_{15}(3) + \Gamma_{25'}^l(3). \quad (1.125)$$

The representation Γ_1^u has the same character of the lowest valence band Γ_1^l arising from the reciprocal wave vector $\mathbf{K}[0, 0, 0]$. Representation Γ_1^u in (1.125) is understood as follows. A summarized combination of orthogonalized plane waves for Γ_1^u is composed from $[\pm 1, \pm 1, \pm 1]$

$$\begin{aligned}
\Gamma_1^u[\pm 1, \pm 1, \pm 1] = \frac{1}{\sqrt{8}} \{ & [1, 1, 1] - [\bar{1}, 1, 1] - [1, \bar{1}, 1] - [1, 1, \bar{1}] \\ & - [\bar{1}, \bar{1}, 1] - [\bar{1}, 1, \bar{1}] - [1, \bar{1}, \bar{1}] + [\bar{1}, \bar{1}, \bar{1}] \} \quad (1.126)
\end{aligned}$$

and the character is the same of $\Gamma_1^l[0, 0, 0]$, where we used the notation

$$[K_x, K_y, K_z] = \exp \left[i \left(\frac{2\pi}{a} \right) (K_x x + K_y y + K_z z) \right]. \quad (1.127)$$

In a similar fashion other symmetrized combinations of the orthogonalized plane waves are composed for $\Gamma_{2'}^u$, Γ_{15} , and $\Gamma_{25'}^l$. The representations of the plane waves are summarized in Table 1.6. In the following several symmetrized combinations of the orthogonalized plane waves [K_x , K_y , K_z] belonging to the Γ -representation are given:

$$\begin{aligned}
 \Gamma_{2'}^l [111] &= \frac{1}{\sqrt{8}} \{ [111] - [1\bar{1}\bar{1}] - [\bar{1}1\bar{1}] - [\bar{1}\bar{1}1] - [\bar{1}\bar{1}\bar{1}] + [\bar{1}11] + [1\bar{1}1] + [11\bar{1}] \}, \\
 \Gamma_{2'}^u [200] &= \frac{1}{\sqrt{6}} \{ [200] + [020] + [002] - [\bar{2}00] - [0\bar{2}0] - [00\bar{2}] \}, \\
 \Gamma_{25'}^l (X) [111] &= \frac{1}{\sqrt{8}} \{ [111] - [1\bar{1}\bar{1}] + [\bar{1}1\bar{1}] + [\bar{1}\bar{1}1] + [\bar{1}\bar{1}\bar{1}] - [\bar{1}11] + [1\bar{1}1] + [11\bar{1}] \}, \\
 \Gamma_{25'}^u (X) [200] &= \frac{1}{\sqrt{2}} \{ [200] + [\bar{2}00] \}, \\
 \Gamma_{15} (x) [111] &= \frac{1}{\sqrt{8}} \{ [111] - [1\bar{1}\bar{1}] + [\bar{1}1\bar{1}] + [\bar{1}\bar{1}1] - [\bar{1}\bar{1}\bar{1}] + [\bar{1}11] - [1\bar{1}1] - [11\bar{1}] \}, \\
 \Gamma_{12'} (1) [200] &= \frac{1}{2} \{ [020] - [002] - [0\bar{2}0] + [00\bar{2}] \}, \\
 \Gamma_{12'} (2) [200] &= \frac{1}{\sqrt{12}} \{ 2[200] - [020] - [002] - 2[\bar{2}00] + [0\bar{2}0] + [00\bar{2}] \}.
 \end{aligned}$$

The Y and Z components of $\Gamma_{25'}^l$, and y and z components of Γ_{15} are obtained by means of cyclic permutation.

1.7.2 Derivation of the $k \cdot p$ Parameters

Energy band calculation by means of $k \cdot p$ perturbation requires estimation of momentum matrix elements such as $\langle \Gamma_{25'}^l | \mathbf{p} | \Gamma_2^l \rangle$ and energy eigenstates at the Γ point of the Brillouin zone ($\mathbf{k} = 0$). For this purpose we use pseudopotential method stated in the previous Sect. 1.6. These values are used for the initial data and then adjusted to the values so that the calculated critical points agree with the experiment. Cardona [16] applied the pseudopotential method for the purpose as described below. First we solve (1.123) with (1.124). For simplicity, irreducible representations of linear combinations of orthogonalized plane waves [000], [111] and [200] are considered, and then we find in Table 1.6 that representations Γ_1 , $\Gamma_{2'}$ and $\Gamma_{25'}$ appear twice, and designated as upper “ u ” and lower “ l ” states. In the case of a diamond crystal such as Ge and Si there exist symmetric pseudopotential terms only, and we obtain eigenvalues and eigenfunctions by diagonalizing 2×2 matrices of Hamiltonian $H_0 = -\nabla^2 + V_{ps}(|G|^2)$ for the Γ_1 , $\Gamma_{2'}$ and $\Gamma_{25'}$ states:

$$\begin{vmatrix} \Gamma_1[000] & \Gamma_1[111] \\ 0 & 2V_3^S \\ 2V_3^S & 3(2\pi/a)^2 + 3V_8^S \end{vmatrix}, \quad (1.128a)$$

$$\begin{vmatrix} \Gamma_{2'}[111] & \Gamma_{2'}[200] \\ 3(2\pi/a)^2 + 3V_3^S & \sqrt{6}(V_3^S + V_{11}^S) \\ \sqrt{6}(V_3^S + V_{11}^S) & 4(2\pi/a)^2 + 4V_8^S \end{vmatrix}, \quad (1.128b)$$

$$\begin{vmatrix} \Gamma_{25'}[111] & \Gamma_{25'}[200] \\ 3(2\pi/a)^2 - V_3^S & \sqrt{2}(V_3^S - V_{11}^S) \\ \sqrt{2}(V_3^S - V_{11}^S) & 4(2\pi/a)^2 \end{vmatrix}. \quad (1.128c)$$

In the following we estimate the eigen energies and eigenfunctions using the pseudopotentials listed in Table 1.2 and thus the obtained results differ a little from those reported by Cardona [16] and Cardona and Pollak [15]. The energies of Γ_1 states are -0.171 [Ry] (-2.326 [eV]) and 1.237 [Ry] (16.8 [eV]) for germanium, and 0.735 [Ry] (10.0 [eV]) and -0.2399 [Ry] (-3.263 [eV]) for silicon. The energies of the $\Gamma_{2'}$ states are given by 1.69 [Ry] (22.9 [eV]) and 0.77 [Ry] (10.5 [eV]) for germanium, and 1.81 [Ry] (24.6 [eV]) and 0.977 [Ry] (13.3 [eV]) for silicon. The eigenstates of the lower energies are

$$\Gamma_{2'}^l \text{ for Ge : } 0.843\Gamma_{2'}[111] + 0.539\Gamma_{2'}[200], \quad (1.129a)$$

$$\Gamma_{2'}^l \text{ for Si, : } 0.906\Gamma_{2'}[111] + 0.422\Gamma_{2'}[200]. \quad (1.129b)$$

In a similar fashion the eigenstates of $\Gamma_{25'}$ are obtained by solving 2×2 Hamiltonian matrix. The eigen energies are 1.74 [Ry] (23.6 [eV]) and 0.909 [Ry] (12.37 [eV]) for Ge, and 1.84 [Ry] (25.0 [eV]) and 1.00 [Ry] (13.6 [eV]) for Si.

$$\Gamma_{25'}^l \text{ for Ge : } 0.755\Gamma_{25'}[111] + 0.656\Gamma_{25'}[200], \quad (1.130a)$$

$$\Gamma_{25'}^l \text{ for Si, : } 0.774\Gamma_{25'}[111] + 0.634\Gamma_{25'}[200]. \quad (1.130b)$$

The energies of the single state Γ_{15} is given by $3(2\pi/a)^2 - V_8^S$, and the doubly-degenerate states $\Gamma_{12'}(1)[200]$ and $\Gamma_{12'}(2)[200]$ are given by $4(2\pi/a)^2 - 2V_8^S$, where matrix elements are 0 between the states $\Gamma_{12'}(1)$ and $\Gamma_{12'}(2)$. The calculated energies at $\mathbf{k} = 0$ (at Γ point) are listed in Table 1.7, where energies of the first row of the material in the table in units of [Ry] are obtained by solving a single band and 2×2 pseudopotential matrices, and the second row of rel.[Ry] is the relative values with respect to the valence band top of $\Gamma_{25'}^l$. The third row of the material shows the eigenvalues calculated by diagonalizing 15×15 pseudopotential matrices. In the 15×15 pseudopotential calculation, 15 reciprocal wave vectors of $[000](1)$, $[\pm 1, \pm 1, \pm 1](8)$, and $[\pm 2, 0, 0](6)$ (numbers in $()$ are degeneracy of the states) are used, and the result reveals that $\Gamma_{25'}^l$, $\Gamma_{25'}^u$, and Γ_{15} states are triply-degenerate, and $\Gamma_{12'}$ states are doubly-degenerate. We find in Table 1.7 that the values deduced from a simplified method give a very good guide to locate the eigenstates of the valence and conduction bands. The results obtained by the simple method are very close to

Table 1.7 Energy eigenvalues at $k = 0$ (Γ point) calculations by simplified matrices of the pseudopotentials. Values are given in atomic unit Rydberg [Ry], and relative values (rel.[Ry]) are with respect to the energy of the top valence band $\Gamma_{25'}^l$. For comparison eigenvalues obtained by solving 15×15 pseudopotential matrix is shown by full [Ry]

At $k = 0$	Waves	Germanium			Silicon		
		[Ry]	rel.[Ry]	full [Ry]	[Ry]	rel.[Ry]	full [Ry]
$\Gamma_{25'}^l$	[111]	0.909	0.00	0.00	1.00	0.00	0.00
$\Gamma_{2'}^l$	[111]	0.769	-0.139	0.0342	0.977	-0.023	0.2396
Γ_{15}	[111]	1.026	0.117	0.2694	1.085	0.086	0.2521
Γ_1^u	[111]	1.237	0.331	0.4805	1.374	0.246	0.5406
Γ_1^l	[000]	-0.171	-1.08	-0.9270	-0.128	-1.28	-0.9611
$\Gamma_{12'}$	[200]	1.36	0.452	0.6044	1.42	0.421	0.5870
$\Gamma_{25'}^u$	[200]	1.74	0.828	0.8938	1.836	0.836	0.9192
$\Gamma_{2'}^u$	[200]	1.687	0.778	0.9396	1.809	0.809	0.9996

the values of “pseudo” in Table 1.8, although the energy levels of $\Gamma_{2'}$ estimated by the simple method are negative and thus lie below the valence band top for both Ge and Si. In the $k \cdot p$ perturbation calculations, however, the parameters are adjusted to fit the data of experimental critical points and thus these estimations will be used for the initial parameters (Table 1.7).

Estimation of the momentum matrix element reported by Cardona [16] is very helpful to understand the energy band structure and thus it is described below in detail. The momentum matrix elements of \mathbf{p} between $\Gamma_{25'}^l$ and $\Gamma_{2'}^l$ which is expressed as P are given by using (1.129a) \sim (1.130b)

$$\begin{aligned}
 \langle \Gamma_{25'}^l(X) | p_x | \Gamma_{2'}^l \rangle &= \langle \Gamma_{25'}^l(Y) | p_y | \Gamma_{2'}^l \rangle = \langle \Gamma_{25'}^l(Z) | p_z | \Gamma_{2'}^l \rangle \\
 &= \frac{2\pi}{a} [0.843 \times 0.755 + 0.539 \times 0.656] \\
 &= 0.58 = P \quad (:\text{ for Ge }), \tag{1.131}
 \end{aligned}$$

$$\begin{aligned}
 \langle \Gamma_{25'}^l(X) | p_x | \Gamma_{2'}^l \rangle &= \langle \Gamma_{25'}^l(Y) | p_y | \Gamma_{2'}^l \rangle = \langle \Gamma_{25'}^l(Z) | p_z | \Gamma_{2'}^l \rangle \\
 &= \frac{2\pi}{a} [0.906 \times 0.774 + 0.422 \times 0.634] \\
 &= 0.59 = P \quad (:\text{ for Si }). \tag{1.132}
 \end{aligned}$$

The momentum matrix elements of \mathbf{p} between $\Gamma_{25'}^l$ and Γ_{15} states are

$$\begin{aligned}
 \langle \Gamma_{25'}^l(Z) | p_x | \Gamma_{15}(y) \rangle &= \langle \Gamma_{25'}^l(X) | p_y | \Gamma_{15}(z) \rangle = \langle \Gamma_{25'}^l(Y) | p_z | \Gamma_{15}(x) \rangle \\
 &= \frac{2\pi}{a} \times 0.755 = 0.44 = Q \quad (:\text{ for Ge }), \tag{1.133}
 \end{aligned}$$

$$\begin{aligned}
 \langle \Gamma_{25'}^l(Z) | p_x | \Gamma_{15}(y) \rangle &= \langle \Gamma_{25'}^l(X) | p_y | \Gamma_{15}(z) \rangle = \langle \Gamma_{25'}^l(Y) | p_z | \Gamma_{15}(x) \rangle \\
 &= \frac{2\pi}{a} \times 0.774 = 0.47 = Q \quad (:\text{ for Si }). \tag{1.134}
 \end{aligned}$$

Table 1.8 Energy eigenvalues used for energy band calculations by the $\mathbf{k} \cdot \mathbf{p}$ perturbation method in units of Rydberg (from reference [15])

At $\mathbf{k} = 0$	Waves	Germanium			Silicon		
		$\mathbf{k} \cdot \mathbf{p}$	OPW ^a	Pseudo	$\mathbf{k} \cdot \mathbf{p}$	OPW ^a	Pseudo
$\Gamma_{25'}^l$	[111]	0.00	0.00	0.00	0.00	0.00	0.00
$\Gamma_{2'}^l$	[111]	0.0728 ^b	-0.081	-0.007	0.265 ^b	0.164	0.23
Γ_{15}	[111]	0.232 ^b	0.231	0.272	0.252 ^b	0.238	0.28
Γ_1^u	[111]	0.571	0.571	0.444	0.520	0.692	0.52
Γ_1^l	[000]	-0.966	-0.929	-0.950	-0.950	-0.863	-0.97
$\Gamma_{12'}$	[200]	0.770	0.770	0.620	0.710	0.696	0.71
$\Gamma_{25'}^u$	[200]	1.25 ^c		0.890	0.940		0.94
$\Gamma_{2'}^u$	[200]	1.35		0.897	0.990		0.99

^aF. Herman, in *Proceedings of the International Conference on the Physics of Semiconductors, Paris, 1964* (Dunod Cie, Paris, 1964), p. 3

^bM. Cardona, J. Phys. Chem. Solids **24**, 1543 (1963)

^cG. Dresselhaus, A.F. Kip, and C. Kittel, Phys. Rev. **98**, 368 (1955); E.O. Kane, J. Phys. Chem. Solids **1**, 82 (1956)

Table 1.9 The values of momentum matrix elements used for the energy band calculations of germanium and silicon by the $\mathbf{k} \cdot \mathbf{p}$ perturbation (atomic units)

Momentum matrix elements	Germanium			Silicon		
	$\mathbf{k} \cdot \mathbf{p}$	Pseudo	c.r. [†]	$\mathbf{k} \cdot \mathbf{p}$	Pseudo	c.r. [†]
$P = 2i\langle\Gamma_{25'}^l \mathbf{p} \Gamma_{2'}^l\rangle$	1.360	1.24	1.36 ^a	1.200	1.27	1.20 ^b
$Q = 2i\langle\Gamma_{25'}^l \mathbf{p} \Gamma_{15}\rangle$	1.070	0.99	1.07 ^a	1.050	1.05	1.05 ^b
$R = 2i\langle\Gamma_{25'}^l \mathbf{p} \Gamma_{12'}\rangle$	0.8049	0.75	0.92 ^c	0.830	0.74	0.68 ^d
$P'' = 2i\langle\Gamma_{25'}^l \mathbf{p} \Gamma_{2'}^u\rangle$	0.1000	0.09		0.100	0.10	
$P' = 2i\langle\Gamma_{25'}^u \mathbf{p} \Gamma_{2'}^l\rangle$	0.1715	0.0092		-0.090	-0.10	
$Q' = 2i\langle\Gamma_{25'}^u \mathbf{p} \Gamma_{15}\rangle$	-0.752	-0.65		-0.807	-0.64	
$R' = 2i\langle\Gamma_{25'}^u \mathbf{p} \Gamma_{12'}\rangle$	1.4357	1.13		1.210	1.21	
$P''' = 2i\langle\Gamma_{25'}^u \mathbf{p} \Gamma_{2'}^u\rangle$	1.6231	1.30		1.32	1.37	
$T = 2i\langle\Gamma_1^l \mathbf{p} \Gamma_{15}\rangle$	1.2003	1.11		1.080	1.18	
$T' = 2i\langle\Gamma_1^l \mathbf{p} \Gamma_{15}\rangle$	0.5323	0.41		0.206	0.34	

[†]Values used to analyze the cyclotron resonance experiments

^aB.W. Levinger and D.R. Frankl, J. Phys. Chem. Solids **20**, 281 (1961)

^bJ.C. Hensel and G. Feher, Phys. Rev. **129**, 1041 (1963)

^cCalculated from cyclotron resonance data

^dCalculated from cyclotron resonance data of reference b

The momentum matrix elements for the $\mathbf{k} \cdot \mathbf{p}$ perturbation should be multiplied by a factor 2, and thus $P = 1.16$ for Ge ($P = 1.18$ for Si) and $Q = 0.88$ for Ge ($Q = 0.94$ for Si), which are very close to the parameters used by Cardona and Pollak [15] in Table 1.9. The matrix elements P play a very important role in the determination of the valence band structure to be dealt with in Chap. 2 and the optical absorption due to the direct transition discussed in Chap. 4.

The 15 states at the Γ point are classified into $\Gamma_1^l(1)$, $\Gamma_1^u(1)$, $\Gamma_2^l(1)$, $\Gamma_2^u(1)$, $\Gamma_{25'}^l(3)$, $\Gamma_{15}(3)$, $\Gamma_{25'}^u(3)$, $\Gamma_{12'}(2)$, where the superscripts l and u correspond to the lower and upper states of the bands, respectively, and number in the parentheses () is the dimension of the representation. It is evident from the character table of the group theory that $\Gamma_{25'}$ is 3-dimensional with three eigenstates. The energy eigenstates are estimated roughly by the pseudopotential method or other approximations [15] as stated above, and shown in Table 1.8. The momentum operator \mathbf{p} has the same symmetry as Γ_{15} and thus the matrix elements of $\mathbf{k} \cdot \mathbf{p}$ for the 15 eigenstates have non-zero components, as shown in the following equations and in Table 1.9.

$$P = 2i\langle\Gamma_{25'}^l|\mathbf{p}|\Gamma_{2'}^l\rangle, \quad (1.135a)$$

$$Q = 2i\langle\Gamma_{25'}^l|\mathbf{p}|\Gamma_{15}\rangle, \quad (1.135b)$$

$$R = 2i\langle\Gamma_{25'}^l|\mathbf{p}|\Gamma_{12'}\rangle, \quad (1.135c)$$

$$P'' = 2i\langle\Gamma_{25'}^l|\mathbf{p}|\Gamma_{2'}^u\rangle, \quad (1.135d)$$

$$P' = 2i\langle\Gamma_{25'}^u|\mathbf{p}|\Gamma_{2'}^l\rangle, \quad (1.135e)$$

$$Q' = 2i\langle\Gamma_{25'}^u|\mathbf{p}|\Gamma_{15}\rangle, \quad (1.135f)$$

$$R' = 2i\langle\Gamma_{25'}^u|\mathbf{p}|\Gamma_{12'}\rangle, \quad (1.135g)$$

$$P''' = 2i\langle\Gamma_{25'}^u|\mathbf{p}|\Gamma_{2'}^u\rangle, \quad (1.135h)$$

$$T = 2i\langle\Gamma_1^u|\mathbf{p}|\Gamma_{15}\rangle, \quad (1.135i)$$

$$T' = 2i\langle\Gamma_1^l|\mathbf{p}|\Gamma_{15}\rangle. \quad (1.135j)$$

The factor 2 of the momentum matrix elements in Table 1.9 and (1.135a) ~ (1.135j) is understood from $\mathbf{k} \cdot \mathbf{p}$ perturbation Hamiltonian given by (1.119) and (1.120), where energy is in Rydberg [Ry] and the length in unit a_B (Bohr radius) as discussed above. We note here the matrix elements of $\langle\Gamma_{25'}|\mathbf{k} \cdot \mathbf{p}|\Gamma_{12'}\rangle$ used in the present calculations. Using the character table and the basis function we may deduce the non-vanishing matrix elements for the $\mathbf{k} \cdot \mathbf{p}$ theory. In the present analysis the matrix elements between $\Gamma_{25'}$ and $\Gamma_{12'}$ are evaluated by using the property of the character table in Table 1.4,

$$\Gamma_{25'} \times \Gamma_{12'} = \Gamma_{15} + \Gamma_{25}, \quad \Gamma_{15} \times \Gamma_{12'} = \Gamma_{25'} + \Gamma_{15'}. \quad (1.136)$$

The wave vectors $\mathbf{p} = [p_x, p_y, p_z]$ have the same property as $[x, y, z]$, and thus the representation is Γ_{15} . Therefore we find non-zero matrix elements $\langle\Gamma_{25'}|\mathbf{p}|\Gamma_{12'}\rangle$ and $\langle\Gamma_{15'}|\mathbf{p}|\Gamma_{12'}\rangle$. However, $\Gamma_{15'}$ states belong to the plane waves $[\pm 3, \pm 1, \pm 1]$ and the free electron energy is $11(2\pi/a)^2$ which is much higher than the upper states of $\Gamma_{25'}$ [200] with the free electron energy $4(2\pi/a)^2$, and thus $\Gamma_{15'}$ states may be disregarded. Therefore the following matrix elements for the states $\Gamma_{12'}$ are included in the 15×15 $\mathbf{k} \cdot \mathbf{p}$ perturbation (see (1.143a) ~ (1.143f) for a detailed treatment).

$$2i\langle\Gamma_{25'}^l(X)|\mathbf{p}|\Gamma_{12'}\rangle = R, \quad (1.137a)$$

$$2i\langle\Gamma_{25'}^u(Y)|\mathbf{p}|\Gamma_{12'}\rangle = R'. \quad (1.137b)$$

Using the parameters listed in Table 1.9 and following the procedures below, the energy band structures of Ge and Si are easily calculated. First, we calculate the

15×15 matrix elements of the $\mathbf{k} \cdot \mathbf{p}$ Hamiltonian, and second diagonalize the matrix to obtain the energy eigenvalues and their eigenstates at \mathbf{k} of the Brillouin zone. The matrix of the $\mathbf{k} \cdot \mathbf{p}$ Hamiltonian has 15×15 *complex* elements. When we include the spin–orbit interaction, the matrix of $\mathbf{k} \cdot \mathbf{p}$ Hamiltonian is given by 30×30 *complex* elements.

1.7.3 15–band $\mathbf{k} \cdot \mathbf{p}$ Method

It is very important to point out here that the 15×15 matrices for Ge and Si are factorized into smaller matrices when we use group theoretical consideration, as shown by Cardona and Pollak [15]. For simplicity we consider the energy bands along the $\langle 100 \rangle$, $\langle 110 \rangle$ and $\langle 111 \rangle$ directions of the \mathbf{k} -vector. The direction $\langle 100 \rangle$ starts from the Γ point and ends at the X point along the Δ axis, and the $\langle 110 \rangle$ direction is from the Γ point to the K point along the Σ axis, while the $\langle 111 \rangle$ direction is from the Γ point to the L point along the Δ axis. With the help of the compatibility relation given in Table 1.10 (see [13]) the matrix elements of the $\mathbf{k} \cdot \mathbf{p}$ Hamiltonian are factorized in several groups of smaller matrices. In the following we use atomic units as stated above, and thus $\hbar^2 k^2/2m$ and $p^2/2m$ are expressed as k^2 and p^2 , respectively. In the following we show the factorized matrices of the $\mathbf{k} \cdot \mathbf{p}$ Hamiltonian in the $[100]$, $[110]$ and $[111]$ directions.

1. $[100]$ direction

(a) Δ_5 bands

From Table 1.10 we find that three Γ bands exist, but the bands in the parentheses () are neglected because of their high energy states.

Δ_5 bands: $(\Gamma_{15'})$, $\Gamma_{25'}^u$, $\Gamma_{25'}^l$, Γ_{15}

The matrix elements for these 3 bands are

Table 1.10 Compatibility relations

Γ_1	Γ_2	Γ_{12}	$\Gamma_{15'}$	$\Gamma_{25'}$	$\Gamma_{1'}$	$\Gamma_{2'}$	$\Gamma_{12'}$	Γ_{15}	Γ_{25}
Δ_1	Δ_2	$\Delta_1 \Delta_2$	$\Delta_{1'} \Delta_5$	$\Delta_{2'} \Delta_5$	$\Delta_{1'}$	$\Delta_{2'}$	$\Delta_{1'} \Delta_{2'}$	$\Delta_1 \Delta_5$	$\Delta_2 \Delta_5$
A_1	A_2	A_3	$A_2 A_3$	$A_1 A_3$	A_2	A_1	A_3	$A_1 A_3$	$A_2 A_3$
Σ_1	Σ_4	$\Sigma_1 \Sigma_4$	$\Sigma_2 \Sigma_3 \Sigma_4$	$\Sigma_1 \Sigma_2 \Sigma_3$	Σ_2	Σ_3	$\Sigma_2 \Sigma_3$	$\Sigma_1 \Sigma_3 \Sigma_4$	$\Sigma_1 \Sigma_2 \Sigma_4$
X_1	X_2	X_3	X_4	X_5	$X_{1'}$	$X_{2'}$	$X_{3'}$	$X_{4'}$	$X_{5'}$
Δ_1	Δ_2	$\Delta_{2'}$	$\Delta_{1'}$	Δ_5	$\Delta_{1'}$	$\Delta_{2'}$	Δ_2	Δ_1	Δ_5
Z_1	Z_1	Z_4	Z_4	$Z_2 Z_3$	Z_2	Z_2	Z_3	Z_3	$Z_1 Z_4$
S_1	S_4	S_1	S_4	$S_2 S_3$	S_2	S_3	S_2	S_3	$S_1 S_4$
M_1	M_2	M_3	M_4	M_5	$M_{1'}$	$M_{2'}$	$M_{3'}$	$M_{4'}$	$M_{5'}$
Σ_1	Σ_1	Σ_4	Σ_4	$\Sigma_2 \Sigma_3$	Σ_2	Σ_2	Σ_3	Σ_3	$\Sigma_1 \Sigma_4$
Z_1	Z_1	Z_3	Z_3	$Z_2 Z_4$	Z_2	Z_2	Z_4	Z_4	$Z_1 Z_3$
T_1	T_2	$T_{2'}$	$T_{1'}$	T_5	$T_{1'}$	$T_{2'}$	T_2	T_1	T_5

$$\begin{vmatrix} |\Gamma_{25}^l\rangle & |\Gamma_{15}\rangle & |\Gamma_{25'}^u\rangle \\ k_x^2 & Qk_x & 0 \\ Qk_x & \mathcal{E}(\Gamma_{15}) + k_x^2 & Q'k_x \\ 0 & Q'k_x & \mathcal{E}(\Gamma_{25'}^u) + k_x^2 \end{vmatrix}. \quad (1.138)$$

(b) Δ_1 bands

Δ_1 bands: $\Gamma_1^l, \Gamma_1^u, (\Gamma_{12}), \Gamma_{15}$

The matrix elements for these three bands are

$$\begin{vmatrix} |\Gamma_{15}\rangle & |\Gamma_1^u\rangle & |\Gamma_1^l\rangle \\ \mathcal{E}(\Gamma_{15}) + k_x^2 & Tk_x & T'k_x \\ Tk_x & \mathcal{E}(\Gamma_1^u) + k_x^2 & 0 \\ T'k_x & 0 & \mathcal{E}(\Gamma_1^l) + k_x^2 \end{vmatrix}. \quad (1.139)$$

(c) $\Delta_{2'}$ bands

$\Delta_{2'}$ bands: $\Gamma_{25'}^l, \Gamma_{25'}^u, \Gamma_{2'}^l, \Gamma_{2'}^u, \Gamma_{12'}$

The matrix elements for these five bands are

$$\begin{vmatrix} |\Gamma_{2'}^l\rangle & |\Gamma_{25'}^l\rangle & |\Gamma_{12'}\rangle & |\Gamma_{25'}^u\rangle & |\Gamma_{2'}^u\rangle \\ \mathcal{E}(\Gamma_{2'}^l) + k_x^2 & Pk_x & 0 & P'k_x & 0 \\ Pk_x & k_x^2 & \sqrt{2}Rk_x & 0 & P''k_x \\ 0 & \sqrt{2}Rk_x & \mathcal{E}(\Gamma_{12'}) + k_x^2 & \sqrt{2}R'k_x & 0 \\ P'k_x & 0 & \sqrt{2}R'k_x & \mathcal{E}(\Gamma_{25'}^u) + k_x^2 & P'''k_x \\ 0 & P''k_x & 0 & P'''k_x & \mathcal{E}(\Gamma_{2'}^u) + k_x^2 \end{vmatrix}, \quad (1.140)$$

where the factor $\sqrt{2}$ of $\sqrt{2}Rk_x$ and $\sqrt{2}R'k_x$ arises from the definition of $\Gamma_{12'}$ states ($\Gamma_{12'}(1)$ and $\Gamma_{12'}(2)$) as given by Cardona and Pollak [15] and the $\Gamma_{12'}(2)$ state does not interact with any other state in the [100] direction and behaves like a free electron band (see (1.143a), (1.143b), (1.144)).

2. [110] direction

From Table 1.10, $\Sigma_1, \Sigma_4, \Sigma_3, \Sigma_2$ are included in this direction.

(a) Σ_1 bands: $\Gamma_1^l, \Gamma_1^u, (\Gamma_{12}), \Gamma_{25'}^l, \Gamma_{25'}^u, \Gamma_{15}$ (: 5 bands)

(b) Σ_4 bands: $(\Gamma_2), (\Gamma_{12}), (\Gamma_{15'}), \Gamma_{15}, (\Gamma_{25})$ (: 1 band)

(c) Σ_3 bands: $(\Gamma_{15'}), \Gamma_{25'}^l, \Gamma_{25'}^u, \Gamma_{2'}^l, \Gamma_{2'}^u, \Gamma_{12'}, \Gamma_{15}$ (: 6 bands)

(d) Σ_2 bands: $(\Gamma_{15'}), \Gamma_{25'}^l, \Gamma_{25'}^u, (\Gamma_{1'}), \Gamma_{12'}, (\Gamma_{25})$ (: 3 bands)

Therefore, for the bands in the [110] direction, Σ bands, 15×15 matrix elements results in irreducible matrix of $6 \times 6, 5 \times 5, 3 \times 3, 1 \times 1$.

3. [111] direction

From Table 1.10, Λ_1, Λ_3 are included in this direction.

(a) 7 bands of Λ_1 bands: $\Gamma_1^l, \Gamma_1^u, \Gamma_{25'}^l, \Gamma_{25'}^u, \Gamma_{2'}^l, \Gamma_{2'}^u, \Gamma_{15}$

(b) 4 bands of Λ_3 bands: $(\Gamma_{12}), (\Gamma_{15'}), \Gamma_{25'}^l, \Gamma_{25'}^u, \Gamma_{12'}, \Gamma_{15}, (\Gamma_{25})$

and the Λ bands in the $[111]$ direction are classified in 7×7 and 4×4 irreducible matrix.

It should be noted here that above $15 \times 15 \mathbf{k} \cdot \mathbf{p}$ matrix is easily extended to include k_y and k_z components. However we have to take account of correct symmetry of the $\Gamma_{12'}(1)$ and $\Gamma_{12'}(2)$ states, which is done by extending the method of Dresselhaus [14] and convert them into the representations of Cardona and Pollak [15] as follows. Using the definition of Dresselhaus et al. and following their procedures, we obtain

$$\langle \Gamma_{25'}(X) | p_x | \gamma_1^- \rangle = R, \quad (1.141a)$$

$$\langle \Gamma_{25'}(X) | p_x | \gamma_2^- \rangle = -R, \quad (1.141b)$$

$$\langle \Gamma_{25'}(Y) | p_y | \gamma_1^- \rangle = \omega R, \quad (1.141c)$$

$$\langle \Gamma_{25'}(Y) | p_y | \gamma_2^- \rangle = -\omega^2 R, \quad (1.141d)$$

$$\langle \Gamma_{25'}(Z) | p_z | \gamma_1^- \rangle = \omega^2 R, \quad (1.141e)$$

$$\langle \Gamma_{25'}(Z) | p_z | \gamma_2^- \rangle = -\omega R, \quad (1.141f)$$

where we have to note that the matrix elements R defined by Dresselhaus, Kip and Kittel [14] (R_{DKK}) and R defined by Cardona and Pollak [15] (R_{CP}) are related by $R_{\text{CP}} = 2R_{\text{DKK}}$. When we choose the eigenstates $\Gamma_{12'}$ defined by Cardona and Pollak [15];

$$\Gamma_{12'}(1) = \frac{1}{\sqrt{2}}(\gamma_1^- - \gamma_2^-), \quad \Gamma_{12'}(2) = \frac{1}{\sqrt{2}}(\gamma_1^- + \gamma_2^-), \quad (1.142)$$

we obtain the following results

$$\langle \Gamma_{25'} | p_x | \Gamma_{12'}(1) \rangle = \sqrt{2}R, \quad (1.143a)$$

$$\langle \Gamma_{25'} | p_x | \Gamma_{12'}(2) \rangle = 0, \quad (1.143b)$$

$$\langle \Gamma_{25'} | p_y | \Gamma_{12'}(1) \rangle = (\omega + \omega^2)R/\sqrt{2} = -R/\sqrt{2}, \quad (1.143c)$$

$$\langle \Gamma_{25'} | p_y | \Gamma_{12'}(2) \rangle = (\omega - \omega^2)R/\sqrt{2} = \omega(1 - \omega)R/\sqrt{2} = iR\sqrt{3}/2, \quad (1.143d)$$

$$\langle \Gamma_{25'} | p_z | \Gamma_{12'}(1) \rangle = (\omega^2 + \omega)R/\sqrt{2} = -R/\sqrt{2}, \quad (1.143e)$$

$$\langle \Gamma_{25'} | p_z | \Gamma_{12'}(2) \rangle = (\omega^2 - \omega)R/\sqrt{2} = \omega(\omega - 1)R/\sqrt{2} = -iR\sqrt{3}/2, \quad (1.143f)$$

where ω is the solutions of $\omega^3 = 1$ (exclude the solution $\omega = 1$) or the solutions of $\omega^2 + \omega + 1 = 0$. The above results are obtained by using the solution $\omega = (-1 + i\sqrt{3})/2$. When we choose the solution $\omega = (-1 - i\sqrt{3})/2$, the sign of the imaginary part is changed, but the energy band calculations give the same result. In addition we have to note that $\omega = 1$, one of the solutions of $\omega^3 = 1$, does not give a correct energy bands. This is because the solution $\omega = 1$ does not represent the correct symmetry of γ_1^- and γ_2^- . Here we show the $15 \times 15 \mathbf{k} \cdot \mathbf{p}$ Hamiltonian matrix without the spin-orbit interaction (antisymmetric potential terms for zinc blende crystals are included);

$ \Gamma_{25'}^l(X)\rangle$	$ \Gamma_{25'}^l(Y)\rangle$	$ \Gamma_{25'}^l(Z)\rangle$	$ \Gamma_{15}(x)\rangle$	$ \Gamma_{15}(y)\rangle$	$ \Gamma_{15}(z)\rangle$
$E(\Gamma_{25'}^l) + k^2$	0	0	$-iV_1^-$	Qk_z	Qk_y
0	$E(\Gamma_{25'}^l) + k^2$	0	Qk_z	$-iV_1^-$	Qk_x
0	0	$E(\Gamma_{25'}^l) + k^2$	Qk_y	Qk_x	$-iV_1^-$
iV_1^-	Qk_z	Qk_y	$E(\Gamma_{15}) + k^2$	0	0
Qk_z	iV_1^-	Qk_x	0	$E(\Gamma_{15}) + k^2$	0
Qk_y	Qk_x	iV_1^-	0	0	$E(\Gamma_{15}) + k^2$
0	0	0	$-iV_4^-$	$Q'k_z$	$Q'k_y$
0	0	0	$Q'k_z$	$-iV_4^-$	$Q'k_x$
0	0	0	$Q'k_y$	$Q'k_x$	$-iV_4^-$
$\sqrt{2}Rk_x$	$-(R/\sqrt{2})k_y$	$-(R/\sqrt{2})k_z$	0	0	0
0	$-iR\sqrt{3/2}k_y$	$iR\sqrt{3/2}k_z$	0	0	0
Pk_x	Pk_y	Pk_z	0	0	0
$P''k_x$	$P''k_y$	$P''k_z$	0	0	0
0	0	0	Tk_x	Tk_y	Tk_z
0	0	0	$T'k_x$	$T'k_y$	$T'k_z$
$ \Gamma_{25'}^u(X)\rangle$	$ \Gamma_{25'}^u(Y)\rangle$	$ \Gamma_{25'}^u(Z)\rangle$	$ \Gamma_{12'}(1)\rangle$	$ \Gamma_{12'}(2)\rangle$	
0	0	0	$\sqrt{2}Rk_x$	0	
0	0	0	$-(R/\sqrt{2})k_y$	$iR\sqrt{3/2}k_y$	
0	0	0	$-(R/\sqrt{2})k_z$	$-iR\sqrt{3/2}k_z$	
iV_4^-	$Q'k_z$	$Q'k_y$	0	0	
$Q'k_z$	iV_4^-	$Q'k_x$	0	0	
$Q'k_y$	$Q'k_x$	iV_4^-	0	0	
$E(\Gamma_{25'}^u) + k^2$	0	0	$\sqrt{2}R'k_x$	0	
0	$E(\Gamma_{25'}^u) + k^2$	0	$-(R'/\sqrt{2})k_y$	$iR'\sqrt{3/2}k_y$	
0	0	$E(\Gamma_{25'}^u) + k^2$	$-(R'/\sqrt{2})k_z$	$-iR'\sqrt{3/2}k_z$	
$\sqrt{2}R'k_x$	$-(R'/\sqrt{2})k_y$	$-(R'/\sqrt{2})k_z$	$E(\Gamma_{12'}) + k^2$	0	
0	$-iR'\sqrt{3/2}k_y$	$iR'\sqrt{3/2}k_z$	0	$E(\Gamma_{12'}) + k^2$	
$P'k_x$	$P'k_y$	$P'k_z$	0	0	
$P'''k_x$	$P'''k_y$	$P'''k_z$	0	0	
0	0	0	0	0	
0	0	0	0	0	
$ \Gamma_2^l(xyz)\rangle$	$ \Gamma_2^u(xyz)\rangle$	$ \Gamma_1^u\rangle$	$ \Gamma_1^l\rangle$		
Pk_x	$P''k_x$	0	0		
Pk_y	$P''k_y$	0	0		
Pk_z	$P''k_z$	0	0		
0	0	Tk_x	$T'k_x$		
0	0	Tk_y	$T'k_y$		
0	0	Tk_z	$T'k_z$		
$P'k_x$	$P'''k_x$	0	0		
$P'k_y$	$P'''k_y$	0	0		
$P'k_z$	$P'''k_z$	0	0		
0	0	0	0		
0	0	0	0		
$E(\Gamma_2^l) + k^2$	0	iV_2^-	iV_3^-		
0	$E(\Gamma_2^u) + k^2$	iV_5^-	iV_6^-		
$-iV_2^-$	$-iV_5^-$	$E(\Gamma_1^u) + k^2$	0		
$-iV_3^-$	$-iV_6^-$	0	$E(\Gamma_1^l) + k^2$		

(1.144)

It should be noted here that $\langle \Gamma_{12'}(2) | p_y | \Gamma_{25'}(Y) \rangle$ is given by the complex conjugate of $\langle \Gamma_{25'}(Y) | p_y | \Gamma_{12'}(2) \rangle$. Energy bands without the spin-orbit interaction are easily

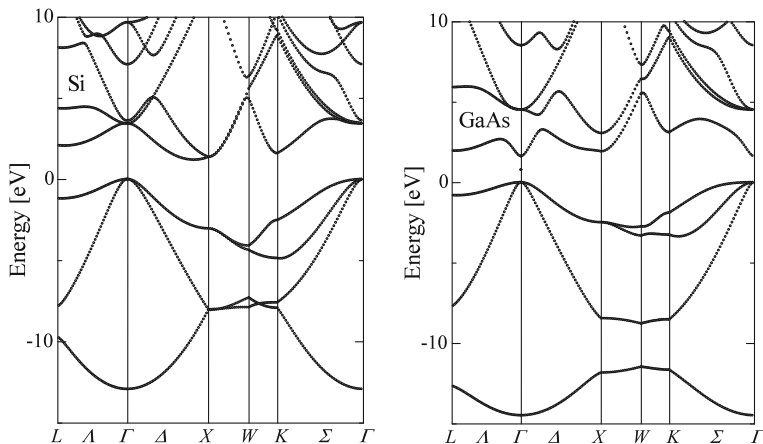


Fig. 1.17 Energy band structure of Si and GaAs calculated by 15 band $\mathbf{k} \cdot \mathbf{p}$ perturbation without spin-orbit interaction. The results are obtained by solving secular equation (1.144) with the parameters given in Table 1.11

calculated by solving (1.144) in any directions of the Brillouin zone. As an example calculated energy band structure of Si along the L, Γ, X, W, K to Γ points is shown in Fig. 1.17. Also in the figure the energy band structure of GaAs is shown, where the antisymmetric potential is taken account (see 1.7.4).

1.7.4 Antisymmetric Potentials for Zinc Blende Crystals

We have to note here the definition of the matrix elements of the anti-symmetric potentials. As discussed in Sect. 1.6, a diamond type crystal has inversion symmetry and thus $V^A(\mathbf{G}) = 0$, while a zinc blende type crystal has no inversion symmetry and thus $V^A(\mathbf{G}) \neq 0$. In order to extend the $\mathbf{k} \cdot \mathbf{p}$ Hamiltonian for a zinc blende crystal we have to evaluate the matrix elements of the anti-symmetric potential as shown in (1.144). Here we present how to evaluate approximate values of the matrix elements of the anti-symmetric potential. First, we obtain non-vanishing matrix elements of the 15 plane waves of $[0, 0, 0]$, $[\pm 1, \pm 1, \pm 1]$, and $[\pm 2, 0, 0]$ which are classified as $\Gamma_1^l, \Gamma_{25'}^l, \Gamma_{15}, \Gamma_{12'}, \Gamma_2^l, \Gamma_1^u, \Gamma_{25'}^u, \Gamma_{12'},$ and Γ_2^u as shown in Table 1.6. In Table 1.4, an inversion operation is expressed by J and representation Γ_i has the inversion symmetry when $J > 0$ but no inversion symmetry when $J < 0$. The product of $\Gamma_i \times \Gamma_j$ has the same symmetry property. Noting the anti-symmetric potential V^- has negative sign for the inversion operation, non-vanishing matrix elements $\langle \Gamma_i | V^- | \Gamma_j \rangle$ are $\langle \Gamma_{15} | V^- | \Gamma_{25'} \rangle$ and $\langle \Gamma_{2'} | V^- | \Gamma_1 \rangle$. When we use the notations of Pollak, Higginbotham, and Cardona [18], these are given by the following relations,

$$V_1^- = \langle \Gamma_{15} | V^- | \Gamma_{25'}^I \rangle = V_4^A, \quad (1.145a)$$

$$V_2^- = \langle \Gamma_{2'}^I | V^- | \Gamma_1^u \rangle = -3V_4^A, \quad (1.145b)$$

$$V_3^- = \langle \Gamma_{2'}^I | V^- | \Gamma_1^I \rangle = 2V_3^A, \quad (1.145c)$$

$$V_4^- = \langle \Gamma_{15} | V^- | \Gamma_{25'}^u \rangle = \sqrt{2} (V_3^A - V_{11}^A), \quad (1.145d)$$

$$V_5^- = \langle \Gamma_{2'}^u | V^- | \Gamma_1^u \rangle = -(\sqrt{6}/3) [(4V_3^A + 2V_{11}^A)], \quad (1.145e)$$

$$V_6^- = \langle \Gamma_{2'}^u | V^- | \Gamma_1^I \rangle = (2\sqrt{6}/3)V_4^A, \quad (1.145f)$$

where the last terms of the above equations are evaluated from the pseudopotentials in Table 1.2 and the relations defined by (1.109a) ~ (1.109d) with linear combinations of the plane waves (1.126) and (1.128 ~ (1.128). As an example we evaluate these terms for GaAs using the pseudopotentials given in Table 1.2. We obtain $V_1^- = 0.05$ (0.12652), $V_2^- = -0.15$ (-0.24791), $V_3^- = 0.14$ (0.38210), $V_4^- = 0.0849$ (0.12297), $V_5^- = -0.245$ (-0.34820), and $V_6^- = 0.0816$ (0.0), where the values in the parentheses are determined from the energy band calculations and summarized in Table 1.11 for several zinc blende type semiconductors. Since the term V_6^- corresponds to interactions between very distant atomic orbitals $\Gamma_{2'}^u$ and Γ_1^I (difference in the free electron energy is $4(2\pi/a)^2 = 1.38$ [a.u.] for GaAs), we may safely assume that $V_6^- = 0.0$ [18].

When we include the spin-orbit interaction, the above equation leads to 30×30 $\mathbf{k} \cdot \mathbf{p}$ complex matrix because each state is doubled with spin-up (\uparrow) and spin-down (\downarrow). In Chap. 2, we will discuss the second order perturbation of the $\mathbf{k} \cdot \mathbf{p}$ Hamiltonian and the parameters defined by Dresselhaus et al. [14] and by Luttinger [2.2], where the above results are used to evaluate the contributions from γ_1^- and γ_2^- ($\Gamma_{12'}(1)$ and $\Gamma_{12'}(2)$).

1.7.5 Spin-orbit Interaction Hamiltonian

When we take account of the spin-orbit interaction, the eigenstates are doubled with spin-up and spin-down as discussed above, and then we have to solve 30×30 complex matrix. In the following we choose the wave functions $|X \uparrow\rangle, |X \downarrow\rangle, |Y \uparrow\rangle, |Y \downarrow\rangle, |Z \uparrow\rangle, |Z \downarrow\rangle$ for $\Gamma_{25'}^I$, and $|x \uparrow\rangle, |x \downarrow\rangle, |y \uparrow\rangle, |y \downarrow\rangle, |z \uparrow\rangle, |z \downarrow\rangle$ for Γ_{15} . This approximation leads to 30×30 complex matrix with the spin-orbit interaction. In this subsection we formulate the spin-orbit matrix elements using these eigenstates. Spin-orbit interaction is also discussed in 2.3 to analyze the valence band structure, in addition to describe the effective mass and effective g factor (Landé g factor) of the conduction band. Evaluation of the matrix elements of spin-orbit Hamiltonian is given in detail in 2.3.

We put the spin-orbit interaction term (H.18) of Appendix H into (1.112), and obtain

$$H_{so} = \frac{\hbar}{4m^2c^2} [\nabla \times \mathbf{p}] \cdot \boldsymbol{\sigma} + \frac{\hbar^2}{4m^2c^2} [\nabla \times \mathbf{k}] \cdot \boldsymbol{\sigma}, \quad (1.146)$$

which should be added to the terms in the brackets of the left hand side of (1.116). The second \mathbf{k} -dependent term is very small compared to the first \mathbf{k} -independent term (see Kane [12]) and thus only the first term is considered in this text. Thus the \mathbf{k} -independent term of the spin-orbit Hamiltonian is rewritten as

$$H_{so} \propto \mathbf{L} \cdot \boldsymbol{\sigma} = (\mathbf{r} \times \mathbf{p}) \cdot \boldsymbol{\sigma} = -i\hbar(\mathbf{r} \times \nabla) \cdot \boldsymbol{\sigma} \quad (1.147)$$

and therefore we find that

$$\begin{aligned} -i\hbar(\mathbf{r} \times \nabla) \cdot \boldsymbol{\sigma} = & -i\hbar \left[\left(y \frac{\partial}{\partial z} - z \frac{\partial}{\partial y} \right) \sigma_x + \left(z \frac{\partial}{\partial x} - x \frac{\partial}{\partial z} \right) \sigma_y \right. \\ & \left. + \left(x \frac{\partial}{\partial y} - y \frac{\partial}{\partial x} \right) \sigma_z \right], \end{aligned} \quad (1.148)$$

where $\boldsymbol{\sigma}$ is Pauli spin operator¹ and the matrix elements are evaluated by using the basis functions given in Table 1.5.

$$\langle X(\Gamma_{25'}^l) \uparrow | H_{so} | Y(\Gamma_{25'}^l) \uparrow \rangle = i\Delta_{25'}^l/3, \quad (1.149a)$$

$$\langle X(\Gamma_{25'}^l) \uparrow | H_{so} | Z(\Gamma_{25'}^l) \downarrow \rangle = \Delta_{25'}^l/3, \quad (1.149b)$$

$$\langle Y(\Gamma_{25'}^l) \uparrow | H_{so} | Z(\Gamma_{25'}^l) \downarrow \rangle = i\Delta_{25'}^l/3. \quad (1.149c)$$

In the same manner the spin-orbit interaction for Γ_{15} is written as

$$\langle x(\Gamma_{15}) \uparrow | H_{so} | y(\Gamma_{15}) \uparrow \rangle = i\Delta_{15}/3, \quad (1.150a)$$

$$\langle x(\Gamma_{15}) \uparrow | H_{so} | z(\Gamma_{15}) \downarrow \rangle = \Delta_{15}/3, \quad (1.150b)$$

$$\langle y(\Gamma_{15}) \uparrow | H_{so} | z(\Gamma_{15}) \downarrow \rangle = i\Delta_{15}/3, \quad (1.150c)$$

and the antisymmetric term of the spin-orbit interaction is treated as

$$\langle X(\Gamma_{25'}^l) \uparrow | H_{so} | y(\Gamma_{15}) \uparrow \rangle = i\Delta^-/3, \quad (1.151a)$$

$$\langle X(\Gamma_{25'}^l) \uparrow | H_{so} | z(\Gamma_{15}) \uparrow \rangle = +\Delta^-/3, \quad (1.151b)$$

$$\langle Y(\Gamma_{25'}^l) \uparrow | H_{so} | z(\Gamma_{15}) \downarrow \rangle = i\Delta^-/3. \quad (1.151c)$$

The spin-orbit interaction in the valence bands is discussed in Chap. 2. Here we will show the present treatment leads to the same results. The $\Gamma_{25'}^l$ valence bands ($|X\rangle$, $|Y\rangle$, $|Z\rangle$) are triply-degenerate at the Γ point ($\mathbf{k} = 0$). The degenerate $\Gamma_{25'}^l$ bands split into doubly-degenerate heavy hole and light hole bands, and the spin-orbit-split-off band as discussed in Chap. 2. Here it is shown that the above matrix elements of the spin-orbit Hamiltonian for the valence bands $\Gamma_{25'}^l$ give the same results of the spin-orbit splitting dealt in Chap. 2. The matrix of the spin-orbit Hamiltonian for the valence band $\Gamma_{25'}^l$ is written as

$$\begin{array}{ccc} |X \uparrow\rangle & |Y \uparrow\rangle & |Z \downarrow\rangle \\ \left| \begin{array}{ccc} 0 & i\Delta_{25'}^l/3 & \Delta_{25'}^l/3 \\ -i\Delta_{25'}^l/3 & 0 & i\Delta_{25'}^l/3 \\ \Delta_{25'}^l/3 & -i\Delta_{25'}^l/3 & 0 \end{array} \right| \begin{array}{c} |X \uparrow\rangle \\ |Y \uparrow\rangle \\ |Z \downarrow\rangle \end{array} \end{array}, \quad (1.152)$$

¹See (2.50) of Chap. 2 for the definition and (H.33c) of Appendix H for the matrix elements.

and diagonalization results in

$$\begin{vmatrix} (1/3)\Delta_{25'}^I & 0 & 0 \\ 0 & (1/3)\Delta_{25'}^I & 0 \\ 0 & 0 & -(2/3)\Delta_{25'}^I \end{vmatrix} \begin{vmatrix} u_{v1} \\ u_{v2} \\ u_{v3} \end{vmatrix}. \quad (1.153)$$

Therefore the spin-orbit splitting of $\Gamma_{25'}^I$ bands is $\Delta_0 = \Delta_{25'}^I$ and the corresponding eigenfunctions are

$$u_{v1} = \frac{i}{\sqrt{2}}(X - iY) \uparrow, \quad (1.154a)$$

$$u_{v2} = \frac{1}{\sqrt{2}}(X \uparrow + Z \downarrow), \quad (1.154b)$$

$$u_{v3} = \frac{-1}{\sqrt{3}}[(X + iY) \uparrow - Z \downarrow]. \quad (1.154c)$$

Using these results we may obtain the matrix elements of the spin-orbit Hamiltonian H_{so} for the $\Gamma_{25'}$ states:

$$\langle \Gamma_{25'} | H_{so} | \Gamma_{25'} \rangle = \frac{\Delta}{3} \begin{vmatrix} |X \uparrow\rangle & |Y \uparrow\rangle & |Z \downarrow\rangle & |X \downarrow\rangle & |Y \downarrow\rangle & |Z \uparrow\rangle \\ 0 & i & 1 & 0 & 0 & 0 \\ -i & 0 & i & 0 & 0 & 0 \\ 1 & -i & 0 & 0 & 0 & 0 \\ 0 & 0 & 0 & 0 & i & 1 \\ 0 & 0 & 0 & -i & 0 & i \\ 0 & 0 & 0 & 1 & -i & 0 \end{vmatrix}, \quad (1.155)$$

and the matrix is separated by two 3×3 matrices and diagonalization of the matrix gives the following eigenvalues and eigen functions,

$$\langle \Gamma_{25'} | H_{so} | \Gamma_{25'} \rangle = \frac{\Delta}{3} \begin{vmatrix} |v_{v1}\rangle & |v_{v2}\rangle & |v_{v3}\rangle & |v_{v4}\rangle & |v_{v5}\rangle & |v_{v6}\rangle \\ 1 & 0 & 0 & 0 & 0 & 0 \\ 0 & 1 & 0 & 0 & 0 & 0 \\ 0 & 0 & 1 & 0 & 0 & 0 \\ 0 & 0 & 0 & 1 & 0 & 0 \\ 0 & 0 & 0 & 0 & -2 & 0 \\ 0 & 0 & 0 & 0 & 0 & -2 \end{vmatrix}, \quad (1.156)$$

The eigenstates of the fourfold degenerate valence bands are

$$\begin{aligned}
u_{v1} &= \frac{1}{\sqrt{2}} [|X \uparrow\rangle + |Z \downarrow\rangle] , \\
u_{v2} &= \frac{1}{\sqrt{2}} [|X \downarrow\rangle + |Z \uparrow\rangle] , \\
u_{v3} &= \frac{i}{\sqrt{2}} [(X - iY) \downarrow] , \\
u_{v4} &= \frac{i}{\sqrt{2}} [(X - iY) \uparrow] ,
\end{aligned}$$

and for twofold degenerate spin-orbit split off bands are

$$\begin{aligned}
u_{v5} &= -\frac{1}{\sqrt{3}} [(X + iY) \uparrow - |Z \downarrow\rangle] , \\
u_{v6} &= -\frac{i}{\sqrt{3}} [(X + iY) \downarrow - |Z \uparrow\rangle] ,
\end{aligned}$$

where we find that the spin-orbit interaction results in the split of valence bands $\Delta/3$, $\Delta/3$, and $-2\Delta/3$. Note here that the obtained eigen functions differ from those defined by (2.63a) ~ (2.63f) in Chap. 2 because of the different definition of the original (unperturbed) basis functions. Similar relations for the Γ_{15} states and antisymmetric parts are easily evaluated.

1.7.6 30-band $\mathbf{k} \cdot \mathbf{p}$ Method with the Spin-Orbit Interaction

We have to note here that the full band calculation (energy states at any points of the Brillouin zone) is easily carried out by extending $15 \times 15 \mathbf{k} \cdot \mathbf{p}$ matrix of (1.144) to $30 \times 30 \mathbf{k} \cdot \mathbf{p}$ matrix with spin-up and spin-down states. The matrices of the spin-orbit interaction Hamiltonian for $\Gamma_{25'}^u$ states, Γ_{15} states, and the antisymmetric parts between $\Gamma_{25'}^u$ and Γ_{15} states are obtained by (1.155). The 30-band $\mathbf{k} \cdot \mathbf{p}$ Hamiltonian with *complex* elements are solved to obtain 30 eigenstates. The full band calculations based on the 30-band $\mathbf{k} \cdot \mathbf{p}$ methods have been reported in the literatures [19, 20], where the treatment of the matrix elements R and R_1 are deduced by Voon and Willatzen [19].² All the $\mathbf{k} \cdot \mathbf{p}$ parameters for semiconductors such as Ge and Si with diamond crystal structure and several III-V compound semiconductors such as GaAs and GaP are summarized in Table 1.11. It should be noted again that III-V compound semiconductors with a zinc blende structure have no inversion symmetry and thus we have to include the anti-symmetric terms of the potentials and spin-orbit interaction as discussed by Pollak et al. [18]. A lack of the inversion symmetry results in the antisymmetric potential V^- , and the antisymmetric parts of Δ^- in the spin-orbit Hamiltonian of which matrix elements are defined by (1.151a) ~ (1.151c).

²The author is thankful for M. Cardona to remind the work by Voon and Willatzen after his visit to Max Planck Institute at Stuttgart in June, 2013.

Table 1.11 Energy eigenvalues (in Rydberg) and momentum matrix elements (in atomic units) used in the $\mathbf{k} \cdot \mathbf{p}$ Hamiltonians for Si, Ge, GaAs, GaP, InP and InSb. Matrix elements of the anti-symmetric potentials V^- and anti-symmetric spin-orbit splitting parameter Δ^- (in Rydberg) for GaAs, GaP, InP and InSb are also listed. Values are from references [15, 18, 21–23]

	Si	Ge	GaAs	GaP	InP	InSb
$\Gamma_{25'}^l$	0.00	0.00	0.00	0.00	0.00	0.00
$\Gamma_{2'}^l$	0.265	0.0728	0.0845	0.2566	0.0929	0.022
Γ_{15}	0.252	0.232	0.2596	0.2511	0.2622	0.232
Γ_1^u	0.520	0.571	0.4940	0.5222	0.5057	0.400
$\Gamma_{12'}$	0.710	0.771	0.6063	0.7126	0.5803	0.494
$\Gamma_{25'}^u$	0.940	1.25	0.9002	0.9535	0.8745	0.726
$\Gamma_{2'}^u$	0.990	1.35	0.9849	1.0056	0.9792	0.765
Γ_1^l	−0.950	−0.966	−0.844	−0.9827	−0.8107	−0.846
P	1.200	1.360	1.3225	1.207	1.0876	1.3460
Q	1.050	1.070	1.1599	1.051	1.1346	1.0990
R	0.830	0.8049	0.7635	0.8289	0.8045	0.5914
P''	0.100	0.100	0.2465	0.100	0.1267	0.5324
P'	−0.090	0.1715	0.0438	−0.07863	0.1031	0.0666
Q'	−0.807	−0.752	−0.5511	−0.8046	−0.6585	−0.2120
R'	1.210	1.436	0.9697	1.220	1.1038	1.0760
P'''	1.320	1.623	1.5530	1.333	1.4281	1.2340
T	1.080	1.200	1.1387	1.0852	1.0806	0.9070
T'	0.206	0.5323	0.5323	0.2202	0.3906	0.0210
$\Delta_{25'}^l$	0.0032	0.0213	0.0251	0.00399	0.00823	0.0590
Δ_{15}	0.0036	0.0265	0.0135	0.00459	0.00573	0.0287
V_1	$= \langle \Gamma_{15} V^- \Gamma_{25'}^l \rangle$		0.12652	0.14924	0.1347	0.0869
V_2	$= \langle \Gamma_{2'}^l V^- \Gamma_1^u \rangle$		−0.24791	−0.26885	−0.2003	−0.1558
V_3	$= \langle \Gamma_{2'}^l V^- \Gamma_1^l \rangle$		0.38210	0.45687	0.2252	0.2391
V_4	$= \langle \Gamma_{15} V^- \Gamma_{25'}^u \rangle$		0.12297	0.21044	0.1131	0.0581
V_5	$= \langle \Gamma_{2'}^u V^- \Gamma_1^u \rangle$		−0.34820	−0.33021	−0.2601	−0.1252
V_6	$= \langle \Gamma_{2'}^u V^- \Gamma_1^l \rangle$		0.0	0.0	0.0	0.0
Δ^-			0.0051	0.00485	0.00682	0.0160

The calculated energy band structures of in the energy range $-15 \sim 10$ [eV] are shown for Ge and GaAs in Fig. 1.18 and for GaP and InP in Fig. 1.19, where we find that the 30-band $\mathbf{k} \cdot \mathbf{p}$ perturbation method gives a reasonable result although the matrix elements are very few compared to the pseudopotential method. Since the energy bands near the lowest conduction band and the top valence bands are very important to understand the electrical and optical properties of semiconductors, the energy band structures in the vicinity of the conduction minima and the valence band maxima calculated by the 30-band $\mathbf{k} \cdot \mathbf{p}$ perturbation method are shown in Fig. 1.20

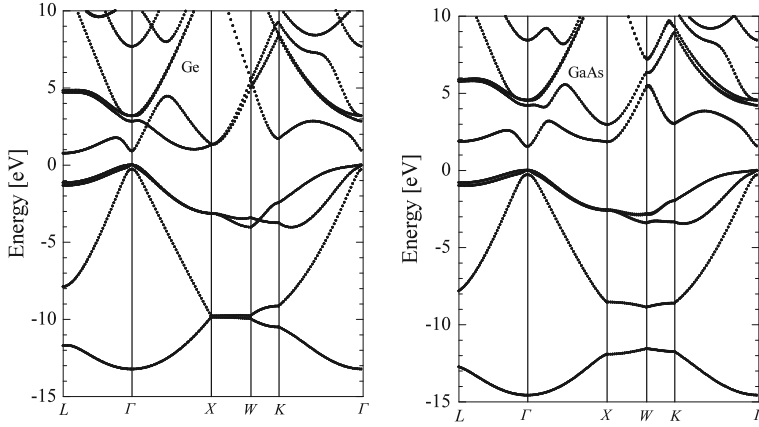


Fig. 1.18 Energy band structure of Ge and GaAs calculated by the 30-band $\mathbf{k} \cdot \mathbf{p}$ method with spin-orbit interaction in \mathbf{k} space along L , Γ , X , W , K , and Γ of the Brillouin zone

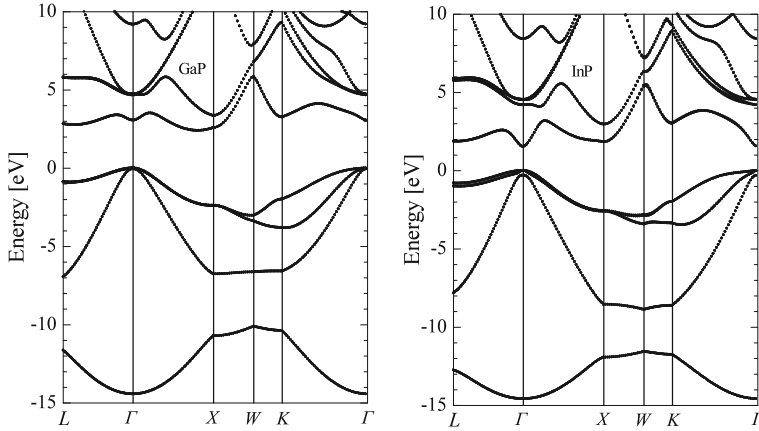


Fig. 1.19 Energy band structures calculated by the 30-band $\mathbf{k} \cdot \mathbf{p}$ perturbation method for GaP and InP, where the spin-orbit interaction is included

for Ge and GaAs, where the parameters are from the references [15, 18, 21–23]. The $\mathbf{k} \cdot \mathbf{p}$ perturbation method is very simple, as shown above, and gives an information about the matrix elements of the optical transition in addition to detailed and accurate energy band structures [15].

We have to note here some difference of the calculated band structures between the empirical pseudopotential method and 30-band $\mathbf{k} \cdot \mathbf{p}$ perturbation method. As seen in the first Brillouin zone of a face centered cubic crystal given in Figs. 1.5a and 1.22 the U point and K point are equivalent and we may expect the same energy eigenvalues at the two points. This feature is understood from the symmetry properties of the free electron band in the region U and K of Fig. 1.6. However,

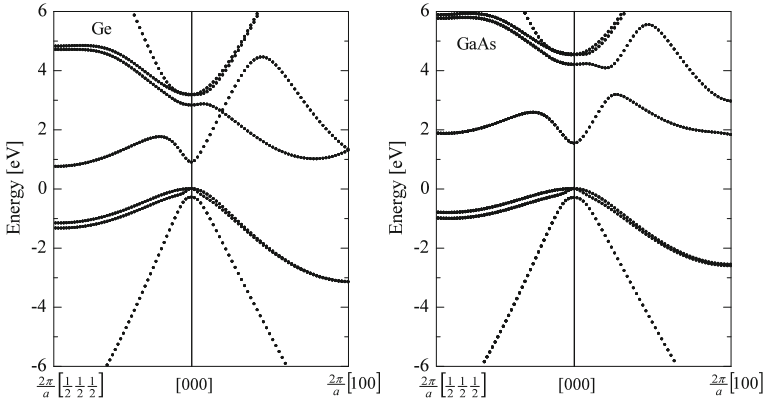


Fig. 1.20 Energy band structures near the conduction and valence bands calculated by the 30-band $k \cdot p$ perturbation method for Ge and GaAs, where the spin-orbit interaction is included

when we plot energy bands obtained by the 30-band $k \cdot p$ method along X point to U point and K point to Γ point, we find a small discontinuity at the points U and K , although the pseudopotential method gives smooth curve in this region. This may be ascribed to the assumption of limited number of eigen states at the Γ point for the $k \cdot p$ perturbation method as follows. The free electron bands of a face centered cubic lattice are shown in Figs. 1.6 and 1.7, where we find that one of the 12 free electron bands of $[220]$ is merged into one of the 6 free electron bands of $[200]$. This is clearly seen in Fig. 1.21, where the energy band structures of GaAs calculated by 30-band $k \cdot p$ are shown in Fig. 1.21a and the results obtained from the empirical pseudopotential method with 65 plane waves (130 plane waves with spin-up and spin-down) are shown in Fig. 1.21b. In the calculations of the local pseudopotential method, we used the following parameters replacing the pseudopotentials V_3^S and V_{11}^A in Table 1.3 by $V_3^S = -0.260$ and $V_{11}^A = 0.015$, and the spin-orbit interaction parameters $\lambda^S = -0.00050$ and $\lambda^A = -0.00012$ in atomic units. Total number of the free electron waves is 113 and the higher lying free electron waves beyond $\mathcal{E} = 16$ are included by Löwdin's perturbation method. These parameters lead to $\mathcal{E}_G = 1.52$ eV and spin-orbit splitting $\Delta = 0.342$ eV. In Fig. 1.21a we find the bands obtained from 30-band $k \cdot p$ method are discontinuous at U and K points, while the bands calculated by the empirical pseudopotential method with 65 plane waves are continuous. In addition the second lowest conduction band in the region $\Gamma-X$ calculated by 30-band $k \cdot p$ method does not appear in the region of between U , K and Γ points. These features are observed in the band structures calculated by the pseudopotential method with 15 plane waves shown in Fig. 1.9, while the energy bands with 65 plane waves show much more smooth (continuous) curves near U and K points.

Although such a small difference exists in the energy band structure calculated by the 30-bands $k \cdot p$ perturbation method, the obtained overall features of the full band structures are very in good agreement with the empirical pseudopotential method and

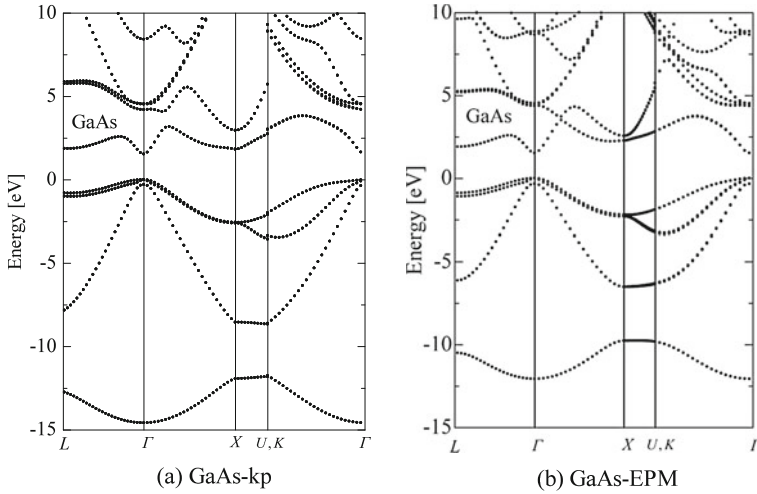


Fig. 1.21 Energy band structures of GaAs along L - Γ , Γ - X , X - U , K , and U , K - Γ points **a** calculated by the 30-band $\mathbf{k} \cdot \mathbf{p}$ perturbation method and **b** calculated by the empirical pseudopotential method with 65 plane waves (130 plane waves with spin-up and spin-down), where the spin-orbit interaction is included. See the textbook for the used parameters

the bands along L , Γ , X , W , K to Γ are very smooth. As discussed in Sect. 1.8, the density of states are calculated by dividing the polyhedron, the $1/48$ volume of the first Brillouin zone, starting the basal plane of L , Γ , X , W , K . Then the calculations of the density of states are straight forward.

From the results of the pseudopotential and $\mathbf{k} \cdot \mathbf{p}$ perturbation methods we find the important features of the energy band structures of the semiconductors which we deal with in this text. All these semiconductors have valence band maxima at $\mathbf{k} = 0$ (Γ point) and most III-V semiconductors (except several compounds such as GaP, AlAs and so on) have the conduction band minimum at $\mathbf{k} = 0$ (Γ point), and so are classified as direct gap semiconductors. On the other hand, other semiconductors such as Ge, Si, GaP, AlAs and so on have the conduction band minima at $\mathbf{k} \neq 0$, and so are called indirect gap semiconductors. Ge has the conduction band minima at $\mathbf{k} = (\pi/a)[111]$ (L point), which are degenerate and consist of equivalent four conduction bands, and thus the conduction bands have a “many-valley structure.” On the other hand, Si has the conduction band minima at the Δ point close to the X point and six equivalent conduction band minima. Later we will discuss the optical properties of semiconductors, where we find that the direct and indirect semiconductors are quite different in their optical properties such as absorption and light emission. The electrical properties also exhibit the features of many-valley structures in Ge and Si, and also the Gunn effect of GaAs, which arises from the inter-valley transfer of electrons in a high electric field from the high electron mobility Γ valley to the low mobility L and/or X valleys. From these results we understand that the energy band structures play a very important role in the understanding of the electrical and

optical properties of semiconductors. In addition, once we know the procedures for calculating energy band structures it is very easy to extend the method to calculate the energy band structures of superlattices (periodic layers of different semiconductors such as GaAs/AlAs) as treated in Chap. 8. It is also possible to predict the basic features of semiconductors from the results of energy band calculations. In this text the basic physics of semiconductors is treated on the basis of their energy band structures.

1.8 Density of States

As shown in Sect. 4.3, density of states (DOS) is defined as the number of states per unit energy. When the number of states in a small volume of \mathbf{k} -space in a small range of energy, $[\mathcal{E}, \mathcal{E} + \Delta\mathcal{E}]$ is given by $(1/2\pi)^3 \Delta v(\mathbf{k})$, the density of states $J_{\text{DOS}}(\mathcal{E})$ is defined by (spin factor 2 is omitted)

$$J_{\text{DOS}}(\mathcal{E}) = \sum_{\mathbf{k}} \frac{1}{(2\pi)^3} \frac{\Delta v(\mathbf{k})}{\Delta\mathcal{E}}. \quad (1.157)$$

Here $v(\mathbf{k})$ is a small volume of the wave vector \mathbf{k} in the first Brillouin zone. The density of states is required to calculate dielectric function (joint density of states) and also to calculate scattering rate of electrons. It is well known that Monte Carlo simulation [24] gives a good description of transport properties at high electric fields. Full band Monte Carlo simulation is used very often, where the calculated energy band structure is used to simulated electron motion in \mathbf{k} -space, and thus the density of states is required to obtain the scattering rate. In this textbook we will not deal with high field transport (see [25] for a review on high field transport) and thus we will not concern with Monte Carlo simulation. However, it is very important to know how to calculate the density of states defined by (1.157) from the calculated energy band structure. Various methods have been reported to calculate DOS from the energy bands. Brust [9] reported a rigorous analysis of the joint density of states in Ge and Si, but the method is very complicated. Here we will show a simple but accurate method to calculate the density of states. First, let's take a look of the Brillouin zone shown in Fig. 1.22 which is the same as shown in Fig. 1.5a. It is clear from the 48-fold symmetry of the Brillouin zone that 1/48th part of the zone shown in Fig. 1.22 is sufficient to calculate the density of states. In other words, all the other \mathbf{k} -points in the first Brillouin zone may be obtained by rotation of the 1/48-th of the Brillouin zone. Using a unit length $k_f = (X - \Gamma)/8 = \pi/4a$ with the lattice constant a , 1/48-th part of the first Brillouin zone can be divided into polyhedrons shown in Fig. 1.23. The bottom plane consists of the critical points Γ , X , W , K . The second plane is displaced by k_f in the k_z direction with respect to the first plane, and intersects Λ , S , Q . The third plane with the same displacement intersects Λ , U , Q , and the fourth intersects Λ , Q , L . The two neighboring planes

Fig. 1.22 The first Brillouin zone of face centered cubic lattice and the symmetry points. The box defined by the lines is $1/48$ -th part of the volume of the first Brillouin zone

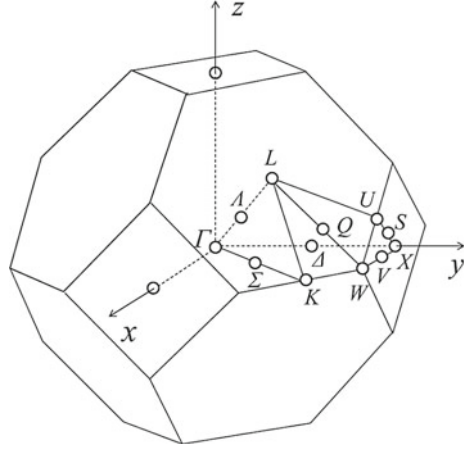
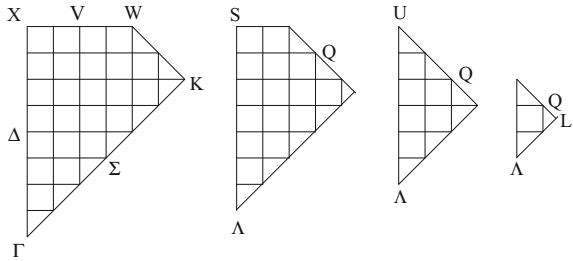


Fig. 1.23 $1/48$ th part of the first Brillouin zone of face centered cubic lattice is discretized into polyhedrons using unit length $k_f = (X - \Gamma)/8 = \pi/4a$, where a is the lattice constant



form polyhedrons of which volume gives the number of states. The discretization shown in Fig. 1.23 is not sufficient to calculate the density of states. Here we have to note the most important idea to use this type of discretization. In order to get smaller volumes of the polyhedrons, use the unit length $k_f/N \rightarrow k_f$, where N is 2, 4, 8, ... Then the volumes of new polyhedrons becomes $1/8$, $1/64$, $1/512$, ... of the original polyhedrons and the number of polyhedrons are 8, 64, 512, ... times of the original number. The density of states are easily calculated using this discretization. We calculate the energy eigenstates at the corners of a polygon and tabulate them. Then pick up the minimum \mathcal{E}_{\min} and the maximum \mathcal{E}_{\max} from the lowest pairs of the tabulated eigenstates. Calculate $\Delta\mathcal{E} = \mathcal{E}_{\max} - \mathcal{E}_{\min}$ and $\mathcal{E} = (\mathcal{E}_{\max} + \mathcal{E}_{\min})/2$. This gives us

$$J_{\text{DOS}}(\mathcal{E}) \simeq \frac{1}{(2\pi)^3} \frac{\Delta v_f(\mathbf{k})}{\Delta\mathcal{E}}, \quad (1.158)$$

where $\Delta v_f(\mathbf{k})$ is the volume of the polyhedron. In a similar fashion we calculate the density of states for the second lowest pairs, third lowest pairs and so on up to a required \mathcal{E} value. The obtained DOS $J_{\text{DOS}}(\mathcal{E})$ is not uniform but scattered in the

Fig. 1.24 Energy band structures of Si calculated by empirical pseudopotential method with the pseudopotentials listed in Table 1.2 and the calculated density of states (DOS)

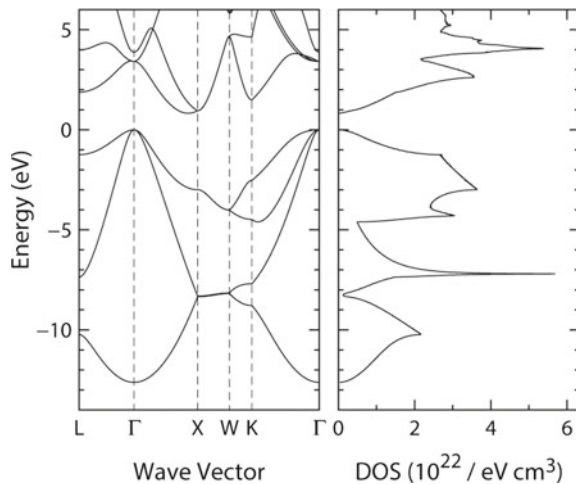
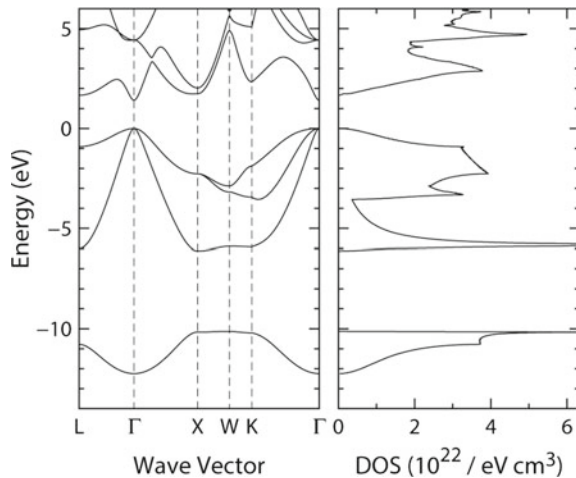


Fig. 1.25 Energy band structures of GaAs calculated by empirical pseudopotential method with the pseudopotentials listed in Table 1.2 and the calculated density of states (DOS)



energy \mathcal{E} and thus we have to rearrange the data in the histogram, 0.1-eV histogram for example. Then smoothing procedure will give a smooth curve of $J_{\text{DOS}}(\mathcal{E})$ as a function of \mathcal{E} . Typical examples of the energy bands and the DOS are shown in Fig. 1.24 for Si and in Fig. 1.25 for GaAs, where the energy bands are obtained by the local pseudopotential method using the pseudopotentials given in Table 1.2 and the density of states in the valence bands and the conduction bands are calculated.

1.9 Problems

- (1.1) Calculate the reciprocal lattice vectors of a zinc blende type crystal structure and compare with the result of Table. 1.1.
- (1.2) Energy band calculations are carried out by using atomic units [a.u.]. Give wave vector $k = 2\pi/a_B$, and energy $(\hbar^2/2m)/a_B^2$ in atomic units, where $a_B = (\epsilon_0 \hbar^2 / \pi m e^2) = 0.529177 \text{ [\AA]}$ is Bohr radius.
- (1.3) Rewrite Equation (1.35), using the atomic units.
- (1.4) Evaluate energy bands of two band model based on the nearly free electron approximation, taking free electron bands of $G_n = 0$ and $G_n = 1$, where $G_n = 2n\pi/a$, $a = 0.543 \text{ [\AA]}$, and $V(G_1) = V_3^s = -0.21 \text{ [a.u.]}$. Calculate the energy band $\mathcal{E}(k_x)$ and plot the energy bands together with the free electron bands.
- (1.5) Derive fundamental vectors $[\mathbf{a}, \mathbf{b}, \mathbf{c}]$ of (i) simple cubic, (ii) body centered cubic, (iii) face centered cubic and hexagonal closed pack crystals, and calculate their unit cell volume v .
- (1.6) Derive the reciprocal lattice vectors $[\mathbf{a}^*, \mathbf{b}^*, \mathbf{c}^*]$ of (i) simple cubic, (ii) body centered cubic, (iii) face centered cubic and hexagonal closed pack crystals, and calculate their unit cell volume v .
- (1.7) Derive spin-orbit interaction given by (1.149a)

$$\langle X(\Gamma_{25'}^I) \uparrow | H_{\text{so}} | Y(\Gamma_{25'}^I) \uparrow \rangle = i\Delta_{25'}^I/3$$

- (1.8) In order to calculate full band structure in the first Brillouin zone, we have to the wave vectors at the critical points (symmetry points) and their lengths. Referring Figs. 1.22 and 1.23, evaluate the symmetry points and the lengths between the symmetry points of a face centered cubic crystal.

References

1. C. Kittel, *Introduction to Solid State Physics*, 7th edn. (Wiley, New York, 1996)
2. M.L. Cohen, J.R. Chelikowsky, *Electronic Structure and Optical Properties of Semiconductors* (Springer, Heidelberg, 1989). This article provides a good review of energy band calculations based on the pseudopotential theory. The bibliography is a good guide to find articles of the energy band calculations and optical properties of various semiconductors
3. V. Heine, The pseudopotential concept. *Solid State Phys.* **24**, 1–36 (1970)
4. M.L. Cohen, V. Heine, The fitting pseudopotentials to experimental data and their subsequent application. *Solid State Phys.* **24**, 37–248 (1970)
5. M.L. Cohen, T.K. Bergstresser, *Phys. Rev.* **141**, 789 (1966)
6. J.R. Chelikowsky, M.L. Cohen, *Phys. Rev. B* **10**, 5095 (1974)
7. J.R. Chelikowsky, M.L. Cohen, *Phys. Rev. B* **14**, 556 (1976)
8. P.O. Löwdin, *J. Chem. Phys.* **19**, 1396 (1951)
9. D. Brust, *Phys. Rev. A* **134**, 1337 (1964)
10. P.J. Melz, *J. Phys. Chem. Solids* **32**, 209 (1971)
11. G. Weisz, *Phys. Rev.* **149**, 504 (1966)
12. E.O. Kane, *J. Phys. Chem. Solids* **1**, 82 (1956); 249 (1957)

13. L.P. Bouckaert, R. Smoluchowski, E. Wigner, *Phys. Rev.* **50**, 58 (1936)
14. G. Dresselhaus, A.F. Kip, C. Kittel, *Phys. Rev.* **98**, 368 (1955)
15. M. Cardona, F.H. Pollak, *Phys. Rev.* **142**, 530 (1966)
16. M. Cardona, Optical properties and band structure of Germanium and Zinblende-type semiconductors, in *Proceedings of the International School of Physics «Enrico Fermi»* (Academic Press, New York, 1972) pp. 514–580
17. F. Bassani, G. Pastori Parravicini, *Electronic States and Optical Transitions in Solids* (Pergamon Press, New York, 1975)
18. F.H. Pollak, C.W. Higginbotham, M. Cardona, *J. Phys. Soc. Jpn.* **21**(Supplement), 20 (1966)
19. L.C.L.Y. Voon, M. Willatzen, *The $k \cdot p$ Method: Electronic Properties of Semiconductors* (Springer, Berlin, 2009)
20. D.W. Bailey, C.J. Stanton, K. Hess, *Phys. Rev. B* **42**, 3423 (1990)
21. H. Hazama, Y. Itoh, C. Hamaguchi, *J. Phys. Soc. Jpn.* **54**, 269 (1985)
22. T. Nakashima, C. Hamaguchi, J. Komeno, M. Ozeki, *J. Phys. Soc. Jpn.* **54**, 725 (1985)
23. H. Hazama, T. Sugimasa, T. Imachi, C. Hamaguchi, *J. Phys. Soc. Jpn.* **55**, 1282 (1986)
24. C. Jacoboni, L. Reggiani, *Rev. Mod. Phys.* **55**, 645 (1983)
25. E.M. Conwell, *High Field Transport in Semiconductors*, vol. 9, Solid State Physics (Academic Press, New York, 1967)



<http://www.springer.com/978-3-319-66859-8>

Basic Semiconductor Physics

Hamaguchi, C.

2017, XXI, 709 p. 315 illus., Hardcover

ISBN: 978-3-319-66859-8